Evaluation of novel enzyme systems for *in-vitro* production of industrial solvents

Steven Reiße

Vollständiger Abdruck der von der Fakultät für Chemie der Technischen Universität München zur Erlangung des akademischen Grades eines Doktors der Naturwissenschaften genehmigten Dissertation.

Eidesstattliche Erklärung

Hiermit versichere ich, dass ich die vorliegende Dissertation selbstständig verfasst, sowie die Ausführungen und Gedanken, welche anderen Schriften sinngemäß oder wörtlich entnommen wurden, sowie weitere Quellen und Hilfsmittel kenntlich gemacht habe. Die vorliegende Arbeit wurde bisher weder in gleicher noch ähnlicher Form einer anderen Prüfungsbehörde vorgelegt oder anderweitig veröffentlicht.

München, den 27.04.2015

Acknowledgments

This thesis represents the end of a five year long journey with ups and downs and amazing moments. On my way, I had the pleasure to meet many wonderful persons and to find exciting perspectives for my personal growth. Now, at the end, I want to thank all the people who contributed to this work in so many ways:

Prof. Dr. Thomas Brück for his excellent support. With his motivating guidance, constructive reviews and trustfully granted scope for my personal development, he has contributed most to the success of this work.

Prof. Dr. Volker Sieber, who gave me a scientific home at his institute at the beginning of the project. He offered me a genuine endorsement through his wide knowledge and his advice.

Prof. Dr. Tom Nilges as chairperson of examination for acceptance of this duty.

Special thanks go to Dr. Daniel Garbe for his great support as team leader and particularly for his valuable comments on this thesis.

I am also grateful to my project partners, Dr. Jan-Karl Guterl, Dr. Bettina Sommer, Martina Haack, Dr. Jörg Carsten, Dr. Fabian Steffler, Anja Schmidt and Broder Rühmann.

My lab and office mates form the group of Industrial Biocatalysis. Not to forget all my other adorable colleagues from WZ-Straubing. We had a great time! Thank you for that.

Especially I want to thank Fabian and André. Together, we were the FumA dream team and, maybe one day, we get a new chance.

I warmly thank Martin Rauscher for the correction of this thesis.

Finally I want to thank my family for their patience and great support that foremost made this thesis feasible.

Zusammenfassung

Die endliche Verfügbarkeit von fossilen Ressourcen forciert eine Neuorientierung in der chemischen Industrie mit Fokus auf bio-basierte, nachhaltige Prozesse. Die zuckerbasierte Produktion der industriellen Alkohole Ethanol, Isobutanol und *n*-Butanol als Plattformchemikalien zur Produktion von Kraftstoffäquivalenten und chemischen Bausteinen ist hier von besonderer Bedeutung. Zellbasierte, fermentative Verfahren zur nachhaltigen Darstellung dieser Moleküle sind bereits in einem fortgeschrittenen Entwicklungsstadium. Jedoch ist der zell-basierte Ansatz speziell zur Darstellung von höherwertigen Alkoholen, wie Isobutanol und *n*-Butanol, auf Ausbeuten um die 2 % (v/v) limitiert. Dies ist auf toxische Effekte des Endproduktes als auch der Umleitung von Schlüsselmetaboliten, wie Pyruvate und Acetyl-CoA, in nicht produktive Stoffwechselwege zurückzuführen. Die Produkttiter-Problematik zellbasierter Systeme bedingt daher energieaufwendige Aufreinigungsverfahren, welche die ökonomische Effizienz des Gesamtprozesses in Frage stellen.

Um diese Flaschenhälse zu umgehen, wurde in einem Verbundprojekt zwischen dem Lehrstuhl für Chemie Biogener Rohstoffe (CBR), dem Fachgebiet Industrielle Biokatalyse (IBK) und einem Industriepartner ein neues zellfreies Verfahren zur Produktion von höherwertigen Alkoholen (Isobutanol, *n*-Butanol) entwickelt. Dieses Verfahren basiert auf minimierten, nicht-natürlichen Enzymkaskaden und erlaubt so eine massen- und energieeffiziente Umsetzung von biogenen Zuckerströmen in die Zielprodukte. Im Vergleich zu einem zellbasierenden System können die katalytischen Eigenschaften und Ko-Faktorspezifitäten sowie Thermo- und Lösemittelstabilitäten von einzelnen Enzymkomponenten schnell genetisch optimiert werden. Dies führt potentiell zu höheren Produkttitern und einer vereinfachten Produktaufarbeitung. Das Design und die Prozessoptimierung dieser Enzymkaskaden bedingt jedoch die Wahl von geeigneten Ausgangsenzymen. Hier muss jede Einzelenzymkomponente in katalytischer Effizienz, Stabilität und Ko-Faktor-Nutzung mit vor- bzw. nachgeschalteten Enzymfunktionen abgestimmt werden.

Das Ziel dieser Arbeit war die Auswahl, Charakterisierung, falls nötig Optimierung und die Bereitstellung geeigneter Enzyme, um ein *in-vitro* Produktionssystem auf Basis nachwachsender Rohstoffe für technisch relevante Lösungsmittel wie Isobutanol und

n-Butanol zu konstruieren. Insbesondere die Enzymaktivitäten der Ketol-Säure-Reduktoisomerase (KARI), Thiolase und Crotonase waren hier im Fokus.

In-vitro Isobutanolsynthese

Das hier beschriebene zellfreie Isobutanol-Produktionssystem basiert auf einer synthetischen, von den Projektmitgliedern entwickelten Enzymkaskade. Diese Enzymkaskade besteht grundsätzlich aus einer minimierten Glykolyse zum zentralen Intermediat Pyruvat. Darauf aufbauend können verschiede Module zur Synthese verschiedener industriell relevanter Produkte angeschlossen werden. Der hier aufgezeigte enzymatische Ansatz hat das Potential, bisherige Produktionsverfahren zu ersetzen oder zumindest zu ergänzen.

In dieser Arbeit wurde u. a. die Reaktion der KARI betrachtet, die Bestandteil des Isobutanol-Syntheseweges ist. KARI katalysiert die reduktive Isomerisierung von 2-Acetolactat zu 2,3-Dihydroxyisolvalerat mit Mg^{2+} und NAD(P)H als Ko-Faktoren. Aufgrund der vorgegebenen Prozessbedingungen musste dafür eine neue KARI in den Produktionsweg integriert werden, die alle Anforderungen erfüllt. Die erforderliche KARI hatte zu den bevorzugten Prozessbedingungen langfristig stabil, NADH-abhängig und bestenfalls sowohl lösemittel- als auch thermotolerant zu sein.

Die entsprechende KARI wurde schließlich aus dem gram-negativen Bakterium *Meiothermus ruber* DSM 1279 (Mr) isoliert. Das Enzym wurde heterolog exprimiert, charakterisiert und anschließend katalytisch optimiert.

Mr-KARI wies einige außergewöhnliche Eigenschaften auf, die es in seiner Enzymklasse einzigartig machen. So verfügte Mr-KARI über eine hohe Temperaturstabiltiät ($\tau_{(50\ °C)}$ = 71 ± 0,2 h) und demonstrierte eine hohe Toleranz gegenüber Isobutanol (IS_{50} ≥ 6 % (v/v)). Auch konnte es die Ko-Faktor-Anforderung der zellfreien Isobutanolsynthese erfüllen, welche auf NADH ausgerichtet wurde. Die beobachteten katalytischen Konstanten betrugen für NADH K_m = 0,24 ± 0,02 mM, k_{cat} = 1,09 ± 0,03 s^{-1} und für das Substrat 2-Acetolactat K_m = 0,55 ± 0,06 mM, k_{cat} = 0,50 ± 0,01 s^{-1}, wobei die spezifische Aktivität 0,7 U mg^{-1} betrug.

Zur Verbesserung der katalytischen Eigenschaften wurden sowohl zufällige als auch gezielte Mutageneseschritte am Enzym durchgeführt. In dieser Studie wurde dafür eigens eine Screening-Prozedur entwickelt, die eine beschleunigte und selektive Auswahl potentieller Enzymvarianten ermöglichte. Auf diese Weise konnte eine Variante mit 350 % verbesserter Aktivität und gleichzeitig erhöhter NADH-Spezifität identifiziert werden. Andere Varianten ermöglichten einen Einblick in die Struktur-Funktions-Beziehung der Mr-KARI.

Im Rahmen dieses Projekts konnte mit der hier beschriebenen Wildtyp-Variante der Mr-KARI bereits erfolgreich Isobutanol durch die entwickelte zellfreie Produktionsroute synthetisiert werden. Die Synthese wurde bei 50 °C und über eine Dauer von 23 h durchgeführt und ergab eine Ausbeute von 53 % Isobutanol. In Betracht aller nachweisbaren Zwischenprodukte und des Produktes wurden sogar 80 % Ausbeute erreicht.

In-vitro Butanolsynthese

Für die *n*-Butanolsynthese wurde zunächst der natürlich vorkommende Stoffwechselweg aus *Clostridium acetobutylicum* betrachtet. Hierbei waren in dieser Arbeit vor allem die Enzymreaktionen der Acetyl-CoA Acetyltransferase (Thiolase) und der Enoyl-CoA Hydratase (Crotonase) von Bedeutung.

Im weiteren Verlauf des Projektes zeigte sich jedoch, dass sich durch die starke Rückkopplungs-Inhibition der Thiolase durch freies CoA und eine erhöhte Temperatursensitivität beteiligter CoA-Derivate die *in-vitro* Prozessführung sehr schwierig gestaltete.

So ergab sich die Überlegung, den Anteil von CoA-Derivaten und damit einhergehend auch die Enzymreaktionen auf ein Minimum zu reduzieren. Die zellfreie Biokatalyse zeigte dabei ihr enormes Potential. So wurde ein alternativer, artifizieller Reaktionsweg erarbeitet, der eine nicht-natürliche Enzymkaskade mit einem organokatalytischen Reaktionsschritt kombiniert.

Acetaldehyd wird hierbei durch eine Prolin-katalysierte Aldolkondensation zu Crotonaldehyd umgesetzt, welches durch eine 2-Enoat Reduktase aus *Bacillus subtilis* und einer Alkoholdehydrogenase aus Geobacillus *stearothermophilus* weiter zu *n*-Butanol reduziert wird.

Durch diesen neuen Syntheseweg können gleich mehrere enzymatische Reaktionsschritte und der Ko-Faktor CoA gänzlich eingespart werden, so dass ausgehend vom Zuckersubstrat nur noch sechs Enzyme und lediglich NAD^+ als Redoxäquivalent für die *n*-Butanolsynthese notwendig sind.

Auf diese Weise konnten wir bereits 7,4 mg L^{-1} *n*-Butanol zellfrei herstellen und unser modulares *in-vitro* Biokatalysesystem für hydrophobe Synthesebausteine vervollständigen.

List of related articles

This thesis is based on the following related articles, which are referred to in the text by their Roman numerals:

I. J.K. Guterl, D. Garbe, J. Carsten, F. Steffler, B. Sommer, S. Reisse, A. Philipp, M. Haack, B. Ruhmann, A. Koltermann, U. Kettling, T. Bruck, V. Sieber, Cell-free metabolic engineering: production of chemicals by minimized reaction cascades, ChemSusChem 5 (2012) 2165-2172.

II. S. Reisse, D. Garbe, T. Bruck, Meiothermus ruber thiolase - a new process stable enzyme for improved butanol synthesis, Biochimie 103 (2014) 16-22.

III. S. Reiße, D. Garbe, T. Brück, Identification and optimization of a novel thermo- and solvent stable ketol-acid reductoisomerase for cell free isobutanol biosynthesis, Biochimie 108C (2014) 76-84.

IV. S. Reiße, D. Garbe, T. Brück, Identification and characterization of a highly thermostable crotonase from Meiothermus ruber, Journal of Molecular Catalysis B: Enzymatic, 112 (2015) 40-44.

V. Minimized butanol biosynthesis via an enamine – aldol – condensation reaction, in preparation.

Content

Virtute fortis!

1 Introduction

With the increasing threat of climate change and rising energy costs, development of sustainable, bio-based processes for production of platform chemicals and biofuels has attracted a great attention during the last few decades. The biological production of fuels from renewable sources is regarded as a feasible solution to the energy and environmental problems in the foreseeable future.

However, to substitute petroleum-based fuels, biofuels have to meet both performance and regulatory standards. All of the petroleum-based fuels consist primarily of alkanes of various lengths and branching patterns. Gasoline, used for internal combustion engines, consists of smaller alkanes containing six to nine carbon atoms on average and must meet specifications for vapor pressure and octane number [1]. In general, increasing carbon chain length lowers the octane number, whereas increasing chain branching increases the octane number [1].

Ethanol is an unbranched alcohol and the most successful biofuel to date because of the simple production process and its high efficiency. Even the recent conflict of the food-versus-fuel issue could be circumvented by using lignocellulose containing agricultural waste as feedstock in second generation ethanol production plants [2, 3].

Nevertheless, ethanol does not compare favorably to gasoline. It contains only 66 % of the gasoline energy content with the consequence of an increased fuel mileage. Furthermore, the high hygroscopicity can lead to corrosion in pipelines and engine ducts (Table 1) [1]. Hence, gasoline can be blended with ethanol only up to 15 % without any engine modifications [4].

Meanwhile, the spectrum of petroleum independent next generation biofuels has expanded from ethanol to other molecules, such as higher alcohols with more desirable fuel properties. Isobutanol (2-methyl-1-propanol) and *n*-butanol have an energy density of only 10 % less than gasoline and a comparable low hygroscopicity, which permits blending with gasoline up to 100 % and the distribution of gasoline / (iso)butanol blends in existing pipelines. While the average octane number of *n*-butanol is similar to gasoline, the octane number of isobutanol is much higher due to its branched-chain nature. Overall, isobutanol and *n*-butanol combine the advantages of gasoline in terms of energy density and hydrophobicity with the renewability of ethanol.

1 Introduction

Table 1: Chemical properties of liquid fuels. [a]

	Ethanol	*n*-Butanol	Isobutanol	Gasoline
Energy density [MJ L^{-1}]	21	29	29	32
Vapor pressure [psi]	1.1	0.077	0.17	0.1-30
Avg octane number [b]	116	87	110	90
Hygroscopicity	high	low	low	low

[a] Adapted from Li et al. [1]

[b] Average of research octane number (RON) and motor octane number (MON)

However, the major challenge in *n*-butanol or isobutanol production is to merge performance and efficiency of the fermentation process. In comparison, ethanol production via fermentation has a long history and is very simple, because of mild, aerobic process conditions and relative low end product toxicity. The ethanol pathway does not emit any byproducts and consequently achieves 95 % yield of the theoretical maximum [1].

In contrast, the *n*-butanol fermentation produces multiple products through the acetone-butanol-ethanol (ABE) process. This traditional biobutanol production, originally established by Weizmann in the beginning of the 20th century [5], is based on an anaerobic fermentation process applying different *Clostridia* species and creates acetone, butanol, ethanol, carbon dioxide, acetic acid, butyric acid, and trace amounts of hydrogen gas [6]. Besides, pH dependent induction of the solventogenesis in addition to the complicated life cycle of the clostridial species including spore formation lead to a much more complex process management [6, 7].

In recent years various organisms were under investigation to overcome this limitations by installing the butanol production pathway in heterologous microorganisms. Therefore, the butanol pathway of *Clostridium acetobutylicum* was successfully re-constructed in *Escherichia coli* [8] or *Saccharomyces cerevisiae* [9]. *Pseudomonas putida* and *Bacillus subtilis* were also explored as alternative production hosts [10].

2

Isobutanol cannot be synthesized in native organisms and is thus reliant on non-natural hosts. Fermentative isobutanol production involves metabolic integration of the last two reactions of the Ehrlich pathway into cellular production systems, such as *E. coli* [11], *B. subtilis* [12] or *Corynebacterium glutamicum* [13]. This strategy allows the metabolic diversion of the conventional branched-chain amino acid biosynthesis of valine, leucine and isoleucine towards the production of isobutanol, via the 2-keto acid intermediate [11].

However, these attempts often suffer from flux imbalances caused by yet unidentified regulatory mechanisms of natural metabolisms [14]. Furthermore, in these cell-based systems end product toxicity at solvent concentrations above 2 % (v/v) remains a main challenge, limiting both product titers and process viability [9-11]. Hydrophobic alcohols, such as *n*-butanol or isobutanol, exert their toxic effects on cellular production systems predominantly by damaging cell wall components [15].

A new approach to overcome these limitations could be the application of *in-vitro* enzyme cascades [16]. This method offers numerous benefits compared to the classical fermentation processes: First the entire process chain and all reaction conditions, like temperature and pH-value, can be modified and controlled.

Secondly, isolated enzymes originating from thermophilic organisms are prone to survive high product and organic solvent titers as well as further industrially relevant process parameters, like high salinity. Additionally, *in-vitro* reaction cascades do not suffer from a product drain into other non-productive metabolic pathways. Furthermore, this approach offers the possibility to create tailor-made, artificial reaction cascades, which are not restricted to the limits of living cells [I].

A major drawback of cell-free production systems is the cost factor. Ideally, the main costs in a butanol or isobutanol production process are feedstock consumption, fermentation equipment, the harvesting equipment and the overall energy consumption during recovery [17].

In this regard, *in-vitro* processes are more expensive than microbial fermentations due to enzyme production and purification. Required cofactors generate a further substantial impact on the cost factor. However, production costs can be significantly decreased by consolidation of the applied enzyme activities and cofactor requirements.

1 Introduction

Accordingly, in cooperation with the Chair of Chemistry of Biogenic Resources a cell-free approach featuring an artificial minimized glycolytic reaction cascade, which provides the key intermediate pyruvate.

Figure 1: Schematic representation of cell-free reaction cascades from glucose to ethanol, isobutanol and *n*-butanol. GDH: Glucose dehydrogenase; DHAD: Dihydroxyacid dehydratase; KDGA: 2-Keto-3-deoxygluconate aldolase; ALDH: Aldehyde dehydrogenase; PDC: Pyruvate decarboxylase; ADH: Alcohol dehydrogenase; ALS: Acetolactate synthase; KARI: Ketol-acid reductoisomerase; KDC: 2-Ketoacid decarboxylase; THL: Thiolase; HBD: Hydroxybutyryl-CoA dehydrogenase; CRT: Crotonase; TCR: Trans-2-enoyl-CoA reductase.

Starting from pyruvate, ethanol, *n*-butanol and isobutanol can be synthesized aerobically and redox balanced (Figure 1) [I].

Here, the ethanol synthesis served as a template to demonstrate the feasibility of the *in-vitro* production system due to the simple pathway design. Glucose is converted to pyruvate via the new glycolysis reaction, which is followed by decarboxylation of pyruvate and further reduction [I].

The isobutanol and *n*-butanol production routes are described in more details in the following sections, including general research issues and specific objectives within each route.

1.1   Aims and scope of this work

This work was part of a collaboration project between the group of Industrial Biocatalysis, the Chair of Chemistry of Biogenic Resources (Technische Universität München, Straubing, Germany) and the industrial partner Clariant Produkte (Deutschland) GmbH. The project pursued the development of a new and advanced technology platform to synthesize industrially relevant solvents or biofuels on the basis of renewable resources.

The underlying idea was to use tailor-made reaction pathways to produce primarily hydrophobic compounds in cell-free processes. The developed toolboxes permitted the *in-vitro* synthesis of ethanol, *n*-butanol or isobutanol. Due to the application of solvent- and thermo-tolerant biocatalysts, the new processes hold the promise of higher titers and simplified product recovery compared to the classical fermentation.

In order to construct an *in-vitro* production system each enzyme component was examined regarding catalytic efficiency, process stability, and cofactor requirements in coordination with upstream and downstream enzyme activities. In this respect the central aim of this study was to select and eventually optimize process-relevant specific biocatalysts. Particularly, the enzyme activities of ketol-acid reductoisomerase, thiolase and crotonase were in focus.

Therefore, all corresponding genes were identified and cloned. The enzymes were heterologously expressed in *E. coli* and subsequently characterized. With provision of all

enzyme components, the whole production routes were assembled *in-vitro* and the desired products were synthesized.

1.2 Cell-free isobutanol catalysis

Isobutanol has the potential to substitute ethanol as next generation biofuel due to its higher energy density and lower hygroscopicity. Additionally, the higher octane number provides isobutanol with an additional benefit compared to the isomer *n*-butanol.
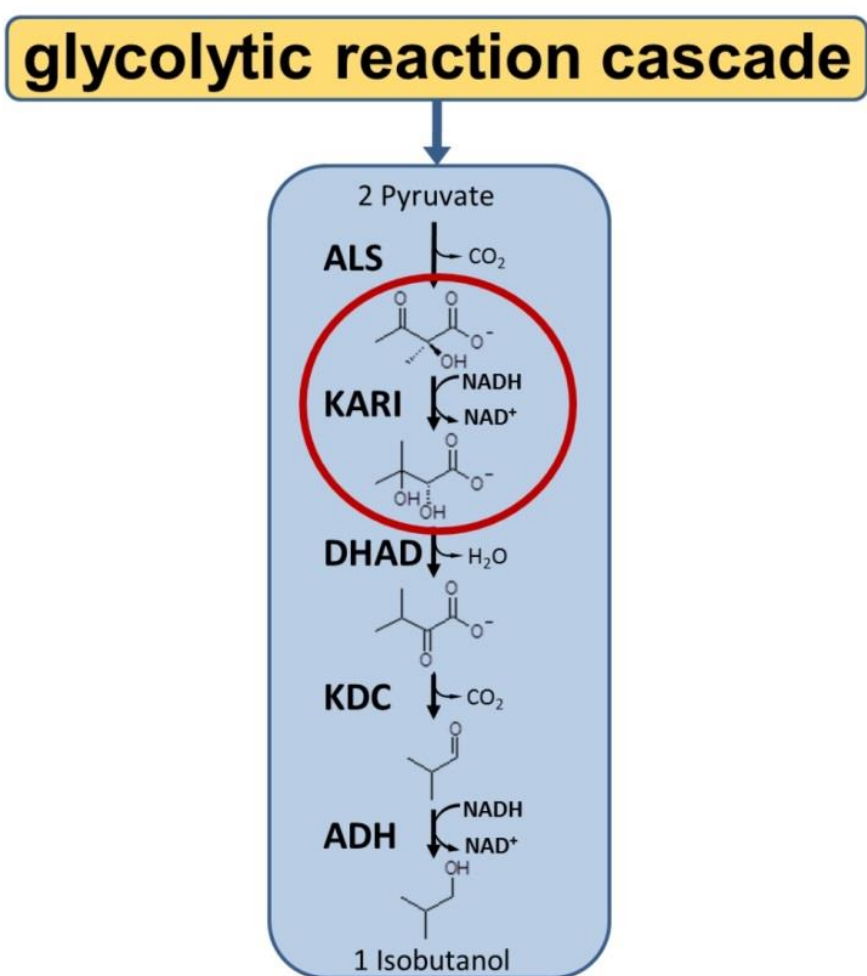

Figure 2: Raction cascade of the *in-vitro* isobutanol biosynthesis, starting from pyruvate.

Although isobutanol offers numerous advantages, the biosynthesis is hampered owing to the lack of an economic native producer. Recently, several metabolically engineered cell-based

and cell-free processes for conversion of sugars to isobutanol have been reported [11-13]. For both cases, the utilized isobutanol production route is depicted in Figure 2.

The advanced *in-vitro* concept for the isobutanol biosynthesis, established during the project phase, converts pyruvate to isobutanol applying only five enzyme activities. Initially, two pyruvate molecules are condensed by acetolactate synthase (ALS) [18] to yield acetolactate, which is further converted by ketol-acid reductoisomerase (KARI) [III] resulting in the natural Dihydroxyacid dehydratase's (DHAD) substrate dihydroxyisovalerate. DHAD then catalyzes the conversion of dihydroxyisovalerate to 2-ketoisovalerate. The enzymes 2-ketoacid decarboxylase (KDC) and an alcohol dehydrogenase (ADH) produce via isobutyraldehyde the final product, isobutanol.

Cell-based and cell-free processes rely on NADH as redox mediator to avoid an imbalanced metabolic flux or a redundant cofactor requirement. Therefore, utilizing NADH as sole electron shuttle would be advantageous [19]. Unfortunately, reported KARI enzymes prefer NADPH as redox equivalent [20-22].

While previous studies deal with engineered *E. coli* KARI enzymes [19, 21], in this work additional criteria like enhanced thermal and solvent stability guided the selection of putative activities as well. With respect to the process specifications, a new KARI enzyme activity should provide excellent catalytic performance as well as process stability at high temperature and high solvent concentrations (see articles I and III).

1.2.1 Ketol-acid reductoisomerase

Ketol-acid reductoisomerase (KARI, EC 1.1.1.86) catalyzes the unusual two-step conversion of 2-acetolactate to 2,3-dihydroxyisovalerate via an initiating alkyl migration and a following NAD(P)H dependent reduction (Figure 3) [20].

The Mg^{2+} dependent KARI activity is present in plants, fungi and microorganisms [20]. Comparison of KARI amino acid sequences among these different phylogenetic groups reveals that there are two KARI enzyme types, which differ in their secondary structure. KARI

enzymes found in fungi and most bacteria display a short form and are therefore defined as class I, whereas the long form, typically found in plants, is defined as class II [23].
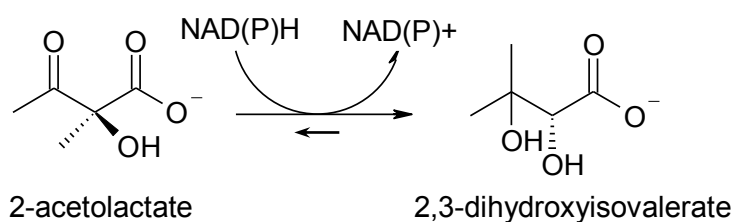

Figure 3: Reaction of ketol-acid reductoisomerase.

The overall tertiary structure of the KARI enzyme family encompasses a mixed α/β N-terminal domain and a C-terminal domain predominately composed of α-helical motifs. The long form differs from the shorter class I KARI enzyme by an evolutionarily evolved duplication of the C-terminal α-helical domain [24].

Some bacteria like *E. coli* possess also a long form comparable in length to the class II. However, the additional residues are not similar to the plant KARI inserts. Conversely, the origin of the *E. coli* KARI is comparable to plant KARI enzymes like spinach [23]. Therefore, *E. coli* KARI and related enzymes are classified as bacterial class II.

Apart from these differences, the KARI enzyme family share many common features. In particular, five regions belonging to the active site are highly conserved among all phylogenetic groups [20]. This work mainly dealt with one of them, the NAD(P)H cofactor binding site. As mentioned earlier, the new developed cell-free isobutanol production system is NADH dependent (see 1.2), while reported native KARI enzymes prefer NADPH as cofactor.

The canonical dinucleotide (cofactor) binding fold (Rossmann-fold) can be found in the N-terminal domain and can be identified by the highly conserved GxGxxG motif. The Rossmann-fold is in general characteristic for NAD(P)H depending oxidoreductases [25].

The binding site for the 2`-phosphate moiety of NAD(P)H can be identified in the loop region 18 amino acids downstream of the GXGXXG motif. This loop connects the second β-strand and the second α-helix of the characteristic βαβαβ motif of the Rossmann-fold (Figure 4).
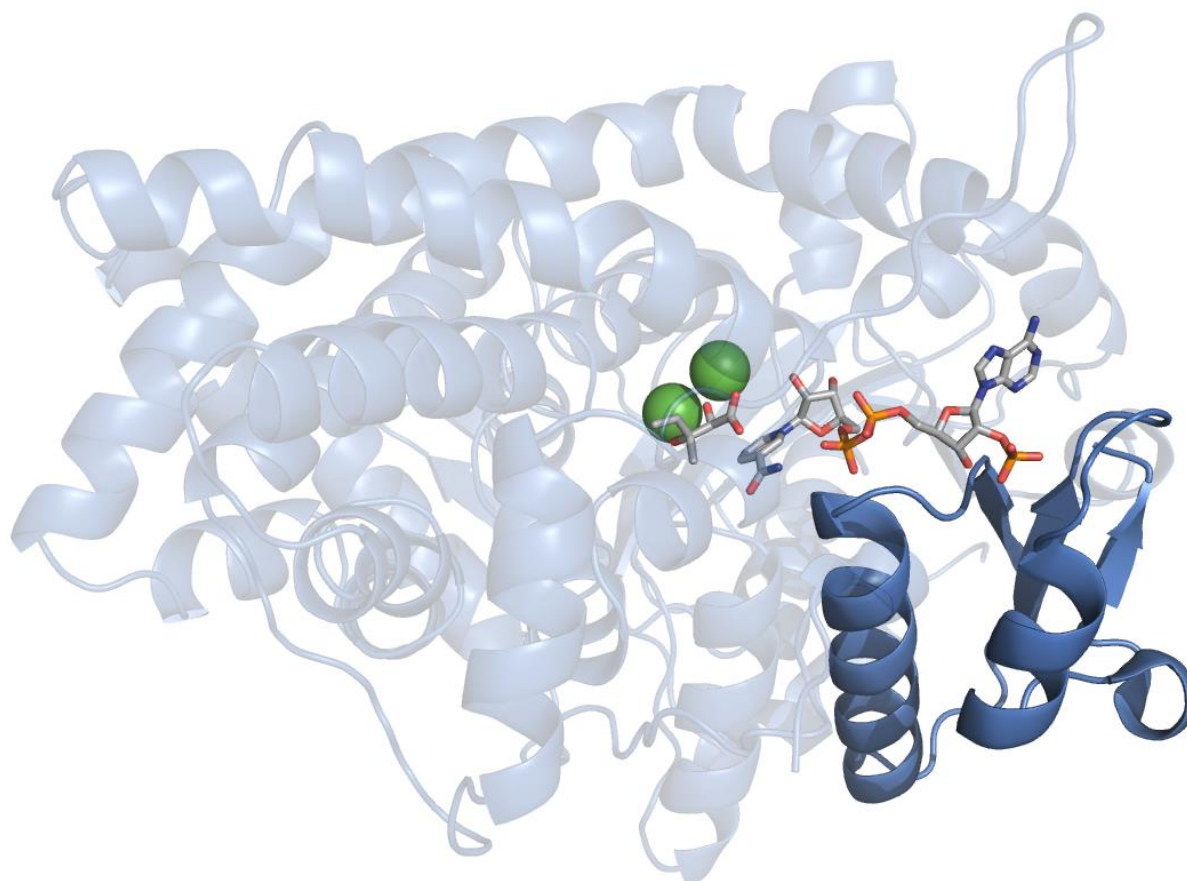
Figure 4: Crystal structure of spinach KARI. The ligands were adopted from PDB 1YVE: Mg^{2+} (green spheres), $NADP^{+}$ (gray sticks) and PDB 1QMG: 2,3-dihydroxy-3-methylvalerate (gray sticks). The Rossmann-fold is highlighted in blue.

The loop region itself varies in length and amino acid sequence and can be thus separated in three groups, depending on the loop length: six, seven and twelve residues [26]. Based on this analysis several KARI activities could already be shifted to prefer NADH [26].

To accomplish a molecular efficient cell-free isobutanol production a novel NADH dependent thermo- and solvent stable KARI was required. The corresponding KARI activity was isolated from the gram-negative bacterium *Meiothermus ruber* DSM 1279. The enzyme was heterologously expressed, characterized and subsequently catalytically optimized (see article III).

1.3 Development of a cell-free *n*-butanol biosynthesis

N-Butanol is a primary alcohol with a 4-carbon structure. It is a flammable, colourless liquid with a restricted solubility in water (8 % at 20 °C) [27]. *N*-Butanol is an important renewable building block for the chemical, textile, polymer and biofuel industry due to its increased energy density. Current biotechnological *n*-butanol production is based on an anaerobic fermentation process applying different solventogenic Clostridia species, such as *C. acetobutylicum* [15, 28-30]. However, by-products such as butyrate, acetone and ethanol accompanied with low tolerance to temperature and butanol concentration lead to a low product yield and impede industrial process realization.
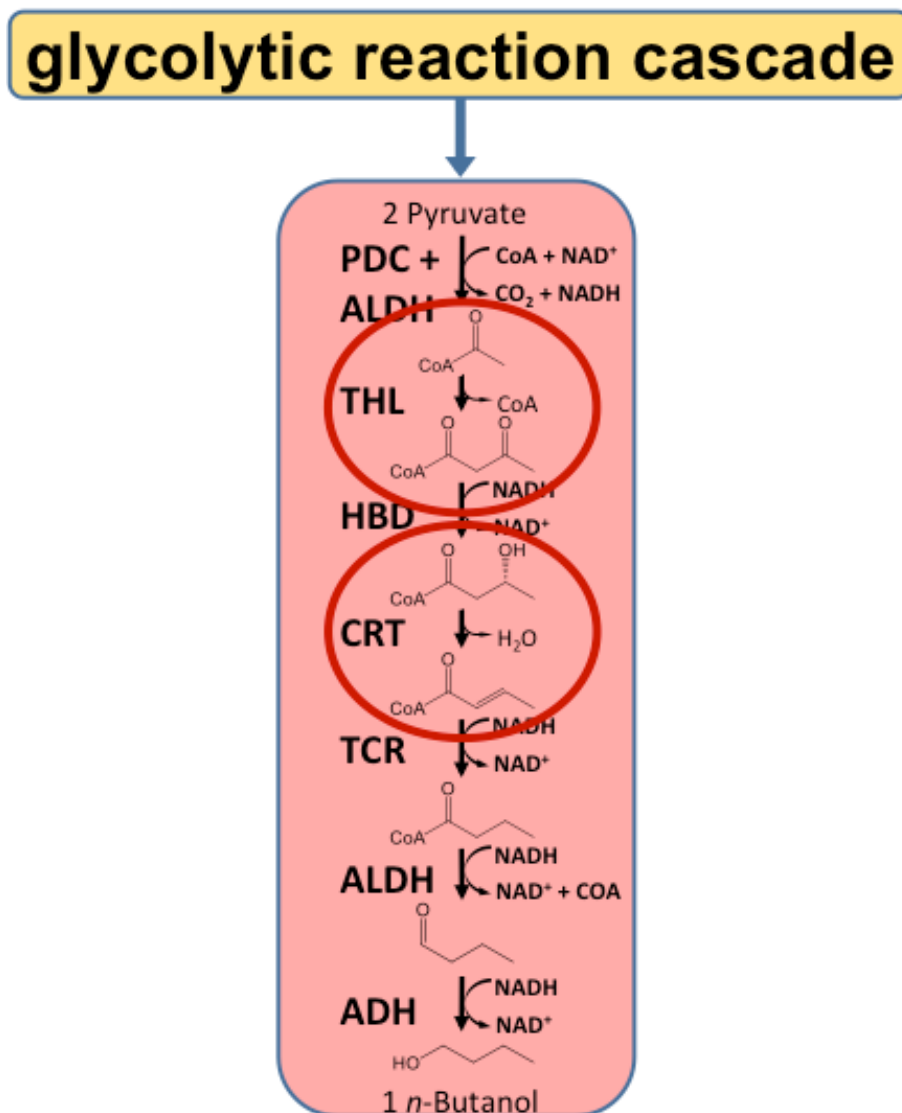

Figure 5: Raction cascade of the *in-vitro n*-butanol biosynthesis, starting from pyruvate.

Alternatively, *in-vitro* biobutanol production systems utilizing tailor made enzyme cascades (Figure 5) offer an alternative and were examined during this study.

This pathway is largly in compliance with the native pathway found in *C. acetobuytylicum*, with the exception of the combined reaction steps encompassing Pyruvate decarboxylase (PDC) and aldehyde dehydrogenase (ALDH). This solution allows to circumvent the provision of the pyruvate dehydrogenase complex, which represents the largest known multienzyme complex [31].

The PDC / ALDH step delivers acetyl-CoA for the thiolase (THL) reaction, which condensates two molecules acetyl-CoA to one molecule acetoacetyl-CoA. Afterwards, acetoacetyl-CoA is reduced to β-hydroxybutyryl-CoA by a dehydrogenase with the same name (β-hydroxybutyryl-CoA dehydrogenase / Hbd) [32]. Then, crotonase (CRT) dehydrates β-hydroxybutyryl-CoA to crotonyl-CoA, which is subsequently reduced to *n*-butanol via trans-2-enoyl-CoA reductase (TCR), ALDH and finally an ADH.

This work was focused on the biophysical and biochemical characterization of the enzymes thiolase and crotonase. In the second stage, the whole *n*-butanol production route should be established as an *in-vitro* system (see II and IV).

1.3.1 Thiolase

Thiolases are omnipresent enzymes that can be found in prokaryotic as well as eukaryotic organisms. This enzyme family can be further subdivided into catabolic (EC 2.3.1.16) and metabolic (EC 2.3.1.9) thiolases, respectively. Both are able to catalyze a Claisen type condensation of two acetyl-CoA molecules to generate acetoacetyl-CoA (Figure 6).
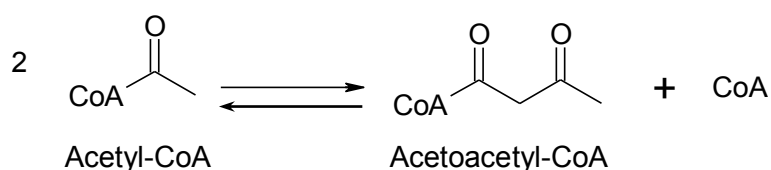

Figure 6: Reaction of thiolase.

Hence, these enzymes are key in forming extended carbon skeletons from the universal metabolic precursor acetyl-CoA. Biosynthetic thiolases (EC 2.3.1.9) are utilizing only acetyl-CoA and acetoacetyl-CoA as substrates [33]. In contrast, catabolic thiolases (EC 2.3.1.16) display a varied substrate spectrum, which includes larger substrates such as 3-ketodecanoyl-CoA [34]. The catabolic enzymes are key to the β-oxidation pathway dedicated to fatty acid degradation. Although both thiolase classes metabolize different substrates, the reaction mechanism is equivalent [33].
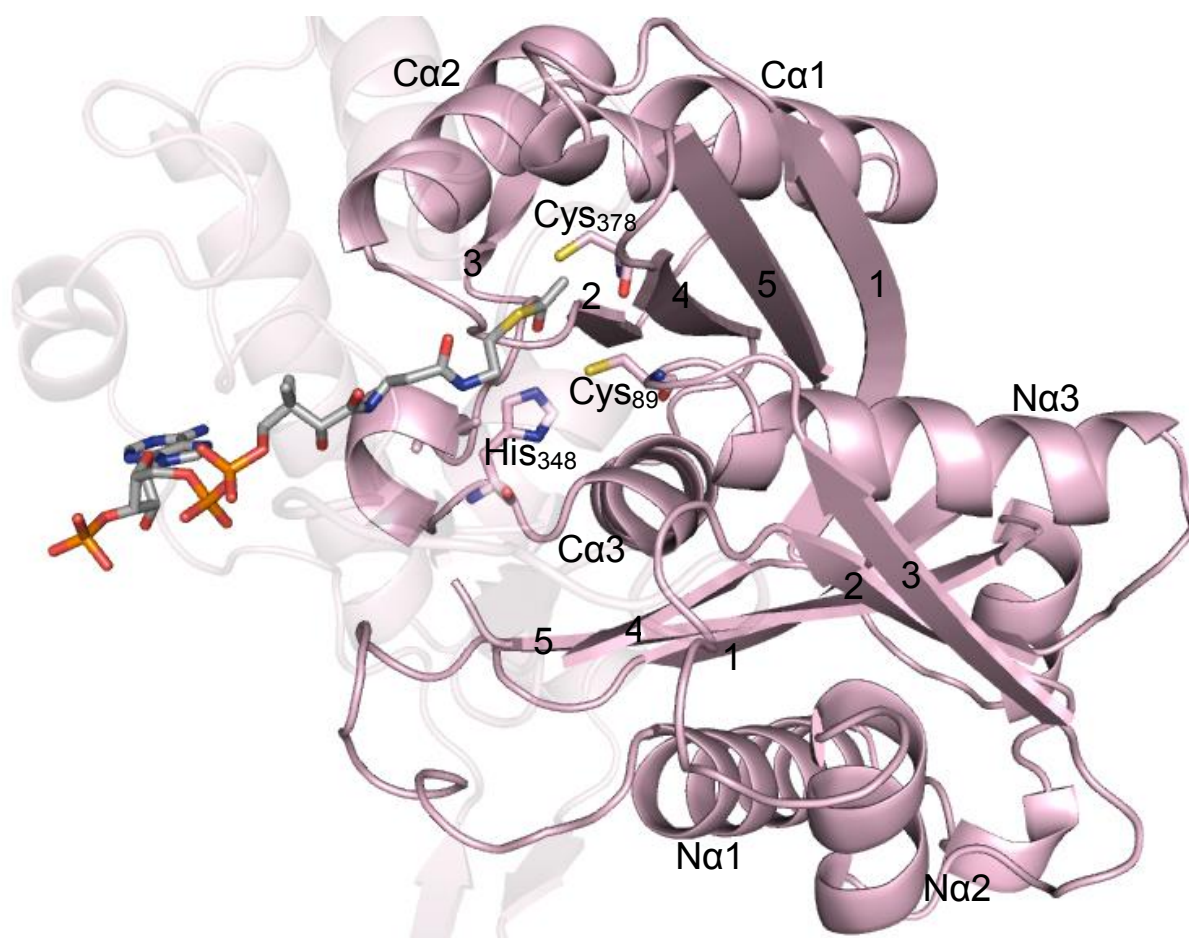
Figure 7: Crystal structure of *Zoogloea ramigera* thiolase (PDB 1DM3). The catalytic relevant residues Cys89, Cys378 and His348 are labeled. The β strands and α helices of the layered βαβαβαββ structure are numbered for each domain as they appear.

The common denominator of the whole thiolase superfamily enzyme structure is the dimer [35]. The monomer subunit itself is arranged in five layers from a C- and N-terminal half, which both display the same βαβαβαββ topology [35]. While the first two helices of both halves facing outwards, the third helix (Nα3 and Cα3) forms the central layer [35]. The C-

terminal half encompasses most of the catalytic loops including the strictly conserved residues Cys378 and His348, whereas Cys89 is part of the N-terminal section of the catalytic site (here exemplary for *Zoogloea ramigera*, PDB 1DM3). These three residues constitute the catalytic triade and are close together in space, shaping the catalytic site, but rather separated in sequence (Figure 7) [35-37].

The thiolase catalyzed Claisen condensation consists of two chemical conversions via a ping-pong mechanism [37]. In the primary step His348 activates the N-terminal Cys89. A subsequent nucleophilic attack on the substrate acetyl-CoA forms a covalent acyl-enzyme intermediate [33, 38]. An additional acetyl-CoA is then added to the initial enzyme-substrate complex. Subsequently, the second, C-terminal located Cys378 deprotonates the enzyme substrate complex intermediate by a second nucleophilic attack to yield acetoacetyl-CoA, which is ultimately released from the active site [36, 39].

In the condensation direction CoA is validated to be a potent inhibitor [40-43]. The thiolase activity is already reduced in micromolar concentrations. Additionally, NAD^+ and NADH were found to inhibit the thiolase activity as well [41]. With respect to kinetic properties and preferred reaction conditions for the *n*-butanol biosynthesis, a thiolase activity was isolated from the thermophilic bacterium *M. ruber* (see article II).

1.3.2 Crotonase

Enoyl-CoA-hydratase (EC 4.2.1.17) catalyzes the reversible addition of water to α,β-unsaturated enoyl-CoA thioesters (Figure 8).

β-Hydroxybutyryl-CoA   Crotonyl-CoA
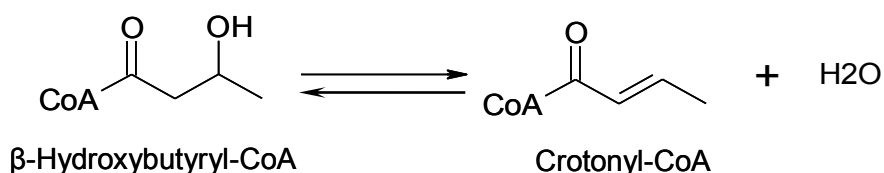
Figure 8: Reaction of crotonase.

The enzyme is commonly referred to as crotonase because of its most active substrate, crotonyl-CoA. Crotonase is part of the physiological important fatty acid β-oxidation pathway and is an essential enzyme component of the related CoA-dependent *n*-butanol biosynthesis

in microbial cells. At present, only a few crotonase type enzyme activities have been reported from pro- and eukaryotic organisms [44-49]. Moreover, only the crystal structure and catalytic mechanism of the crotonase from *Rattus norvegicus* was examined in detail (Figure 9) [50-52].
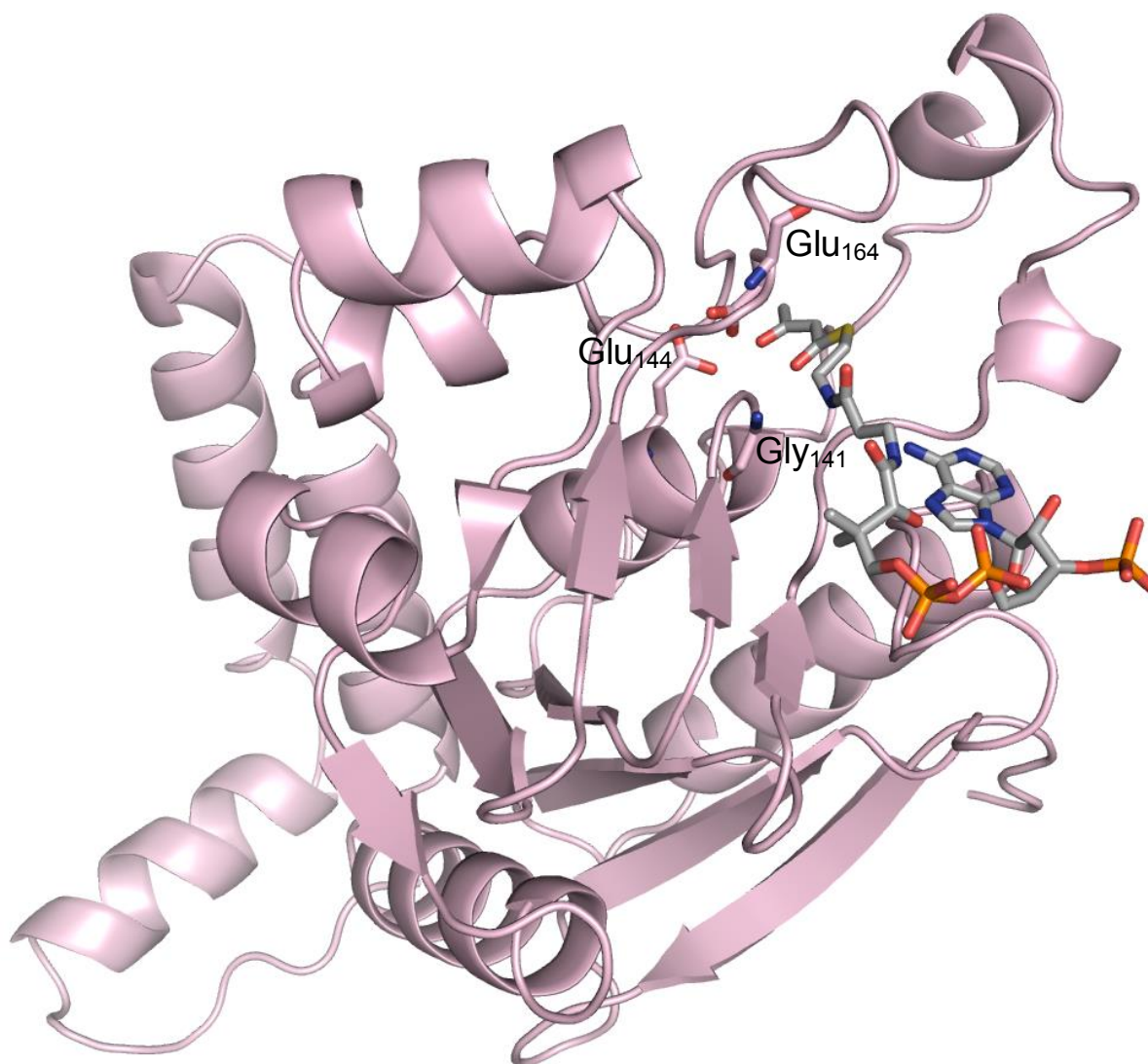
Figure 9: Crystal structure of *Rattus norvegicus* crotonase (PDB 1DUB). The catalytic triad, consisting of Gly141, Glu144 and Glu164, is labeled.

The catalytic mechanism comprises the three key residues Gly141, Glu144 and Glu164 (here for *R. norvegicus*, PDB 1DUB). In a concerted attack of the two glutamate residues the Glu164 protonates the substrate, while Glu144 abstracts a proton from a bound water molecule. The Gly141 activates the substrate by a hydrogen bond to the oxygen of the enoyl moiety of the

CoA ester [50, 53]. The binding pocket for the CoA moiety is formed by hydrophobic amino acids and lysine residues of two adjacent subunits [50].

Since isolated KARI and thiolase activities showed required parameters to achieve an enzymatic based isobutanol or *n*-butanol synthesis, the *M. ruber* strain was also evaluated for isolation of the necessary crotonase activity (see article IV).

1.3.3 Alternative condensed *n*-butanol cascade

As already mentioned, designing a cell-free enzyme cascade for *n*-butanol is complex and accompanied by several bottlenecks which had to be overcome. Described cascades require a minimum of eight enzymes, CoA and NADH as cofactors to convert pyruvate to *n*-butanol [14]. However, CoA intermediates and resulting NAD^+ inhibit the required enzymes in micro- and millimolar concentrations [32, 50]. Under practical terms managing the cofactor balance and adjusting a linear production rate is very difficult to achieve. A complete inhibition of one of the enzymes would result in the termination of the whole process. Moreover, CoA intermediates are not very stable under process conditions and therefore had to be dosed over time, which lead to high costs. Further, the enzyme cost is a major factor itself, due to complicated production routes. Hence, a solution can be the minimized *n*-butanol reaction cascade presented in the following paragraph, which focuses on decreasing the biocatalyst and cofactor quantities to the essential.

To circumvent inhibitory and additional cost effects by CoA a new reaction step is implemented. This step directly converts acetaldehyde to crotonaldehyde by an enamine-aldol-condensation. With implementation of this enamine condensation it is now possible to bypass most of the enzymatic reaction steps of the native *n*-butanol pathway (Figure 5) and provide for a direct access into an alternative *n*-butanol cascade stated by Sommer et al. [54]. That implies a completely new and condensed *n*-butanol pathway (Figure 10).
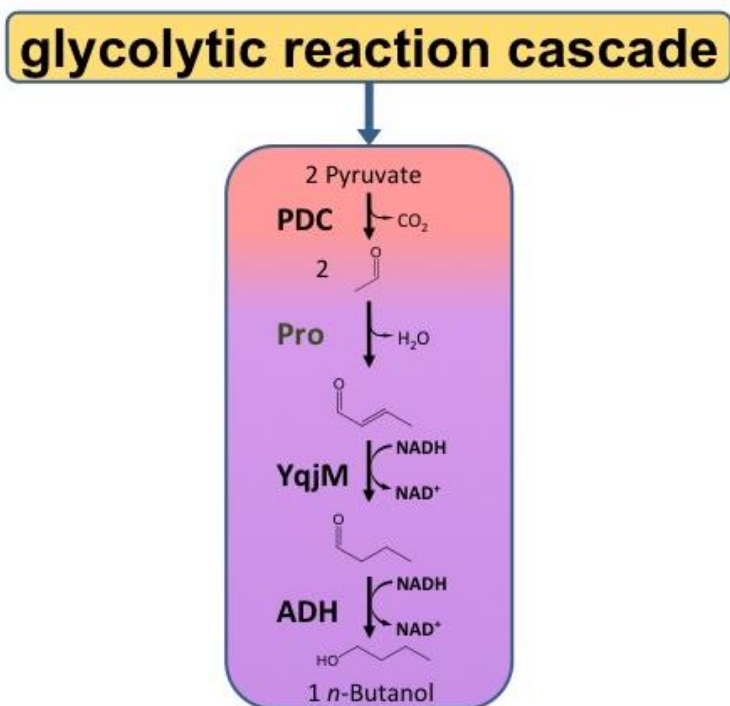
Figure 10: Schematic illustration of the *n*-butanol reaction cascade via the enamine-aldol-condensation.

The common starting point is, analogous pyruvate as the central intermediate. In a first step pyruvate is decarboxylated to acetaldehyde, which again serves as substrate for the implemented enamine-aldol-condensation. The underlying mechanism of the reaction is displayed in Figure 11 for a proline catalyst.

Proline is thereby unique due to the nucleophilic reactivity because of the pyrrolidine portion. Although the pyrrolidine forms iminium ions and enamines readily [55], even arginine or tryptophan possess secondary amines and constitute suitable catalysts. In this regard polyamines like spermidine or putrescine could also be used as catalysts [56].

In a subsequent two-step reaction the resulting crotonaldehyde is converted to butanal and finally to *n*-butanol by action of YqjM and ADH.

Consequently, the new *n*-butanol reaction cascade is consolidated to use only three enzyme activities and NADH as reducing equivalent.

Figure 11: Catalytic cycle of the enamine-aldol-condensation of acetaldehyde, here for proline as catalyst.

In combination with the already published artificial glycolytic reaction cascade [I] the whole *n*-butanol production route is thus completely redox balanced (see article V).

1.4   Original articles

1.4.1   Cell-free metabolic engineering: production of chemicals by minimized reaction cascades

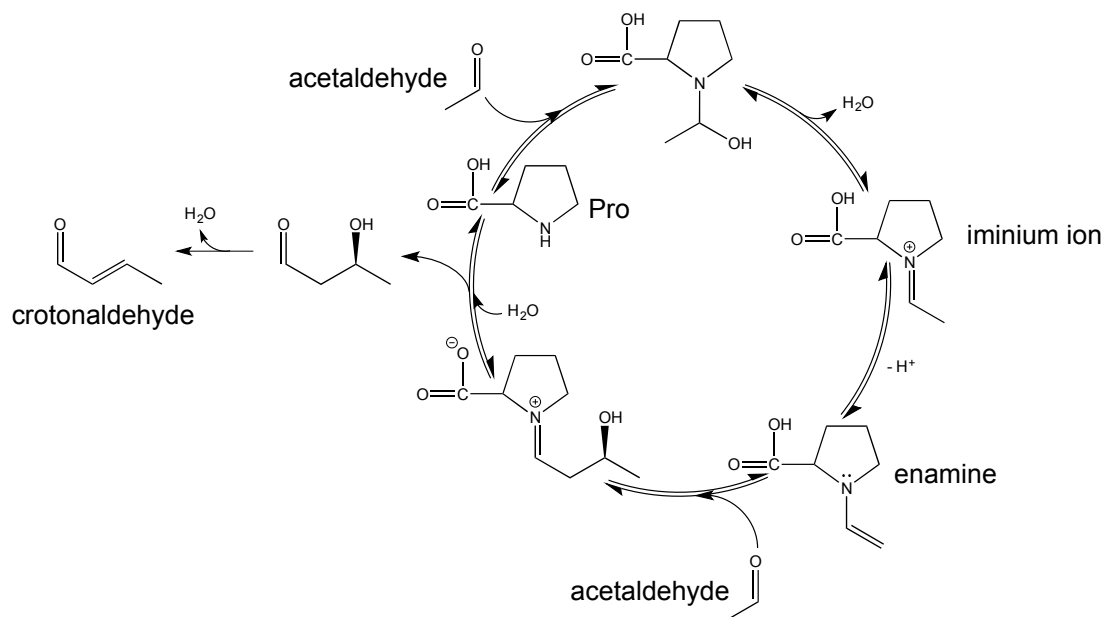J.K. Guterl, D. Garbe, J. Carsten, F. Steffler, B. Sommer, S. Reisse, A. Philipp, M. Haack, B. Ruhmann, A. Koltermann, U. Kettling, T. Bruck, V. Sieber

Bio-based higher alcohols such as isobutanol are versatile platform molecules for the synthesis of chemical produces and fuels. However, their fermentation-based processes are restricted to the physiological limits of cellular production systems. Key barriers include end-product toxicity effects, undesirable by-products and a complex process management.

This article presents an innovative cell-free approach, utilizing an artificial minimized glycolytic reaction cascade. The developed toolbox allows the cell-free production of ethanol and isobutanol from glucose via pyruvate as central intermediate and can be extended to an array of industrially relevant molecules. The whole cell-free system is additionally consolidated to use only NAD^+ as the universal cofactor.

Although the enzyme-catalyzed reaction was not completed over the course of the experiment, the cumulative mass of all detectable intermediates and products gave a yield in excess of 80 %. The reactions were carried out at 50 °C and neutral process conditions. To demonstrate the feasibility of the *in-vitro* production system, the ethanol production route was additionally conducted in presence of varying isobutanol concentrations. We could demonstrate that the cell-free ethanol productivity and reaction kinetics were not significantly affected by isobutanol concentrations up to 4 % (v/v).

S. R. was coauthor of this article and was involved in enzyme production and characterization, in analytics development and in conducting experiments that resulted in data reported herein. In particular, S. R. implemented the KARI enzyme activity, adopted the required glucose assay for the experimental procedure and analyzed the corresponding results.

1.4.2 *Meiothermus ruber* thiolase - a new process stable enzyme for improved butanol synthesis

Steven Reiße, Daniel Garbe, Thomas Brück

Thiolase (EC 2.3.1.9 / EC 2.3.1.16) is a key enzyme in the biosynthetic conversion of glucose to *n*-butanol, where it is responsible for the formation of carbon-carbon bonds by catalyzing a thioester dependent Claisen-condensation. Specifically, thiolase condenses two acetyl-CoA molecules to build up acetoacetyl-CoA, the first committed step in *n*-butanol biosynthesis. The well characterized clostridial thiolase show high sensitivity to oxygen and are neither solvent nor thermostable, which limits *n*-butanol yields.

This article describes the isolation, heterologous expression and biochemical characterization of a new thermo- (IT_{50} (50 °C) = 199 ± 0.1 h) and solvent stable (IS_{50} > 4 %) thiolase derived from the thermophilic bacterium *M. ruber*. The structural and kinetic properties of the enzyme indicated that it belongs to the catabolic thiolases family. The observed catalytic constants were K_m = 0.07 ± 0.01 mM and k_{cat} = 0.80 ± 0.01 s^{-1}. In analogy to other thiolases, the enzyme was inhibited by NAD$^+$ (K_i = 38.7 ± 5.8 mM) and CoA (K_i = 105.1 ± 6.6 µM) but not via NADH. The enzyme was stable under harsh process conditions (T = 50 °C, *n*-butanol = 4 % (v/v)) for prolonged time periods (τ = 7 h).

The lower sensitivity of Mr-thiolase towards CoA compared to other reported thiolases and the superior stability under industrially relevant process conditions allow the application of Mr-thiolase as catalyst to improve the metabolic flux in order to achieve higher *n*-butanol titer in cell-free as well as cell-based approaches.

The first author S. R. selected the bacterial strain, conducted all experiments and drafted the manuscript. The co-author D. G. and the corresponding author T. B. supervised this study and finalized the manuscript. Patrick Schrepfer modeled the Mr-thiolase structure based on the *Z. ramigera* scaffold.

1.4.3 Identification and optimization of a novel thermo- and solvent stable ketol-acid reductoisomerase for cell-free isobutanol biosynthesis

Steven Reiße, Daniel Garbe, Thomas Brück

Ketol-acid reductoisomerase (EC 1.1.1.86) catalyzes the two-step conversion of 2-acetolactate into 2,3-dihydroxyisovalerate. The Mg^{2+} dependent KARI activity is part of the branched-chain amino acid biosynthesis of valine, leucine and isoleucine.

The metabolic conversion of this pathway at the 2-keto acid intermediate via integration of the last two reactions of the Ehrlich pathway allows the production of higher alcohols, such as isobutanol. To enhance cellular or cell-free isobutanol production systems NADH dependent enzyme systems are favored.

This article deals with a new thermo- and solvent stable KARI activity derived from the bacterial strain *M. ruber* DSM 1279. Furthermore, a novel screening procedure for accelerated molecular optimization of KARI enzymes is presented.

The native Mr-KARI (39 kDa) exhibited an extended half-life (IT_{50} (50 °C) = 71 ± 0.2 h) and retained activity at high levels of organic solvents (IS_{50} ≥ 6 % (v/v)). To simplify cofactor requirements, the cell-free isobutanol biosynthesis was focused on NADH as cofactor. In this regard, the observed catalytic constants for NADH were K_m = 0.24 ± 0.02 mM and k_{cat} = 1.09 ± 0.03 s^{-1} and for 2-acetolactate K_m = 0.55 ± 0.06 mM and k_{cat} = 0.50 ± 0.01 s^{-1}, whereby the specific activity was 0.7 U mg^{-1}.

The new screening procedure, developed in this study, based on an *E. coli* KARI knockout strain as the central *in-vivo* selection vehicle and generated optimized KARI mutants. Via this method a *T84S* variant was identified, which showed a 350 % increase in the NADH dependent catalytic activity.

The first author S. R. selected the bacterial strain, performed all experiments, developed the screening procedure and drafted the manuscript. The co-author D. G. and the corresponding author T. B. supervised this study and finalized the manuscript.

1.4.4 Identification and characterization of a highly thermo stable crotonase from *Meiothermus ruber*

Steven Reiße, Daniel Garbe, Thomas Brück

In this article, a new crotonase (Crt, EC 4.2.1.17) activity derived from *M. ruber*, which catalyzes the reversible hydration of crotonyl-CoA, is presented. The new Mr-Crt was cloned, heterologously expressed in *E. coli* and finally characterized with respect to industrial applications, such as *n*-butanol synthesis.

As part of the *n*-butanol biosynthesis pathway, crotonase is responsible for the reversible hydration of crotonyl-CoA. Homology studies of the predicted Mr-Crt amino acid sequence indicated a relationship to previously reported enzyme activities among the crotonase family. In comparison to the amino acid sequences of *C. acetobutylicum* (46 %) and *R. norvegicus* (36 %) the gene of *M. ruber* crotonase encodes the similar highly conserved active site regions.

The enzyme exhibits an optimal pH at 7.0 and highest activity at 55 °C, whereby an activity of 80 % is retained in a broad temperature range from 50 °C – 70 °C. Furthermore, at relevant process conditions Mr-Crt displayed an extended half-life of over one month (IT$_{50}$ (50 °C) = 743 ± 0.7 h) and represents therefore a unique member within the crotonase enzyme family. The observed catalytic constants were K_m = 0.03 ± 0.01 mM and k_{cat} = 14.9 ± 0.9 s^{-1}, whereby the specific activity was 20.9 ± 0.3 U mg^{-1}.

The first author S. R. selected the bacterial strain, conducted all experiments and drafted the manuscript. The co-author D. G. and the corresponding author T. B. conceived this study and finalized the manuscript.

1.4.5   Minimized butanol biosynthesis via an enamine – aldol – condensation reaction

Steven Reiße, Daniel Garbe, Thomas Brück

Due to the comparable chemical properties, *n*-butanol represents an excellent substitute for gasoline. However, the current cellular fermentative process is limited by end product toxicity. Neither examination of different solventogenic *Clostridia* species nor the integration of the clostridial *n*-butanol pathway into other species could improve this process.

A new approach to overcome the limitations is to leave out the cell and realize an *in-vitro* *n*-butanol process. Here we present a tailor made enzyme *n*-butnaol cascade, which combines enzymatic activities with an organocatalytic reaction step. The implemented enamine – aldol – condensation converts acetaldehyde to crotonaldehyde, which is directly reduced to *n*-butanol by action of a 2-enoate reductase and finally an alcohol dehydrogenase. This way the whole pathway is condensed to a minimum of required enzyme reactions and cofactor quantities and can be excellently integrated into our developed toolbox.

In a proof-of-concept experiment *n*-butanol was synthesized at 50 °C and neutral pH conditions. Due to the smart concept, all intermediates and the product could be simply determined by GC analysis. We could successfully produce 7,4 mg L^{-1} *n*-butanol and demonstrated the possibilities of modern enzymatic technologies.

In combination with our previously developed minimized glycolysis reaction cascade the presented new *n*-butanol *in-vitro* concept requires only six enzymes in total and NADH as sole electron shuttle.

The first author S. R. conceived the condensed *n*-butanol cascade, conducted all experiments and drafted the manuscript. The co-author D. G. and the corresponding author T. B. supervised this study and finalized the manuscript. Bettina Sommer characterized and provided the 2-enoate reductase. Martina Haack assisted during the GC analysis.

2 Methods

2.1 Sequence alignment and structural modeling

As mentioned earlier, previously reported enzyme activities for KARI, thiolase and crotonase did not fulfill required process parameters. In particular, thermo- and solvent stability were driving forces to find new enzymes for both, isobutanol and *n*-butanol biosynthesis.

Therefore, the bacterial strain *M. ruber* DSM 1279 was selected to isolate and to characterize appropriate enzyme activities due to its mildly thermophilic and aerobic growth conditions.

Initially amino acid sequences of representative prokaryotic as well as eukaryotic enzymes were aligned and searched against the reported *M. ruber* genome. For the alignment, we used only the sequences from already reported enzyme activities. Sources of sequence information are listed in Table 2. Clustal W [57] was used to conduct the sequence alignment and ESPript [58] for further editing.

Table 2: Sequence sources. [a]

Target enzyme	Gene	Protein accession number
KARI	Mrub_1907	YP_003507684.1
Thiolase	Mrub_1917	YP_003507694.1
Crotonase	Mrub_2284	YP_003508056.1

[a] www.ncbi.nlm.nih.gov

Additionally, structure models for Mr-KARI, Mr-thiolase and Mr-Crt were prepared. The Mr-KARI and Mr-Crt models were calculated by the Phyre[2] server [59] and aligned with already characterized structures. Mr-KARI was aligned to the reported spinach scaffold (PDB: 1YVE and 1QMG) and Mr-Crt to *R. norvegicus* (PDB: 1DUB). The putative Mr-thiolase sequence was used as template for a structural prediction via the HHpred server [60], which employs profile

Hidden Markov Models. To carry out a tertiary structure alignment the MUSTANG algorithm [61] of the YASARA bioinformatics toolbox was used, in line with manufacturers' guidelines.

2.2   DNA isolation and cloning

2.2.1   Isolation of genomic- and plasmid DNA

The isolation of genomic DNA from *M. ruber* was carried out according to a modified protocol of Saha [62]. The strain was grown aerobically at 50 °C for 24 h in *Thermus ruber* medium containing trypton (5 g L^{-1}), yeast extract (1 g L^{-1}) and soluble starch (1 g L^{-1}), adjusted to pH 8. A volume of 2 - 4 mL was taken from the culture and centrifuged (4500 x g, 10 min, 4 °C). The supernatant was discarded and the pellet was washed twice with dd H_2O. Afterwards, the resulting pellet was re-suspended in TE buffer (50 mM Tris pH 8, 10 mM EDTA), supplemented with 50 µL lysozyme (25 mg mL^{-1}) and incubated at 37 °C for 60 min. Immediately after lysozyme treatment,, the mixture was supplemented with 50 µL of 10 % (w/v) SDS, gently mixed and further incubated for additional 10 min at room temperature (RT). Thereafter, 3 µL of a proteinase-K solution (20 mg mL^{-1}) were added, followed by an additional incubation step of 60 min at 60 °C. The mixture was neutralized with ice cold 300 µL Na-acetate (3 M, pH 4.8) and gently mixed by inverting. The cell lysate was then centrifuged (10,000 × g, 10 min, 4 °C) and the clear supernatant was transferred to a sterile microcentrifuge tube. Contained DNA was extracted in two steps with 300 µL phenol-chloroform-isoamyl alcohol (25:24:1) (Roth) and finally 300 µL of pure chloroform (Sigma). The clear supernatants along with the middle white layer were every time carefully pooled in another microcentrifuge tube. After that, the DNA was precipitated with 1 mL of chilled ethanol (-20 °C). After gently mixing by inversion and incubation (60 min, -20 °C), the precipitated DNA was centrifuged (15 min, 15,000 x g) and subsequently washed in 70 % ethanol at 4 °C overnight. Washed pellets were air dried (30 min) and re-suspended in 50 µL of dd H_2O.

Plasmid DNA from *E. coli* was purified applying the GeneJET Plasmid Miniprep Kit (Thermo Scientific, Braunschweig), according to the manufacturer's manual.

2.2.2 Amplification of the target genes

The isolated DNA from *M. ruber* was used as template for the polymerase chain reaction (PCR) to amplify the respective gene. The reaction was performed in a volume of 50 µL with the following composition: 1 – 10 ng genomic DNA, 10 pmol phosphorylated primers (Eurofins MWG Operon) (Table 3), 0.2 mM of each deoxynucleotide triphosphate (dNTPs), 0.02 U µL^{-1} Phusion™ DNA polymerase (Thermo Scientific, Braunschweig), reaction buffer and dd H$_2$O ad 50 µL. The temperature program was based on the applied oligonucleotides and the manufacturer's specifications for the polymerase.

Table 3: Oligonucleotides.

Primer	Sequence (5' -> 3')	Restriction site	Annealing temperature	Melting temperature
Mr-KARI fwd	CAGCAA<u>CGTCTC</u>GCATATGAAGA TTTACTACGACCAGGACGCAG	BsmBI	68 °C	74 °C
Mr-KARI rev	GCTACCGACCTCTTCCTTCGTGA AC	/	68 °C	68 °C
Mr-Thl fwd	CAGCAA<u>CGTCTC</u>ACATATGCGTG AGGTGTGGGTGGTTTC	BsmBI	65 °C	74 °C
Mr-Thl rev	CAGCAA<u>GTCGAC</u>GCCCACAGCC TCCAC	SalI	65 °C	74 °C
Mr-Crt fwd	CAGCAA<u>GGTCTC</u>GCATATGGCAC AGACCTTTGAACTC	BsaI	62 °C	72 °C
Mr-Crt rev	CAGCAA<u>GTCGAC</u>CTCCCCTTTAA ACTGCGCC	SalI	63 °C	73 °C

PCR products and enzymatically manipulated DNA were analyzed by 1 % (v/v) agarose gel electrophoresis and purified via the innuPREP DOUBLEpure Kit (Analytik Jena, Jena).

2.2.3 Determination of the DNA concentration

DNA concentration was determined by the absorbance at 260 nm in a UV / Vis spectrophotometer in a quartz cuvette. An absorbance of A_{260} = 1 corresponds to a concentration of double-stranded DNA of 50 mg L^{-1}. To assess the purity of the DNA the absorbance ratio A_{260}/A_{280} was used, whereby a value between 1.8 and 2.0 indicated a high purity [63].

2.2.4 Cloning

The plasmid pET28a (Novagen) was used as basis for a new constructed cloning vector, pCBR. The whole procedure is explained in detail by Guterl et al. [I]. The resulting pCBR vector backbone including C-terminal His-Tag and the DNA fragments gained from PCR were each digested with the restriction enzymes listed in table 3. Subsequently, the DNA fragments were ligated into the pCBR vector.

The obtained plasmids (pCBR-KARI-CHis, pCBR-Thl-CHis, pCBR-Crt-CHis) were transformed in *E. coli* as described elsewhere [63]. DNA sequencing validated all cloning procedures.

2.3 Heterologous Protein expression

For protein expression, plasmids were transformed into *E. coli* Rosetta cells ((F- ompT hsdSB(rB- mB-) gal dcm (DE3) pLysSRARE (CamR)) (Merck, Darmstadt). The pCBR-KARI-CHis plasmid was additionally transformed into the KARI knockout strain *E. coli* JW3747 (F-, Δ(araD-araB)567, ΔlacZ4787(::rrnB-3), λ-, rph-1, ΔilvC725::kan, Δ(rhaD-rhaB)568, hsdR514), obtained from the Keio collection [64].

Rosetta cells were cultivated in TB-medium supplemented with kanamycin (30 μg mL^{-1}) and chloramphenicol (34 μg mL^{-1}). A preculture was inoculated with a single colony from an agar plate and incubated at 37 °C in a shaking incubator overnight. For expression, shake flasks were filled up to 20 % of the nominal volume with TB medium and the appropriate antibiotics, inoculated with preculture ad OD_{600} = 0.1 and incubated at 37 °C until an OD_{600} of

0.5 – 0.8 was reached. Then, the cells were induced with 1 mM IPTG. Mr-thiolase and Mr-Crt were subsequently incubated at 37 °C for 4 h. Mr-KARI was additionally incubated at 20 °C for 20 h. Afterwards, the cells were harvested and stored at -20 °C until further use.

The basal expression of Mr-KARI in the knockout strain *E. coli* JW3747 was conducted in M9 minimal medium supplemented with 0.4 % (w/v) glucose and kanamycin (30 µg ml^{-1}) as indicated [63]. The culture was inoculated with a single colony of transformed cells and cultivated at 37 °C overnight. Cells were subsequently harvested and frozen at -20 °C.

2.4 Enzyme purification

For cell disruption, cell pellets were re-suspended in binding buffer (50 mM HEPES pH 8, 20 mM imidazole, 10 % (v/v) glycerol, 0.1 % (v/v) Tween 20), supplemented with DNAse (10 mg mL^{-1}). The cells were lysed with an Avestin EmulsiFlex-B15 homogenizer (Mannheim, Germany). Cell debris was removed by centrifugation at 20,000 x g and 4 °C for 30 min.

HisTrap™ columns (GE Healthcare), packed with nickel ions (Ni^{2+}) immobilized by highly cross-linked agarose were used for enzyme purification. After equilibration with 5 column volumes of binding buffer, the supernatant was loaded onto the column and washed with 5 column volumes of binding buffer. The profile of the protein concentration was monitored by the UV signal at 280 nm. Undesirably bound bacterial proteins were removed by washing with binding buffer until the UV signal reached the baseline. Then, His-tagged enzymes were eluted in one step with two column volumes of elution buffer (50 mM HEPES pH 8, 500 mM imidazole,
10 % (v/v) glycerol, 0.1 % (v/v) Tween 20). Collected fractions were identified by the UV signal and analyzed by 12 % SDS-PAGE.

The purified enzyme was subsequently desalted via HiPrep 26/10 Desalting-column (GE Healthcare) in either 20 mM ammonium carbonate for lyophilization purposes or in 50 mM HEPES pH 7.5 plus 10 % (v/v) glycerol for storage at -80 °C.

Protein contents were quantified photometrically by measuring the absorbance at 215 and 225 nm [65-67]. The method based on the strong absorbance of peptide bonds in this wavelength range provides considerable advantages. First, the measurements are unaffected

by variation of protein composition and structure. Specific extinction coefficients are thus unnecessary. Secondly, a calibration with a protein reference standard is not required. In this context, the protein concentration was calculated according to the following formula 2.4.1:

$$c_E = 144 \cdot (A_{215} - A_{225}) \cdot f \qquad\qquad 2.4.1$$

c_E enzyme concentration, µg ml^{-1}

A_x absorbance at specific wavelength x

f dilution factor

2.5 Analytical methods

2.5.1 Photometrical measurements

Photometrical measurements were carried out in flat-bottom microtiter plates using an Enspire 2 plate reader (Perkin Elmer, Rodgau). Specific activities were determined from the photometric data based on Beer's law (equation 2.5.1)

$$E = \varepsilon \cdot c \cdot l \qquad\qquad 2.5.1$$

E extinction

ε molar extinction coefficient, L mmol^{-1} cm^{-1}

c molar concentration, mmol L^{-1}

l path length, cm

2.5.2 Gas chromatography

Aldehydes and alcohols were separated and quantified by gas chromatography (GC) using a Trace GC Ultra (Thermo Scientific, Braunschweig), equipped with a Headspace Tri Plus autosampler, an agitator and a flame ionization detector (FID). All compounds were separated via a Stabilwax column (length 30 m, 0.25 mm internal diameter, 0.25 µm film

thickness; Restek, Bad Homburg), with helium (1.2 mL min^{-1}) as carrier gas. The oven temperature was programmed to be held at 50 °C for 2 min, raised with a ramp of 10 °C min^{-1} to 200 °C and held for 1 min. Injector and detector were kept at 200 °C. Samples were incubated prior to injection at 40 °C for 15 min. For the analysis 700 µL of the headspace were injected (headspace syringe 100 °C) in the split mode with a flow of 10 mL min^{-1}. For quantification of crotonaldehyde, butanal and *n*-butanol concentrations, the FID response in each sample was related to control measurements of a known concentration (20 mM).

2.5.3 High performance liquid chromatography

CoA-esters were analyzed via high performance liquid chromatography (HPLC; Agilent 1100 Series; Agilent, Waldbronn). The system was equipped with an autosampler, a column oven and a diode-array detector (DAD). Separation of the CoA-esters was achieved on a Luna 3 µm C18(2) 100Å column (Phenomenex, Aschaffenburg) at 25 °C. The two step elution started with a mixture of buffer A (10 mM potassium phosphate buffer, pH 6.5) and 30 % buffer B (10 mM potassium phosphate buffer, pH 6.5 and methanol, ratio 60 / 40), followed by a gradient up to 80 % buffer B within 10 min. The level of 80 % buffer B was finally kept for 5 min, whereby the overall mobile phase flow was adjusted to 0.4 mL min^{-1}. The system was calibrated using external standards of each CoA-ester. All samples were pretreated by filtration (10 kDa MWCO, modified PES; VWR, Darmstadt) prior to injection. The injection volume was 10 µL in each case.

2.5.4 Nuclear magnetic resonance

Nuclear magnetic resonance (NMR) spectroscopy was used to determine the 2-acetolactate concentration. Before every experiment, 2-acetolactate was freshly synthesized with a purified acetolactate synthase (ALS) from *Bacillus subtillis*, existing in our lab. The reaction mixture contained 50 mM HEPES pH 7, 0.1 mM thiamine pyrophosphate, 2.5 µM FAD, 50 mM sodium pyruvate. After addition of ALS the reaction was incubated at 40 °C for 40 min. The 2-acetolactate concentration was determined via NMR: 500 MHz, D_2O, δ = 1.46 (s, 3H,

COHC$H3$); δ = 2.26 (s, 3H, COC$H3$). The measurements were adjusted to δ = 0 with the internal standard Sodium 3-(trimethylsilyl)propanoate (TSP). Additionally, the integrals of the signals were derived from the one of (s, 9H) of TSP.

2.6 Enzymatic characterization

Since the reaction conditions for the cell-free production system were previously specified, all enzymes were characterized according to a definite screening panel to find the optimal reaction conditions. This panel included the examination of the optimal reaction temperature, the thermal stability, the optimal pH setting and the resistance towards the desired alcohol products. Finally, the kinetic properties were examined at the agreed process conditions.

To reduce microbial contamination in the reaction vessel and enhance space-time yield the production would be preferably carried out at elevated temperatures, primarily 50 °C. Furthermore, the consolidated cell-free reaction cascade was set to operate at neutral pH. This setting represented a feasible compromise that maintains activity for all required enzyme components albeit not operating at their individual pH optimum.

With respect to optimal reaction conditions, the enzymes were initially examined for their temperature and pH optimum. Since thermo-tolerance is a key process parameter to establish the *in-vivo* system, the residence time of the enzymes were additionally tested by incubating the purified enzymes at 50 °C, followed by determination of the residual activity. The half-life of the enzyme could be determined via the reaction constant. The corresponding calculation was derived by the first-order reaction equation (2.6.1).

$$-\frac{dc}{dt} = k \cdot c \qquad\qquad 2.6.1$$

c concentration of the reactant, mol L^{-1}

t time, h

k reaction rate constant, s^{-1}

Equation 2.6.1 can be solved by conversion and integration at the initial time t=0, to get the following equation 2.6.2.

$$ln\left(\frac{c}{c_0}\right) = -k \cdot t$$ 2.6.2

c_0 initial concentration of the reactant, mol L^{-1}

This equation is valid for the entire course of a first-order reaction. Considering the half-life τ ($t_{1/2}$), in which the concentration of c has decreased by the half of c_0, we get equation 2.6.3

$$ln\left(\frac{\frac{1}{2}c_0}{c_0}\right) = ln\frac{1}{2} = -k \cdot \tau$$ 2.6.3

By plotting the natural logarithm of the enzyme activity against time the reaction constant k was received as the slope. The half-life was then calculated from equation 2.6.4.

$$\tau = \frac{\ln 2}{k}$$ 2.6.4

τ half-life, h

As solvent tolerance is a further crucial parameter to enhance solvent productivity in biotechnological production processes the enzyme activities were determined in the presence of increasing concentrations of the desired alcohols. Mr-KARI was tested in presence of isobutanol, Mr-thiolase and Mr-Crt in presence of *n*-butanol.

Determination of the enzyme kinetic properties was carried out by measuring the initial reaction rates. From all tested Mr enzymes only Mr-KARI had a two-substrate enzyme mechanism. Consequently, the initial reaction rate for Mr-KARI was measured with either the substrate or the cofactor in excess. As each Mr-thiolase and Mr-Crt, had an one-substrate mechanism, they were measured with their substrates in excess, whereby Mr-thiolase had to be examined in a coupled enzyme assay. Thus, the initial enzyme rates could be described

with classical Michaelis-Menten kinetics by equation 2.6.5. Kinetic parameters were determined by non-linear regression using SigmaPlot 12.

$$v_0 = V_{max} \cdot \frac{[S]}{K_m + [S]} \qquad\qquad 2.6.5$$

v_0	initial reaction rate, mol L^{-1} s^{-1}
V_{max}	maximal reaction rate, mol L^{-1} s^{-1}
$[S]$	substrate concentration, mol L^{-1}
K_m	Michaelis constant, mol L^{-1}

The turnover number, which describes the maximum number of substrate molecules that an enzyme active site can convert to product per second, could be subsequently calculated as follows (2.6.6):

$$k_{cat} = \frac{V_{max}}{[E]} \qquad\qquad 2.6.6$$

k_{cat}	Turnover number, s^{-1}
$[E]$	enzyme concentration, mol L^{-1}

Specific assay setup and examination of all involved Mr enzymes can be taken from the following sections.

2.6.1 Ketol-acid reductoisomerase

The reaction was initiated by addition of 180 µl assay mixture to 20 µl enzyme solution. Assay mixtures were preincubated in a thermomixer for accurate temperature control. The pH was adjusted to the corresponding temperature.

The KARI activity was quantified spectrophotometrically by the NADH consumption connected with the conversion of 2-acetolactate to 2,3-dihydroxyisovalerate at 50 °C. The

assay mixture contained 5 mM acetolactate, 0.3 mM NADH, 10 mM MgCl$_2$ and 50 mM HEPES pH 7. The specific activity was calculated with the following formula 2.6.7:

$$a = \frac{\Delta c_{NAD(P)H} \cdot V_R \cdot f}{\Delta t \cdot V_E \cdot c_E} = \frac{\Delta A_{340} \cdot V_R \cdot f}{\Delta t \cdot \varepsilon \cdot l \cdot V_E \cdot c_E} \qquad 2.6.7$$

a	specific enzyme activity, U mg^{-1}
$\dfrac{\Delta c_{NAD(P)H}}{\Delta t}$	change of NAD(P)H concentration over time, mM min^{-1}
V_R	total reaction volume, mL
V_E	enzyme solution volume, mL
c_E	enzyme concentration, µg mL^{-1}
f	dilution factor
$\dfrac{\Delta A_{340}}{\Delta t}$	change of absorbance at 340 nm over time, min^{-1}
ε	molar extinction coefficient, L mmol^{-1} cm^{-1}
l	path length, cm

2.6.2 Thiolase

The Claisen condensation of 2-molecules acetyl-CoA to yield acetoacetyl-CoA catalyzed by the purified Mr-thiolase was quantified in a coupled enzyme assay with β-Hydroxybutyryl-CoA Dehydrogenase (Hbd) via monitoring the decrease in absorbance at 340 nm due to the oxidation of NADH (Figure 12). The standard assay mixture contained 50 mM HEPES pH 7, 1 mM acetyl-CoA, 0.3 mM NADH and Hbd from *C. acetobutylicum* [32].
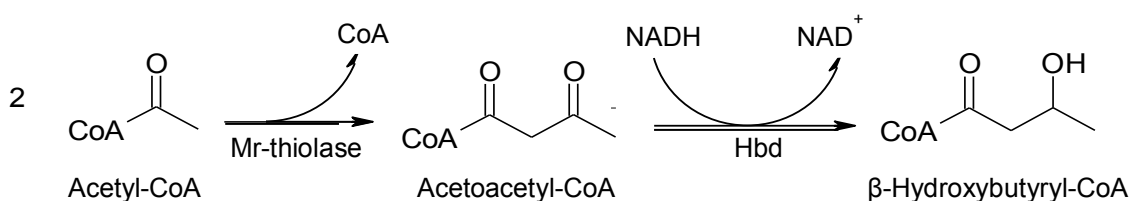

Figure 12: Schematic illustration of the Mr-thiolase activity assay.

2 Methods

Assays for pH dependence were quantified via DTNB (5,5'-dithiobis-(2-nitrobenzoic acid)), substituting a reversed catalyzing direction of Hbd. During this assay the thiol moiety of the released CoA molecule cleaves the disulfide bond of DTNB to form one equivalent of a yellow coloured NTB^{2-} anion (Figure 13), which can be detected at 412 nm.
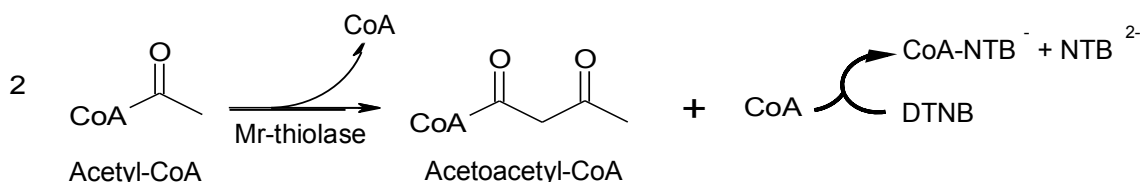

Figure 13: Schematic illustration of the Mr-thiolase DTNB assay.

The standard assay mixture contained 50 mM HEPES, 0.2 mM acetyl-CoA, 0.1 mM DTNB. 5 mM DTNB stock solution was prepared with 100 mM phosphate buffer pH 7.2. The molar extinction coefficient of 14.15 mM^{-1} cm^{-1} was derived from Riener et al. [68]. The specific activity was calculated according to equation 2.6.7.

Previous literature references reported inhibitory effects by NAD$^+$, NADH and CoA [32, 41]. Particularly CoA is classified as strong competitive inhibitor. Hence, all cofactors were examined with respect to their inhibitory effects. According to the general equation for competitive inhibition (2.6.8) a pattern of double reciprocal plots was fitted to Lineweaver-Burk diagrams.

$$v_0 = \frac{V_{max}[S]}{K_m \left(1 + \frac{[I]}{K_i}\right) + [S]}$$

2.6.8

$[I]$ inhibitor concentration, mol L^{-1}

K_i dissociation constant of the inhibitor, mol L^{-1}

The resulting slopes were related to their corresponding inhibitor concentration by a linear regression. The dissociation constant of the inhibitor K_i could be subsequently taken from the intersection on the abscissa.

2.6.3 Crotonase

Enzyme activities of Mr-Crt were determined by HPLC analysis, monitoring the formation of 3-hydroxybutyryl-CoA at 50 °C. The assay mixture contained 50 mM HEPES (pH 7) and 50 µM crotonyl-CoA and was preincubated in a thermomixer for accurate temperature control. The pH was adjusted to the corresponding temperature. Reactions were performed in 1.5 ml safe-lock tubes and initiated by addition of 180 µl assay mixture to 20 µl enzyme solution and finally stopped on ice at 0, 1, 2.5 and 5 min. The specific activity was calculated following equation 2.6.9.

$$a = \frac{\Delta[P] \cdot V_R \cdot f}{\Delta t \cdot V_E \cdot c_E}$$

<div align="right">2.6.9</div>

a	specific enzyme activity, U mg^{-1}
$\dfrac{\Delta[P]}{\Delta t}$	change of product concentration over time, mM min^{-1}
V_R	total reaction volume, mL
V_E	enzyme solution volume, mL
c_E	enzyme concentration, µg mL^{-1}
f	dilution factor

2.7 Development of a new screening method for ketol-acid reductoisomerases

The underlying mechanism of the screening platform was the application of an *E. coli* KARI knockout strain as *in-vivo* selection tool. This strategy promised a simple and rapid analysis of large KARI variant libraries by selecting viable phenotypes. In the absence of the amino acids valine, leucine and isoleucine the knockout strain was not able to grow on minimal medium, unless a functional KARI activity was introduced into the cell. For cellular supplementation of functional KARI activities, the basal expression provided by the pET vector system was used.

The most critical step of the library screen was the assay development. Hence, an efficient validation of the applied methods was essential. In order to achieve a reproducible

and reliable assay design, the whole procedure was simulated with the Mr-KARI wild type (WT) enzyme. Variability and distribution were statistically analyzed by determining the coefficient of variance (CV) and the quality by the Z'-factor as reported by Zhang et al. [69]. In this respect, the Z'-factor is a dimensionless parameter that provides a qualitative sensitivity measure of the applied assay and can be calculated using the control data (equation 2.7.1). The Z'-calculation compares thereby the mean value of the positive control (Mr-KARI WT activity) to the mean value of the negative control (blank). Whereas negative or zero Z' values indicate poor assay quality, values close to one, mark ideal assay conditions [69].

$$Z' = 1 - \frac{(3 \cdot \sigma_{ctrl+} + 3 \cdot \sigma_{ctrl-})}{|(\mu_{ctrl+} - \mu_{ctrl-})|}$$

2.7.1

Z'	dimensionless parameter for the quality of an assay itself
σ	standard deviation
ctrl +	positive control
ctrl -	negative control
μ	mean

While the CV (equation 2.7.2) is defined as the ratio of the standard deviation to the mean and gives an indication of the capability to identify improved variants, the Z'-factor ensures that the assay format has already been properly implemented and that the assay has sufficient dynamic range and acceptable signal variability and will provide useful data [69].

$$CV = 100 \cdot \left(\frac{\sigma_{ctrl+}}{\mu_{ctrl+}} \right)$$

2.7.2

CV	coefficient of variation, %

The dynamic range is defined by the difference between the mean of the positive controls and the mean of the negative control and is also part of the Z-factor calculation (equation 2.7.3), which validates the quality of the whole library screen. The Z-factor in turn is defined as the ratio of the separation band to the signal dynamic range of the assay [69].

$$Z = 1 - \frac{(3 \cdot \sigma_L + 3 \cdot \sigma_{ctrl+})}{|(\mu_L - \mu_{ctrl+})|}$$

2.7.3

Z	dimensionless parameter for the quality of an array of tested variants
L	mutant library

That way a direct estimation of a hit identification can be taken into account to the WT control measurement.

2.7.1 Library construction and screening procedure

The primary library was constructed via error prone PCR in accordance to Jaeger et al. [70] and subsequently cloned in the pCBR vector using NdeI and SalI restriction sites. The plasmids were transformed into the KARI knockout strain JW3747 via electroporation. The pET28a vector without insert was used as control. The library was plated on M9 minimal media agar plates supplemented with 30 µg ml^{-1} kanamycin (M9 + kana). Grown colonies were transferred into 96-well microtiter plates containing 200 µl M9 + kana and incubated at 37 °C for 24 h. Afterwards, deep-well plates containing 1.5 ml M9 + kana were inoculated with this preculture and grown at 37 °C for 48 h. The cells were harvested and resuspended in 100 µl of 50 mM HEPES pH 7.35, 0.5 mg ml^{-1} lysozyme and 10 mg ml^{-1} DNAse to prepare the crude cell extracts. The crude extracts were preincubated for 60 min and subsequently centrifuged. All activity measurements were performed in 96-well microtiter plates at 50 °C with 20 µl of the supernatant by determining the NADH consumption according to section 2.6.1.

The whole screening procedure was assessed on the basis of the formulas 2.7.2 and 2.7.3. Potential hits were verified by rescreening. Plasmids of improved variants were subsequently isolated and sequenced. Individual amino acid exchanges, received by the error prone PCR,

were segregated via quick change mutagenesis following the protocols from Papworth et al. [71], using Phusion polymerase. Applied oligonucleotides can be found in Table 4.

Table 4: Oligonucleotides for point mutagenesis.

Primer	Sequence (5' -> 3')
Mr-KARI E54V fwd	CAGCCGCAACGAGGTGAAGGCCCGTAAAGCG
Mr-KARI E54V rev	CGCTTTACGGGCCTTCACCTCGTTGCGGCTG
Mr-KARI T84S fwd	CCTGCTCCCGGACGAGTCCCAGGGGGCCGTTTAC
Mr-KARI T84S rev	GTAAACGGCCCCCTGGGACTCGTCCGGGAGCAGG
Mr-KARI Q115R fwd	GGCTTCAACATCCATTTCGGCCGGATCAAGCCGCGCCGC
Mr-KARI Q115R rev	GCGGCGCGGCTTGATCCGGCCGAAATGGATGTTGAAGCC
Mr-KARI T253S fwd	GCGCTACTCCATCTCCAACTCCGCCGAGTACGGC
Mr-KARI T253S rev	GCCGTACTCGGCGGAGTTGGAGATGGAGTAGCGC
Mr-KARI K329Q fwd	CCATGATGCCCTTCCTCCAGTCCAGGTTCACGAAG
Mr-KARI K329Q rev	CTTCGTGAACCTGGACTGGAGGAAGGGCATCATGG

Site saturation mutagenesis was carried out with primers (Table 5) degenerated at specific target sites according to the same protocol. Caster 2.0 [72, 73] was used to calculate the individual library sizes and the number of variants to be screened.

Table 5: Degenerated primers for site saturation mutagenesis. [a]

Primer	Sequence (5' -> 3')
R47(DH) fwd	CAAGGTGGTGGTGGGGCTG**DHC**CCCGGCAGCCGCAAC
R47(DH) rev	GTTGCGGCTGCCGGG**GDH**CAGCCCCACCACCACCTTG
S50(BH) fwd	GGGCTGCGCCCCGGC**BHC**CGCAACGAGGAGAAGGCCCG
S50(DV) rev	CGGGCCTTCTCCTCGTTGCG**GDV**GCCGGGGCGCAGCCC
R51(DH) fwd	CTGCGCCCCGGCAGC**DHC**AACGAGGAGAAGGCCCGTAAAG
R51(DH) rev	CTTTACGGGCCTTCTCCTCGTT**GDH**GCTGCCGGGGCGCAG
Q85(RB) fwd	CTGCTCCCGGACGAGACC**RBG**GGGGCCGTTTACAAGGCC
Q85(VY) rev	GGCCTTGTAAACGGCCCC**CVY**GGTCTCGTCCGGGAGCAG
V88(VBV) fwd	GACGAGACCCAGGGGGCC**VBV**TACAAGGCCGAGGTGGAACCC
V88(BVB) rev	GGGTTCCACCTCGGCCTTGTA**BVB**GGCCCCCTGGGTCTCGTC

[a] the degenerated bases representing: D = A/G/T, H = A/C/T, R = A/G, B = C/G/T, V = A/C/G, Y = C/T

2.8 Development of a cell-free *n*-butanol biosynthesis

The adapted native *n*-butanol pathway could only be established as an *in-vitro* production system with difficulties, because of the discussed inhibition dilemma and unstable CoA esters. To circumvent these limitations and reduce required enzyme activities, a new *n*-butanol pathway was designed. This pathway based on an implemented enamine – aldol – condensation as key intermediate reaction step.

Potential catalysts for the enamine condensation were tested with different concentrations in 2 ml GC vials containing 20 mM acetaldehyde and 50 mM HEPES (pH 7). The vials were incubated at 50 °C for 20 h in a water bath and subsequently analyzed via GC. Control measurements were determined with both, 20 mM acetaldehyde and crotonaldehyde, without any catalyst.

2 Methods

The whole production route starting from pyruvate was evaluated in 2 ml GC vials in three separated experiments. All required biocatalysts and their ligands are stated in Table 6.

Table 6: Biocatalyst combination to produce *n*-butanol from pyruvate.

#	Biocatalyst	EC #	Substrate	Product
1	pyruvate decarboxylase (PDC)	4.1.1.1	pyruvate	acetaldehyde
2	proline / arginine / polyamine	--------	acetaldehyde	crotonaldehyde
3	2-enoate reductase (YqjM)	1.6.99.1	crotonaldehyde	butyraldehyde
4	alcohol dehydrogenase (ADH)	1.1.1.1	butyraldehyde	*n*-butanol

The reaction mixture contained 50 mM HEPES (pH 7), 20 mM pyruvate, 20 mM proline, 0.05 mM FMN, 20 mM NADH, 2.5 mM $MgSO_4$ and 0.1 mM thiamine pyrophosphate (TPP). Enzymes were added as follows: 0.5 U PDC, 0.5 U YqjM, 0.5 U ADH. Control reactions were performed without enzyme addition. The vials were placed in a water bath and incubated at 50 °C for 6 h. All reaction intermediates and products were subsequently determined by GC analysis (see 2.5.2).

3 Discussion

The aim of this work was the selection, characterization and partial optimization of suitable enzymes to design an *in-vitro* production system for industrially relevant solvents, such as isobutanol and *n*-butanol, on the basis of renewable resources.

The cell-free process conditions were previously specified. All required enzyme activities were matched to the defined process parameters. Their consolidated performance in a defined reaction cascade was subsequently evaluated. To reduce microbial contamination in the reaction vessel and enhance space–time yields the cell-free production was preferably carried out at 50 °C. The reaction cascades were implemented at neutral pH conditions and therefore represent a feasible compromise that maintains activity of all required enzyme components albeit not at their pH optimum. Additionally, in the context of cell-free alcohol production the solvent stability was of utmost importance.

Consequently, each enzyme component was examined in regard to its catalytic efficiency, process stability, and cofactor requirements in coordination with upstream and downstream enzyme activities. Particularly, the enzyme activities of ketol-acid reductoisomerase, thiolase and crotonase were in the focus.

A variety of methods were employed in this thesis in order to establish a new and advanced cell-free technology platform to synthesize higher alcohols. These methods included molecular modeling, directed evolution, rational protein design, enzyme screening and reaction engineering.

To complement this approach, a novel CoA independent and substantially condensed *n*-butanol pathway was designed. Finally, the new reaction cascade was applied to the *n*-butanol *in-vitro* synthesis, starting from pyruvate.

This chapter is intended to give an overview over the specific characteristics of the examined enzymes in correlation with already characterized members of the same enzyme family, their application as a biocatalyst within the *in-vitro* production routes and opened up new opportunities for further research.

3 Discussion

3.1 Characteristic properties of the native Mr-KARI

Considering the reaction specifications, a new KARI activity derived from *M. ruber* which catalyzes the reductive isomerization of 2-acetolactate to 2,3-dihydroxyisovalerate was isolated. The new Mr-KARI was cloned, heterologously expressed in *E. coli* and finally characterized (see article III).

Mr-KARI could be expressed in *E. coli* with a very high expression level of over 90 % soluble protein in the supernatant cell fraction. The purified enzyme showed both common and extraordinary biochemical properties in the KARI family. The obtained pH optimum for Mr-KARI was 7.0, which is consistent with previous values described for KARI enzymes. In comparison, the KARI enzymes of *C. glutamicum* [74], *Hordeum vulgare* [75], *Neurospora crassa* [76] and *Spinacea oleracea* [77] all display a pH optimum at 7.5. In line with the data observed for Mr-KARI, all other reported enzyme activities exhibited a significant activity decrease below pH 7 [74, 76-78].

The enzyme was active throughout a broad temperature range (30-65 °C), the temperature optimum of Mr-KARI being beyond 65 °C. This value marked the instrumental limit of our assay procedure and is concurrently the highest operational temperature ever measured for any KARI enzyme.

At the desired process conditions (50 °C, pH 7), Mr-KARI demonstrated an extended time-dependent stability (half-life (IT_{50}) = 71 ± 0.2 h). A previously stated lower value of 34 h [I] was due to the application of lyophilized enzyme preparation used in the reported experimental procedures. Clearly, the freshly prepared or glycerol stock used in this study showed enhanced viability and is therefore recommended.

In correlation to the previously defined process parameters, the neutral pH optimum and the high tolerance towards isobutanol ($IS_{50} \geq 6$ %) were a strong benefit. Moreover, kinetic examinations demonstrated that Mr-KARI accepts NADH as cofactor with a 10 times higher specific activity compared to *E. coli* KARI (0.7 U mg^{-1} vs. 0.08 U mg^{-1}). The catalytic efficiency was even 15 times higher (4.6 mM^{-1} s^{-1} vs. 0.3 mM^{-1} s-^{1}).

The overall features of Mr-KARI make this enzyme an ideal candidate not only for *in-vitro* isobutanol synthesis, but also suitable for *in-vivo* production systems. Hence, this enzyme

could be successfully applied in our previously reported cell-free isobutanol production system [I].

3.1.1 The Mr-KARI upgrade

In the reported experimental set-up the relatively low catalytic activity of Mr-KARI (0.7 U mg^{-1}) was a significant bottleneck in achieving high product titers. Hence, large amounts of enzyme had to be supplied to the reaction to compensate the low catalytic performance. To provide an efficient metabolic flux and minimize enzyme quantities in the reaction cascade it was necessary to amplify the catalytic activity of the enzyme. Therefore, we developed a new screening method, which was based on an *E. coli* knockout strain as an *in-vivo* selection tool. This simple procedure allowed selection of significantly improved KARI variants by simple phenotype selection (see article III).

To quantify the sensitivity of the applied screening procedure the CV and the Z'-factor were determined as mentioned above (see 2.7). The calculated CV of 22 % indicated that in our screening system we could only segregate variants with significantly improved activities. Even though this was in line with our experimental goals, the design of a more sensitive assay procedure would require a lower CV. The calculated Z'-factor was 0.2.

The subsequent screening for optimized KARI variants delivered a library of 432 clones in a primary screening round. The mutants displayed a wide range of both, increased and reduced activity values compared to the WT Mr-KARI control. The calculated Z-factor for the initial library screen was 0.3 and was therefore in line with the expected quality values for the procedure. Our analysis indicated that 11 clones showed an enhanced activity of 150-200 % compared to the Mr-KARI WT. Two clones were identified with a significantly increased activity of more than 200 % with respect to the WT. A refinement of the primary screen and a site directed segregation of the most promising amino acid sites provided evidence that the greatest impact could be attributed to a substitution of threonine at position 84 by serine.

In analogy to our data mutagenesis studies with *E. coli* and *Slackia exigua* (Se-KARI) KARI identified amino acid positions equivalent to T84 as optimization hot spots. Particularly, the position Q110 of the *E. coli* KARI is equivalent to I95 of Se-KARI and T84 of Mr-KARI, which

are all positioned at the beginning of the α5-helix covering the Rossmann-fold. Additionally, Q110 and I95 were selected as they can affect the cofactor orientation by coordinating with the adenine moiety [19, 26]. As illustrated in Figure 14, the position of both substitutions in Mr-KARI (T84) and Se-KARI (I95) are comparable. In both instances we can refer to conservative missense mutations. In case of Se-KARI (I95) the nonpolar residue isoleucine was replaced by an equivalent valine residue [26]. In Mr-KARI the polar threonine was substituted by serine. The difference consists only in the hydrophobicity of the residues. In *E. coli* the mutation corresponds to *Q110V* and is likewise speculated to influence the cofactor orientation [26].
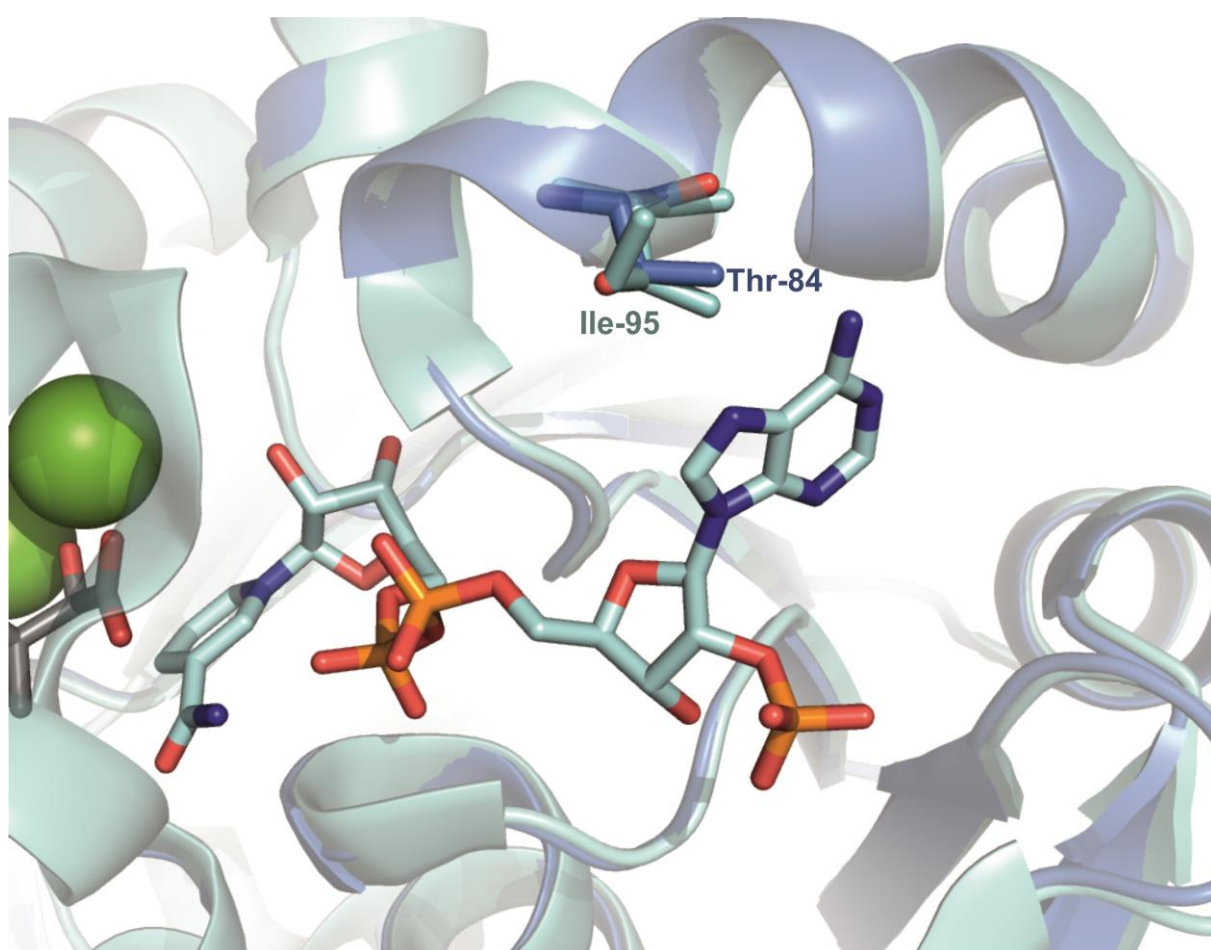
Figure 14: Structural alignment of modeled Mr-KARI and native Se-KARI. The modeled Mr-KARI structure is colored in dark blue. The crystal structure of the native Se-KARI (PDB 4KQW) is colored in light blue. The cofactor NADP$^+$ was adopted from Se-KARI and is also colored in light blue. The other ligands were adopted from spinach KARI (PDB 1YVE, 1QMG). Specific positions for substitutions are labeled.

The directed evolution approach led to a wide variety of enzyme variants, which were screened and handpicked via the established *in-vivo* screening system (see 2.7). The resulting improved variant *T84S* exhibited a specific activity of 2.7 U mg^{-1}, which was a 350 % improvement over the WT. The catalytic properties of the cofactors shifted towards a higher preference of NADH as well. The mutation within the cofactor-binding site was therefore in line with other mutagenesis studies for *E. coli* and Se-KARI.

While the optimized *E. coli* KARI (IlvC$^{6E6-his6}$) demonstrated an improved specific activity of 0.7 U mg^{-1} [19], the corresponding Se-KARI variant (Se_KARI^{DDV}) exhibited a specific activity of 1.6 U mg^{-1} [26]. However, the NADH / NADPH catalytic efficiency ratios of IlvC$^{6E6-his6}$ and Se_KARI^{DDV} could be increased up to 185 and 88, respectively [19, 26]. In comparison, the NADH / NADPH ratio for Mr-KARI was 1.3. This can be attributed to the mentioned mutagenic impacts to the α5-helix that influence both, the NADH and NADPH depending activity [19, 26]. Consequently, additional modifications were implemented into the IlvC$^{6E6-his6}$ and Se_KARI^{DDV} active sites, which caused the higher NADH / NADPH catalytic efficiency ratios. For Mr-KARI corresponding target sites had to be examined.

3.1.2 Investigation of further targets for molecular engineering of Mr-KARI

Since the *E. coli* and Se-KARI reports gave us deeper insights into the structural-function relationship of this enzyme family, we used a rational approach to identify further amino acid residues as targets for the molecular engineering of Mr-KARI (see article III). In accordance with structural and kinetic analysis of the *E. coli* KARI and Se-KARI [19, 26], we selected the residues Arg47, Arg51 and Ser50 because of their position within the NAD(P)H binding loop and their supposed interaction with the phosphate group of NADPH (Figure 15) [19, 26, 79].

The residues Gln85 and Val88 located within the α5-helix across the Rossmann-fold were also selected for site saturation based optimization due to their presumed effect in analogy to *T84S*.
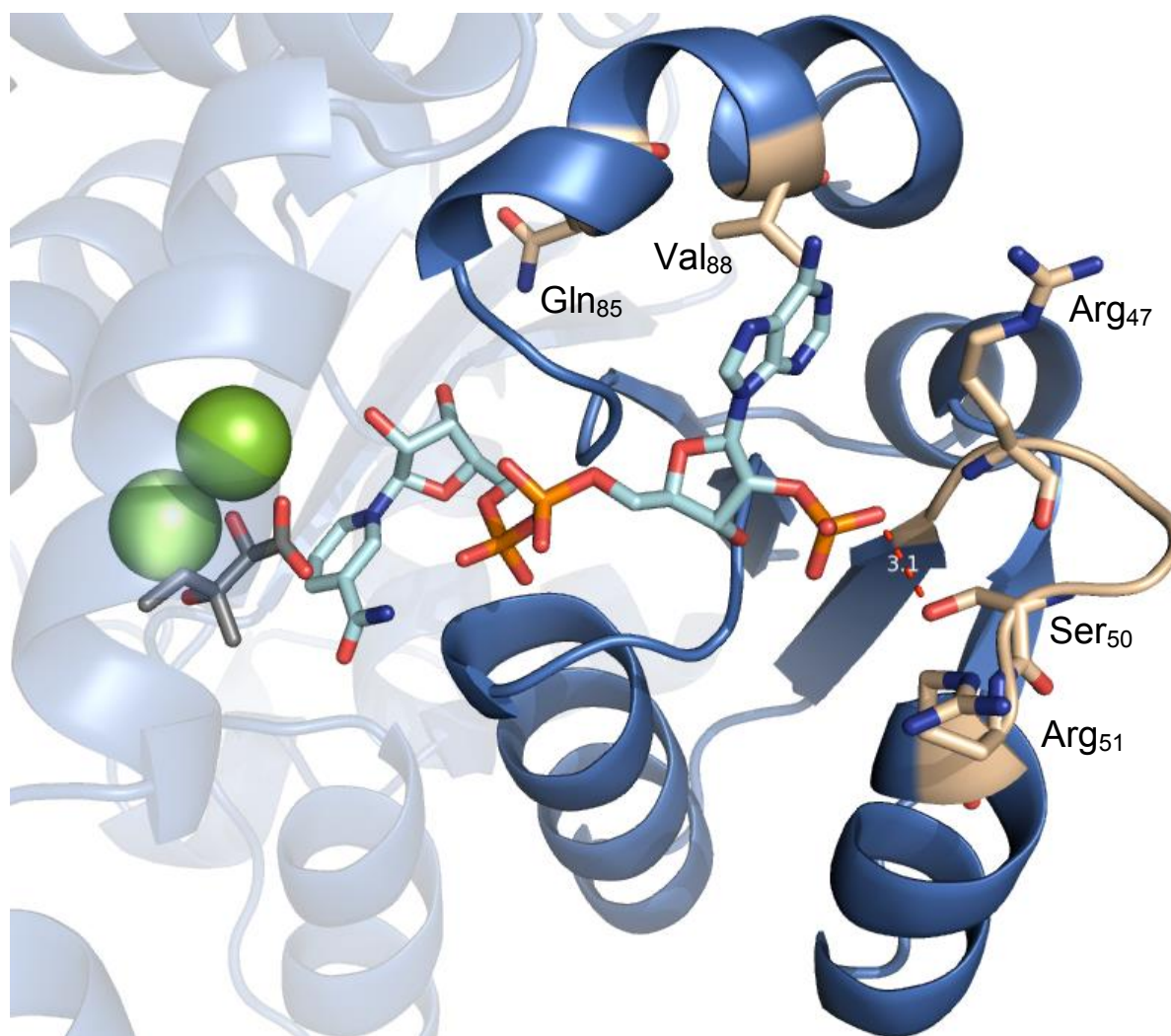
Figure 15: Cofactor-binding site of the Mr-KARI model. The region for site directed mutagenesis including the positively charged loop, which interacts with the 2'-phosphate of the $NADP^+$, are highlighted in gold. The corresponding residues are labeled. The cofactor $NADP^+$ was adopted from Se-KARI and is also colored in light blue. The other ligands were adopted from spinach KARI (PDB 1YVE, 1QMG).

The site saturation mutagenesis was subsequently carried out with primers degenerated at specific target sites (see table 5). Caster 2.0 [72, 73] was used to calculate the individual library sizes and the number of variants to be screened. Potential hits were verified by rescreening.

However, the new Mr-KARI variants obtained by site-saturation could not be purified in the active form and were thus deemed not to be process-relevant. Nevertheless, the obtained results gave us new insights into the structure-function relationships and catalytic interactions of Mr-KARI.

The best improvements with respect to the relative activity were achieved at the positions Ser50 (+ 180 % to WT) within the loop region and Val88 (+ 211 % to WT), which is part of the α5-helix. Surprisingly, the libraries at positions Arg47 and Arg51 resulted in variants with only low enhanced activities or, in case of Arg51, no improvements (data not shown). This data contrasts previous reports on *E. coli* KARI optimization, where amino acid exchanges of the basic arginine to the acidic aspartate resulted in increased catalytic properties towards NADH [19, 21, 26].

The different enzyme behavior may be due to a difference between the loop regions of the Mr-KARI and other analyzed KARI sequences, where the positions of Ser50 and Arg51 at the end of the loop are reversed.

Figure 15 illustrates that only Ser50 is positioned to build a hydrogen bond to an oxygen atom of the phosphate group. By contrast, the arginine residues would not be able to build salt bridges as they are too far away from the phosphate moiety. The low catalytic effects induced by the mutation of the arginine residues confirmed this hypothesis.

The substitution of valine by alanine at position 88 is, like *T84S*, a conservative missense mutation. The enhanced catalytic activity can therefore be attributed to the same effects.

In contrast to previously reported KARI enzymes, our data indicated that the enhanced NADH acceptance of WT Mr-KARI could be attributed to minor interactions between the residues of the binding loop and the cofactor.

In summary, the overall rational approach via a site saturation mutagenesis at specific target sites gave us primary new insights into the catalytic center of Mr-KARI. The obtained variants demonstrated increased catalytic activities, but were not process relevant, as they could not be purified in the active form.

3.2   KARI in the final *in-vitro* isobutanol synthesis

The cell-free isobutanol production route developed during this project based on a minimized non-natural enzyme cascade. The enzymatic approach demonstrated here has the potential to serve as a next generation bio-production system.

3 Discussion

Due to the predefined process conditions, a new KARI enzyme activity had to be integrated into the production route, which satisfied all specified requirements. The required KARI enzyme had to be both solvent- and thermo-tolerant, as well as long term stable at the preferred process conditions and finally NADH dependent.

With the presented native Mr-KARI, the target, isobutanol, could be successfully synthesized from glucose within 23 h in a molar yield of 53 %. The cumulative mass of all detectable intermediates and products even gave a yield in excess of 80 %. The whole cell-free system was thereby consolidated to use only NAD^+ as the universal cofactor, due to the natural acceptance of NADH by Mr-KARI (see article I).

Although the native Mr-KARI showed here extraordinary characteristics, there are two potential targets to improve this enzyme with regard to the cell-free isobutanol production.

The first target can be attributed to the enhancement of the isobutanol tolerance. In our studies, 60 % of the Mr-KARI remains active even in the presence of 6 % (v/v) isobutanol. In comparison, a two-phase isobutanol/water system is formed at product concentrations above 12 % (v/v) [27]. A two-phase system significantly simplifies the downstream process by a simple phase separation [17] and is thus favored.

The second aspect concerns the NADH depending enzyme activity of Mr-KARI. The relatively low catalytic activity of Mr-KARI results in a high enzyme consumption to compensate the low catalytic performance. Although we could generate a Mr-KARI variant with 350 % increased activity, this *T84S* variant and all other variants were accompanied by a reduced structural stability.

In summary, molecular optimizations are continuing necessary and permit iterative improvements with focus on activity and solvent tolerance, in particular with respect to the structural stability. Two opportunities to improve the Mr-KARI enzyme activity could already be demonstrated.

3.3 Thiolase

Thiolase is part of the *n*-butanol production route, which was initially adopted from *C. acetobutylicum*. The enzyme catalyzes the second committed step in the *n*-butanol cascade, downstream to the combined reaction of PDC and ALDH (see 1.3).

The cell-free *n*-butanol process followed the same parameters as the cell-free isobutanol process (see 3.1). In this regard, a new thiolase was derived from *M. ruber*. The new Mr-thiolase was cloned, heterologously expressed in *E. coli* and finally characterized (see article II).

The structural and kinetic properties of Mr-thiolase (K_m = 0.1 mM; k_{cat} = 0.8 s^{-1}) indicated this enzyme belongs to the family of catabolic thiolases. The data was in line with the best performing catabolic thiolase from pig heart (K_m = 0.3 mM; k_{cat} = 0.8 s^{-1}) ([39, 80]. Additionally, we could simultaneously demonstrate the functional cooperation of Mr-thiolase with Hbd resulting in the efficient conversion of acetyl-CoA to β-hydroxybutyryl CoA. Thus, half of the *n*-butanol production route starting from pyruvate could be reconstructed *in-vitro*.

In contrast to previous reports we examined the interaction of Mr-thiolase with alternative cofactors and process intermediates in line with the predefined screening procedure. We could demonstrate that NAD$^+$ and CoA are both competitive inhibitors, whereby CoA seems to be most inhibitory ($K_{i\ NAD^+}$= 38.7 * 10^3 ± 5.8 * 10^3 μM versus $K_{i\ CoA}$= 105.1 ± 6.6 μM). Particularly noteworthy in this context is the lower sensitivity of Mr-thiolase towards CoA compared to other reported thiolases ($K_{i\ CoA\ Rhizobium\ sp.}$= 11 μM; $K_{i\ CoA\ A.\ latus}$= 20 μM) [41, 81]. This particular feature could be used to improve metabolic flux in order to achieve higher butanol titer in cell-free as well as cell-based approaches.

The half-life at the dedicated process temperature of 50 °C was 199 h, which corresponds to a dwell time of over one week in the process. Interestingly, the Mr-thiolase activity remained stable over an extended time periods (7 h) even under extreme temperature and high solvent (T = 50 °C, Butanol = 4 % v/v) concentrations.

In this study I developed a new DTNB based assay, which, for the first time, allowed to overcome limitations of the coupled assay with Hbd. The new DTNB assay allowed the determination of the Mr-thiolase pH optimum at 10. In our reaction set-up the functional

incorporation of Mr-thiolase into the *n*-butanol process cascade was possible as the enzyme was operative at neutral pH.

The pronounced biochemical properties observed for Mr-thiolase suggested that this enzyme is a suitable component for the construction of a cell-free *n*-butanol production cascade. However, further studies towards CoA sensitivity and improved catalytic characteristics are required. Although the Mr-thiolase operates at neutral pH conditions, the shift of the pH optimum towards a more neutral pH while focusing on the catalytic parameters is desirable to enhance the cooperation with the other enzymes in the butanol pathway. The molecular optimization towards a less sensitive and more active thiolase at neutral pH conditions can be addressed by e.g. rational or random enzyme engineering methods.

3.4   Crotonase

In the n-butanol pathway, the crotonase functionality is positioned after the Hbd reaction (see 1.3). To identify a process-relevant crotonase activity, equivalent screening procedures as used for Mr-KARI and Mr-thiolase were applied (see article IV).

We could likewise identify a new crotonase activity in *M. ruber*. The enzyme was cloned, heterologously expressed in *E. coli* and its physical parameters were characterized (see article IV). Unfortunately, the kinetic data for the crotonase family is inhomogeneous and does not allow a direct comparison.

Optimal Mr-Crt activities were determined at pH 7.0 and 55 °C. Interestingly, the enzyme was active over a very broad temperature range of 50 to 70 °C where it retained 80 % of its initial activity. Moreover, Mr-Crt displayed an extended half-life of over one month (IT$_{50}$ (50 °C) = 743 ± 0.7 h) at elevated temperature, which has not been reported for any other member of the crotonase enzyme family.

A further aspect concerns butanol toxicity. Cell-based butanol production systems are limited in both product titers and process viability at 2 % (v/v) butanol [9-11] due to toxic effects on cell wall components [15]. The pronounced butanol stability of Mr-Crt beyond 2 % (v/v) suggests that this enzyme is a suitable component for the construction of a cell-free *n*-butanol synthesis.

In light of process-engineering perspectives the excellent thermostability of Mr-Crt at neutral pH conditions provide extended operation capacity and reduced enzyme costs for cell-free *n*-butanol production approaches.

In this regard, the identification of the new Mr-Crt and thiolase enzyme together with our previous results on the cell-free conversion of glucose to pyruvate provide a platform for a consolidated cell-free reaction cascade that allows direct, aerobic conversion of glucose to *n*-butanol.

3.5 *In-vitro n*-butanol synthesis

The developed toolbox utilizes a minimized glycolytic reaction cascade and allows a great variety to produce industrial relevant molecules. While the *in-vitro* production of ethanol and isobutanol could already be demonstrated (see article I), designing a cell-free enzyme cascade for *n*-butanol was more complex and accompanied by several bottlenecks, which had to be overcome.

Although the initially designed pathway was broadly in compliance with the native pathway of *C. acetobutylicum*, the pyruvate dehydrogenase complex had to be substituted by a combined reaction step of PDC and ALDH (see 1.3) due to the large dimension of the complex [31].

Besides, the *n*-butanol pathway requires CoA as an additional cofactor. Herein, both cofactors CoA and NAD^+ inhibit the thiolase and hbd activity in micro- and millimolar concentrations, respectively [32]. A complete inhibition of one of the enzymes would result in the termination of the whole process. In light of these circumstances it is very difficult to manage the cofactor balance and adjust a linear production rate.

Nevertheless, we launched an *n*-butanol *in-vitro* synthesis in a one-pot reaction comparable to the isobutanol synthesis (see article I), after all components were characterized and provided. Similarly to the isobutanol mixture, 25 mM glucose was added to start the reaction. Apart from the different *n*-butanol enzyme mix, 0.05 mM CoA and 5 mM NAD^+ were used as cofactors. The reaction was likewise set up in 20 ml GC vials at pH 7 and 50 °C.

3 Discussion

Online measurements of all intermediates and the product could not detect any *n*-butanol within the whole experimental period. Instead, we observed enrichments of acetyl-CoA and free CoA, so we assumed that the CoA intermediates decayed and the released CoA inhibited the thiolase activity. This led to the termination of the whole process as we suspected.

To scavenge the free CoA, e.g. with DTNB to impede the related thiolase inhibition would not be appropriate under practical terms. The decayed products would still accumulate and the CoA intermediates would need to be added regularly into the process, which would lead to high production costs.

We were therefore forced to completely redesign our *in-vitro n*-butanol production system. Hence, we employed computational methodologies to predict non-natural reaction steps for the conversion of pyruvate to *n*-butanol. As a result, we implemented an organocatalytic reaction step that directly converts acetaldehyde to crotonaldehyde by an enamine-aldol-condensation. This way, we got a direct access into an alternative *n*-butanol cascade stated by Sommer et al. [54]. That implies a completely new and condensed *n*-butanol pathway (see 1.3.3 and article V).

First of all, potential catalysts for the enamine condensation were selected and tested with acetaldehyde in 50 mM HEPES (pH 7) at 50 °C for 20 h. The following catalysts were examined: arginine, proline, lysine, spermidine, putrescine and alanine as negative control. While proline [55] and lysine [82] are known for their nucleophilic reactivity, arginine was selected due to its side chain's secondary amine function. Polyamines like spermidine and putrescine also possess secondary amines and constitute suitable catalysts [56].

The best conversion of acetaldehyde to crotonaldehyde was demonstrated by proline ($v = 2.2 * 10^{-3}$ µmol ml^{-1} min^{-1}) and arginine ($v = 1.8 * 10^{-3}$ µmol ml^{-1} min^{-1}), followed by lysine ($v = 1.1 * 10^{-3}$ µmol ml^{-1} min^{-1}) and spermidine ($v = 0.5 * 10^{-3}$ µmol ml^{-1} min^{-1}). As we suspected, alanine ($v = 0.1 * 10^{-3}$ µmol ml^{-1} min^{-1}) exhibited the lowest reaction rate.

Due to this result, proline was used for a first validation of the *n*-butanol synthesis via the new condensed pathway. The whole production route starting from pyruvate was tested in 2 ml GC vials in three separated experiments. Also, similar to the isobutanol experiments, the

reactions were performed at neutral pH and 50 °C. All intermediates and the product could be merely determined by GC analysis.

This proof-of-concept experiment demonstrated the possibilities of modern enzymatic technologies. We started the experiment with 2.2 g L^{-1} pyruvate and could successfully produce 7.4 mg L^{-1} n-butanol. With emphasis on the prototypic approach we could already reach more than twice as much as the recently engineered *S. cerevisiae* (2.5 mg L^{-1}) concept [9]. Nevertheless, the comparison to the native n-butanol producer *C. acetobutylicum* (~ 12 g L^{-1}) [7, 83], or the engineered *E. coli* strains (~ 500 mg L^{-1}) [8, 10] provides targets for further improvements.

A glance at an alternative cell-free n-butanol production route also demonstrates the potential of the *in-vitro* technique. This production route developed by the Ohtake group applied almost the whole native clostridial pathway. The pathway was reconstructed *in-vitro* with a final n-butanol titer of 260 mg L^{-1} [14]. However, this approach required 16 enzymes, three metabolic cofactors (ATP, NAD^+ and CoA) and was divided into 7 parts. In contrast, our condensed n-butanol *in-vitro* concept requires only three enzymes and NAD^+ as single cofactor. Hence, this production route can be excellently integrated into our developed toolbox [I]. The total enzyme requirement would thus be increased to six.

The combined organocatalytic and enzymatic n-butanol pathway eliminates the discussed barriers. But the aldol-condensation step equally restricts the overall reaction due to the slow reaction rate. Addition of catalysts to enhance the reaction rate might be possible but have to be coordinated with the enzyme activities within the production route. It is perfectly conceivable to find or to engineer an aldolase, which exhibits the appropriate specific activity. A slightly different approach would be the usage of aldolase active antibodies [84].

Additionally, considering the new pathway the utilized ADH prefers acetaldehyde as substrate, which result in a bypass towards ethanol and reduce the n-butanol yield. A new or engineered ADH that favors higher aldehydes like butyraldehyde would be advantages.

4 Concluding remarks

This thesis gives an insight into current research objectives in the field of white biotechnology. The project pursued the development of a new and advanced technology platform to synthesize hydrophobic building blocks from renewable resources. Based on a new and artificial glycolytic reaction cascade for pyruvate a modular system was created. Considering the defined process configuration, we could successfully implement appropriate modules for ethanol, isobutanol and *n*-butanol (Figure 16).
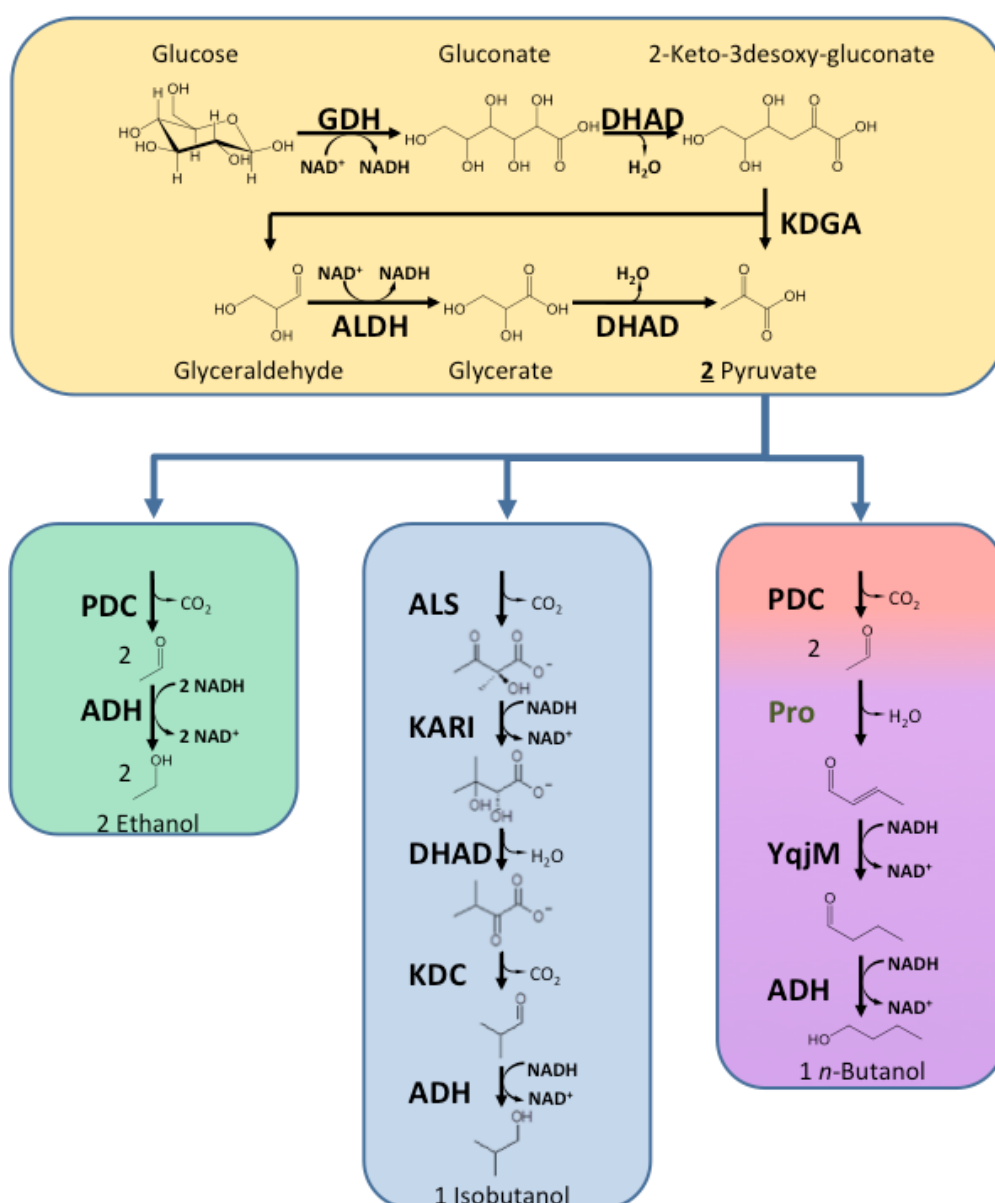

Figure 16: The final toolbox, including the new *n*-butanol module.

5 References

[1] H. Li, A.F. Cann, J.C. Liao, Biofuels: biomolecular engineering fundamentals and advances, Annual review of chemical and biomolecular engineering, 1 (2010) 19-36.

[2] C.N. Hamelinck, G.v. Hooijdonk, A.P.C. Faaij, Ethanol from lignocellulosic biomass: techno-economic performance in short-, middle- and long-term, Biomass and Bioenergy, 28 (2005) 384-410.

[3] M.E. Himmel, S.Y. Ding, D.K. Johnson, W.S. Adney, M.R. Nimlos, J.W. Brady, T.D. Foust, Biomass recalcitrance: engineering plants and enzymes for biofuels production, Science, 315 (2007) 804-807.

[4] A.K. Agarwal, Biofuels (alcohols and biodiesel) applications as fuels for internal combustion engines, Prog Energ Combust, 33 (2007) 233-271.

[5] C. Weizmann, Production of Acetone and Alcohol by Bacteriological Processes, US Patent 1.315.585, 1919.

[6] P. Durre, Biobutanol: an attractive biofuel, Biotechnology journal, 2 (2007) 1525-1534.

[7] S.Y. Lee, J.H. Park, S.H. Jang, L.K. Nielsen, J. Kim, K.S. Jung, Fermentative butanol production by Clostridia, Biotechnology and bioengineering, 101 (2008) 209-228.

[8] S. Atsumi, A.F. Cann, M.R. Connor, C.R. Shen, K.M. Smith, M.P. Brynildsen, K.J. Chou, T. Hanai, J.C. Liao, Metabolic engineering of Escherichia coli for 1-butanol production, Metabolic engineering, 10 (2008) 305-311.

[9] E.J. Steen, R. Chan, N. Prasad, S. Myers, C.J. Petzold, A. Redding, M. Ouellet, J.D. Keasling, Metabolic engineering of Saccharomyces cerevisiae for the production of n-butanol, Microbial cell factories, 7 (2008) 36.

[10] D.R. Nielsen, E. Leonard, S.H. Yoon, H.C. Tseng, C. Yuan, K.L. Prather, Engineering alternative butanol production platforms in heterologous bacteria, Metabolic engineering, 11 (2009) 262-273.

5 References

[11] S. Atsumi, T. Hanai, J.C. Liao, Non-fermentative pathways for synthesis of branched-chain higher alcohols as biofuels, Nature, 451 (2008) 86-89.

[12] S. Li, J. Wen, X. Jia, Engineering Bacillus subtilis for isobutanol production by heterologous Ehrlich pathway construction and the biosynthetic 2-ketoisovalerate precursor pathway overexpression, Applied microbiology and biotechnology, 91 (2011) 577-589.

[13] K.M. Smith, K.M. Cho, J.C. Liao, Engineering Corynebacterium glutamicum for isobutanol production, Applied microbiology and biotechnology, 87 (2010) 1045-1055.

[14] B. Krutsakorn, K. Honda, X. Ye, T. Imagawa, X. Bei, K. Okano, H. Ohtake, In vitro production of n-butanol from glucose, Metabolic engineering, 20 (2013) 84-91.

[15] K. Vollherbst-Schneck, J.A. Sands, B.S. Montenecourt, Effect of butanol on lipid composition and fluidity of Clostridium acetobutylicum ATCC 824, Applied and environmental microbiology, 47 (1984) 193-194.

[16] Y.H.P. Zhang, Simpler Is Better: High-Yield and Potential Low-Cost Biofuels Production through Cell-Free Synthetic Pathway Biotransformation (SyPaB), Acs Catal, 1 (2011) 998-1009.

[17] A. Oudshoorn, L.A.M. van der Wielen, A.J.J. Straathof, Assessment of Options for Selective 1-Butanol Recovery from Aqueous Solution, Ind Eng Chem Res, 48 (2009) 7325-7336.

[18] B. Sommer, H. von Moeller, M. Haack, F. Qoura, C. Langner, G. Bourenkov, D. Garbe, B. Loll, T. Bruck, Detailed Structure-Function Correlations of Bacillus subtilis Acetolactate Synthase, Chembiochem : a European journal of chemical biology, (2014).

[19] S. Bastian, X. Liu, J.T. Meyerowitz, C.D. Snow, M.M. Chen, F.H. Arnold, Engineered ketol-acid reductoisomerase and alcohol dehydrogenase enable anaerobic 2-methylpropan-1-ol production at theoretical yield in Escherichia coli, Metabolic engineering, 13 (2011) 345-352.

[20]   R. Dumas, V. Biou, F. Halgand, R. Douce, R.G. Duggleby, Enzymology, structure, and dynamics of acetohydroxy acid isomeroreductase, Accounts of chemical research, 34 (2001) 399-408.

[21]   M.J. Rane, K.C. Calvo, Reversal of the nucleotide specificity of ketol acid reductoisomerase by site-directed mutagenesis identifies the NADPH binding site, Archives of biochemistry and biophysics, 338 (1997) 83-89.

[22]   R. Dumas, D. Job, J.Y. Ortholand, G. Emeric, A. Greiner, R. Douce, Isolation and kinetic properties of acetohydroxy acid isomeroreductase from spinach (Spinacia oleracea) chloroplasts overexpressed in Escherichia coli, The Biochemical journal, 288 (Pt 3) (1992) 865-874.

[23]   R. Tyagi, S. Duquerroy, J. Navaza, L.W. Guddat, R.G. Duggleby, The crystal structure of a bacterial class II ketol-acid reductoisomerase: domain conservation and evolution, Protein science : a publication of the Protein Society, 14 (2005) 3089-3100.

[24]   H.J. Ahn, S.J. Eom, H.J. Yoon, B.I. Lee, H. Cho, S.W. Suh, Crystal structure of class I acetohydroxy acid isomeroreductase from Pseudomonas aeruginosa, Journal of molecular biology, 328 (2003) 505-515.

[25]   A.M. Lesk, NAD-binding domains of dehydrogenases, Current opinion in structural biology, 5 (1995) 775-783.

[26]   S. Brinkmann-Chen, T. Flock, J.K.B. Cahn, C.D. Snow, E.M. Brustad, J.A. McIntosh, P. Meinhold, L. Zhang, F.H. Arnold, General approach to reversing ketol-acid reductoisomerase cofactor dependence from NADPH to NADH, P Natl Acad Sci USA, 110 (2013) 10946-10951.

[27]   GESTIS Substance Database.

[28]   P. Durre, Fermentative butanol production: bulk chemical and biofuel, Annals of the New York Academy of Sciences, 1125 (2008) 353-362.

[29]   S. Dusseaux, C. Croux, P. Soucaille, I. Meynial-Salles, Metabolic engineering of Clostridium acetobutylicum ATCC 824 for the high-yield production of a biofuel

composed of an isopropanol/butanol/ethanol mixture, Metabolic engineering, 18 (2013) 1-8.

[30] Y.L. Lin, H.P. Blaschek, Butanol Production by a Butanol-Tolerant Strain of Clostridium acetobutylicum in Extruded Corn Broth, Applied and environmental microbiology, 45 (1983) 966-973.

[31] Z.H. Zhou, W.C. Liao, R.H. Cheng, J.E. Lawson, D.B. McCarthy, L.J. Reed, J.K. Stoops, Direct evidence for the size and conformational variability of the pyruvate dehydrogenase complex revealed by three-dimensional electron microscopy - The "breathing" core and its functional relationship to protein dynamics, J Biol Chem, 276 (2001) 21704-21713.

[32] B. Sommer, D. Garbe, P. Schrepfer, T. Bruck, Characterization of a highly thermostable beta-hydroxybutyryl CoA dehydrogenase from Clostridium acetobutylicum ATCC 824, J Mol Catal B-Enzym, 98 (2013) 138-144.

[33] P. Kursula, J. Ojala, A.M. Lambeir, R.K. Wierenga, The catalytic cycle of biosynthetic thiolase: a conformational journey of an acetyl group through four binding modes and two oxyanion holes, Biochemistry, 41 (2002) 15543-15556.

[34] H. Staack, J.F. Binstock, H. Schulz, Purification and properties of a pig heart thiolase with broad chain length specificity and comparison of thiolases from pig heart and Escherichia coli, J Biol Chem, 253 (1978) 1827-1831.

[35] A.M. Haapalainen, G. Merilainen, R.K. Wierenga, The thiolase superfamily: condensing enzymes with diverse reaction specificities, Trends in biochemical sciences, 31 (2006) 64-71.

[36] G. Merilainen, V. Poikela, P. Kursula, R.K. Wierenga, The thiolase reaction mechanism: the importance of Asn316 and His348 for stabilizing the enolate intermediate of the Claisen condensation, Biochemistry, 48 (2009) 11011-11025.

[37] G. Merilainen, W. Schmitz, R.K. Wierenga, P. Kursula, The sulfur atoms of the substrate CoA and the catalytic cysteine are required for a productive mode of substrate binding

in bacterial biosynthetic thiolase, a thioester-dependent enzyme, The FEBS journal, 275 (2008) 6136-6148.

[38] M.A. Palmer, E. Differding, R. Gamboni, S.F. Williams, O.P. Peoples, C.T. Walsh, A.J. Sinskey, S. Masamune, Biosynthetic thiolase from Zoogloea ramigera. Evidence for a mechanism involving Cys-378 as the active site base, J Biol Chem, 266 (1991) 8369-8375.

[39] Y. Modis, R.K. Wierenga, Crystallographic analysis of the reaction pathway of Zoogloea ramigera biosynthetic thiolase, Journal of molecular biology, 297 (2000) 1171-1182.

[40] M. Hedl, A. Sutherlin, E.I. Wilding, M. Mazzulla, D. McDevitt, P. Lane, J.W. Burgner, 2nd, K.R. Lehnbeuter, C.V. Stauffacher, M.N. Gwynn, V.W. Rodwell, Enterococcus faecalis acetoacetyl-coenzyme A thiolase/3-hydroxy-3-methylglutaryl-coenzyme A reductase, a dual-function protein of isopentenyl diphosphate biosynthesis, Journal of bacteriology, 184 (2002) 2116-2122.

[41] S.A. Kim, L. Copeland, Acetyl Coenzyme A Acetyltransferase of Rhizobium sp. (Cicer) Strain CC 1192, Applied and environmental microbiology, 63 (1997) 3432-3437.

[42] B. Middleton, The kinetic mechanism and properties of the cytoplasmic acetoacetyl-coenzyme A thiolase from rat liver, Biochem J, 139 (1974) 109-121.

[43] D.P. Wiesenborn, F.B. Rudolph, E.T. Papoutsakis, Thiolase from Clostridium acetobutylicum ATCC 824 and Its Role in the Synthesis of Acids and Solvents, Applied and environmental microbiology, 54 (1988) 2717-2722.

[44] Z.L. Boynton, G.N. Bennet, F.B. Rudolph, Cloning, sequencing, and expression of clustered genes encoding beta-hydroxybutyryl-coenzyme A (CoA) dehydrogenase, crotonase, and butyryl-CoA dehydrogenase from Clostridium acetobutylicum ATCC 824, Journal of bacteriology, 178 (1996) 3015-3024.

[45] A. Dhar, K. Dhar, J.P. Rosazza, Purification and characterization of a Galactomyces reessii hydratase that converts 3-methylcrotonic acid to 3-hydroxy-3-methylbutyric acid, Journal of industrial microbiology & biotechnology, 28 (2002) 81-87.

5 References

[46] M. Dieuaide-Noubhani, D. Novikov, J. Vandekerckhove, P.P. Veldhoven, G.P. Mannaerts, Identification and characterization of the 2-enoyl-CoA hydratases involved in peroxisomal beta-oxidation in rat liver, The Biochemical journal, 321 (Pt 1) (1997) 253-259.

[47] A. Frandi, P. Zucca, M. Marvasi, G. Mastromei, E. Sanjust, B. Perito, Bacillus subtilis fadB (ysiB) gene encodes an enoyl-CoA hydratase, Ann Microbiol, 61 (2011) 371-374.

[48] S.J. Park, S.Y. Lee, Identification and characterization of a new enoyl coenzyme A hydratase involved in biosynthesis of medium-chain-length polyhydroxyalkanoates in recombinant Escherichia coli, Journal of bacteriology, 185 (2003) 5391-5397.

[49] R.M. Waterson, R.L. Hill, G.M. Hass, Castelli.Fj, Purification and Characterization of Crotonase from Clostridium-Acetobutylicum, Journal of Biological Chemistry, 247 (1972) 5266-5271.

[50] C.K. Engel, M. Mathieu, J.P. Zeelen, J.K. Hiltunen, R.K. Wierenga, Crystal structure of enoyl-coenzyme A (CoA) hydratase at 2.5 angstroms resolution: a spiral fold defines the CoA-binding pocket, The EMBO journal, 15 (1996) 5135-5145.

[51] Y. Feng, H.A. Hofstein, J. Zwahlen, P.J. Tonge, Effect of mutagenesis on the stereochemistry of enoyl-CoA hydratase, Biochemistry, 41 (2002) 12883-12890.

[52] H.A. Hofstein, Y. Feng, V.E. Anderson, P.J. Tonge, Role of glutamate 144 and glutamate 164 in the catalytic mechanism of enoyl-CoA hydratase, Biochemistry, 38 (1999) 9508-9516.

[53] C.K. Engel, T.R. Kiema, J.K. Hiltunen, R.K. Wierenga, The Crystal Structure of Enoyl-CoA Hydratase Complexed with Octanoyl-CoA Reveals the Structural Adaptations Required for Binding of a Long Chain Fatty Acid-CoA Molecule, Journal of molecular biology, 275 (1998) 859-847.

[54] B. Sommer, M. Haack, D. Garbe, T. Brück, Catalytic Modules in Non-Natural Butanol Biosynthesis: Conversion of the Key Intermediate Crotylalcohol to NButanol via a Designed Enzyme Cascade., JSM Biotechnol Bioeng, 1 (2013).

[55]   B. List, Proline-catalyzed asymmetric reactions, Tetrahedron, 58 (2002) 5573-5590.

[56]   J.A. Theruvathu, P. Jaruga, R.G. Nath, M. Dizdaroglu, P.J. Brooks, Polyamines stimulate the formation of mutagenic 1,N2-propanodeoxyguanosine adducts from acetaldehyde, Nucleic acids research, 33 (2005) 3513-3520.

[57]   M.A. Larkin, G. Blackshields, N.P. Brown, R. Chenna, P.A. McGettigan, H. McWilliam, F. Valentin, I.M. Wallace, A. Wilm, R. Lopez, J.D. Thompson, T.J. Gibson, D.G. Higgins, Clustal W and Clustal X version 2.0, Bioinformatics, 23 (2007) 2947-2948.

[58]   P. Gouet, X. Robert, E. Courcelle, ESPript/ENDscript: Extracting and rendering sequence and 3D information from atomic structures of proteins, Nucleic acids research, 31 (2003) 3320-3323.

[59]   L.A. Kelley, M.J. Sternberg, Protein structure prediction on the Web: a case study using the Phyre server, Nature protocols, 4 (2009) 363-371.

[60]   J. Soding, A. Biegert, A.N. Lupas, The HHpred interactive server for protein homology detection and structure prediction, Nucleic Acids Res, 33 (2005) W244-248.

[61]   A.S. Konagurthu, J.C. Whisstock, P.J. Stuckey, A.M. Lesk, MUSTANG: a multiple structural alignment algorithm, Proteins, 64 (2006) 559-574.

[62]   S.K. Saha, L. Uma, G. Subramanian, An improved method for marine cyanobacterial DNA isolation, World J Microb Biot, 21 (2005) 877-881.

[63]   J. Sambrook, D.W. Russell, Molecular cloning: a laboratory manual, Cold Spring Harbor Laboratory2001.

[64]   T. Baba, T. Ara, M. Hasegawa, Y. Takai, Y. Okumura, M. Baba, K.A. Datsenko, M. Tomita, B.L. Wanner, H. Mori, Construction of Escherichia coli K-12 in-frame, single-gene knockout mutants: the Keio collection, Molecular systems biology, 2 (2006) 2006 0008.

[65]   A. Aitken, M. Learmonth, Protein Determination by UV Absorption, in: J. Walker (Ed.) The Protein Protocols Handbook, Humana Press2002, pp. 3-6.

5 References

[66] W.J. Waddell, A simple ultraviolet spectrophotometric method for the determination of protein, The Journal of laboratory and clinical medicine, 48 (1956) 311-314.

[67] P. Wolf, A critical reappraisal of Waddell's technique for ultraviolet spectrophotometric protein estimation, Analytical biochemistry, 129 (1983) 145-155.

[68] C.K. Riener, G. Kada, H.J. Gruber, Quick measurement of protein sulfhydryls with Ellman's reagent and with 4,4'-dithiodipyridine, Analytical and bioanalytical chemistry, 373 (2002) 266-276.

[69] J.H. Zhang, T.D. Chung, K.R. Oldenburg, A Simple Statistical Parameter for Use in Evaluation and Validation of High Throughput Screening Assays, Journal of biomolecular screening, 4 (1999) 67-73.

[70] K.E. Jaeger, T. Eggert, A. Eipper, M.T. Reetz, Directed evolution and the creation of enantioselective biocatalysts, Appl Microbiol Biot, 55 (2001) 519-530.

[71] Papworth C, Bauer JC, Braman J, W. DA, QuikChange site-directed mutagenesis, Strategies, 9 (1996) 3-4.

[72] M.T. Reetz, Caster 2.0.

[73] M.T. Reetz, J.D. Carballeira, Iterative saturation mutagenesis (ISM) for rapid directed evolution of functional enzymes, Nat Protoc, 2 (2007) 891-903.

[74] D. Leyval, D. Uy, S. Delaunay, J.L. Goergen, J.M. Engasser, Characterisation of the enzyme activities involved in the valine biosynthetic pathway in a valine-producing strain of Corynebacterium glutamicum, Journal of biotechnology, 104 (2003) 241-252.

[75] J. Durner, O.C. Knorzer, P. Boger, Ketol-Acid Reductoisomerase from Barley (Hordeum vulgare) (Purification, Properties, and Specific Inhibition), Plant physiology, 103 (1993) 903-910.

[76] K. Kiritani, S. Narise, R.P. Wagner, The dihydroxy acid dehydratase of Neurospora crassa, The Journal of biological chemistry, 241 (1966) 2042-2046.

[77]   R. Dumas, J. Joyard, R. Douce, Purification and characterization of acetohydroxyacid reductoisomerase from spinach chloroplasts, The Biochemical journal, 262 (1989) 971-976.

[78]   S.M. Arfin, H.E. Umbarger, Purification and properties of the acetohydroxy acid isomeroreductase of Salmonella typhimurium, The Journal of biological chemistry, 244 (1969) 1118-1127.

[79]   N.S. Scrutton, A. Berry, R.N. Perham, Redesign of the coenzyme specificity of a dehydrogenase by protein engineering, Nature, 343 (1990) 38-43.

[80]   H.F. Gilbert, B.J. Lennox, C.D. Mossman, W.C. Carle, The relation of acyl transfer to the overall reaction of thiolase I from porcine heart, J Biol Chem, 256 (1981) 7371-7377.

[81]   B. Maekawa, N. Koyama, Y. Doi, Purification and Properties of 3-Ketothiolase from Alcaligenes-Latus, Biotechnology letters, 15 (1993) 691-696.

[82]   A. Karlstrom, G. Zhong, C. Rader, N.A. Larsen, A. Heine, R. Fuller, B. List, F. Tanaka, I.A. Wilson, C.F. Barbas, 3rd, R.A. Lerner, Using antibody catalysis to study the outcome of multiple evolutionary trials of a chemical task, Proceedings of the National Academy of Sciences of the United States of America, 97 (2000) 3878-3883.

[83]   L.M. Harris, L. Blank, R.P. Desai, N.E. Welker, E.T. Papoutsakis, Fermentation characterization and flux analysis of recombinant strains of Clostridium acetobutylicum with an inactivated solR gene, Journal of industrial microbiology & biotechnology, 27 (2001) 322-328.

[84]   J. Wagner, R.A. Lerner, C.F. Barbas, 3rd, Efficient aldolase catalytic antibodies that use the enamine mechanism of natural enzymes, Science, 270 (1995) 1797-1800.

6 Appendix

6.1 List of abbreviations and symbols

%	percent	EC	enzyme commission
% v/v	percent volume per volume	EDTA	ethylenediaminetetraacetic acid
% w/v	percent weight per volume	FAD	flavin adenine dinucleotide
°C	degree Celsius	FMN	flavin mononucleotide
μ	micro ($1 * 10^{-6}$)	FPLC	fast protein liquid
μl	micro liter	fwd	forward
A	absorbance	g	gram
ADH	alcohol dehydrogenase	GC	gas chromatography
ALDH	aldehyde dehydrogenase	GDH	glucose dehydrogenase
ALS	acetolactate synthase	HBD	Hydroxybutyryl-CoA dehydrogenase
Avg	average	HEPES	4-(2-hydroxyethyl)-1-piperazineethanesulfonic acid
Crt	crotonase	HPLC	high-performance liquid chromatography
CV	coefficient of variation	IPTG	isopropyl-ß-1-thiogalactopyranoside
dd	double distilled	IS_{50}	solvent concentration which causes loss of 50 % activity
DHAD	dihydroxyacid dehydratase	IT_{50}	temperature which causes loss of 50 % activity

DNA	deoxyribonucleic acid	kana	Kanamycin
dNTP	deoxyribonucleoside triphosphate	KARI	Ketol-acid reductoisomerase
E. coli	*Escherichia coli*	k_{cat}	turnover number
KDC	2-ketoacid decarboxylase	rev	reverse
KDGA	2-keto-3-deoxygluconate aldolase	RT	room temperature
k_i	inactivation constant	SDS	sodium dodecyl sulfate
K_m	Michaelis Menten constant	TB	terrific broth
LB	Luria-Bertani broth	TCR	trans-2-enoyl-CoA reductase
ml	milliliter	TE	Tris-EDTA
mM	millimol per liter	Thl	thiolase
Mr	*Meiothermus ruber*	TPP	thiamine pyrophosphate
NADH NADP$^+$	nicotinamide adenine dinucleotide	Tris	tris(hydroxymethyl)aminomethane
NADPH NADP$^+$	nicotinamide adenine dinucleotide phosphate	U	unit [μmol min^{-1}]
NMR	nuclear magnetic resonance	UV	ultra violet
OD	optical density	Vis	visible
PAGE	polyacrylamide gel electrophoresis	WT	wild type
PCR	polymerase chain reaction	YASARA	Yet Another Scientific Artificial Reality Application (software)
PDC	pyruvate decarboxylase	YqjM	2-enoate reductase
Pfu	*Pyrococcus furiosus*	τ	half-life

6 Appendix

6.2   List of figures

6.3 List of tables

Related scientific journal articles

Cell-Free Metabolic Engineering: Production of Chemicals by Minimized Reaction Cascades

Jan-Karl Guterl,[a] Daniel Garbe,[b] Jörg Carsten,[a] Fabian Steffler,[a] Bettina Sommer,[b] Steven Reiße,[b] Anja Philipp,[a] Martina Haack,[b] Broder Rühmann,[a] Andre Koltermann,[c] Ulrich Kettling,[c] Thomas Brück,[b] and Volker Sieber*[a]

The limited supply of fossil resources demands the development of renewable alternatives to petroleum-based products. Here, biobased higher alcohols such as isobutanol are versatile platform molecules for the synthesis of chemical commodities and fuels. Currently, their fermentation-based production is limited by the low tolerance of microbial production systems to the end products and also by the low substrate flux into cell metabolism. We developed an innovative cell-free approach, utilizing an artificial minimized glycolytic reaction cascade that only requires one single coenzyme. Using this toolbox the cell-free production of ethanol and isobutanol from glucose was achieved. We also confirmed that these streamlined cascades functioned under conditions at which microbial production would have ceased. Our system can be extended to an array of industrially-relevant molecules. Application of solvent-tolerant biocatalysts potentially allows for high product yields, which significantly simplifies downstream product recovery.

Introduction

The development of sustainable, biomass-based production strategies is influenced by factors such as availability of cheap, nonfood biomass, its efficient depolymerization into key intermediates (i.e., sugars), and flexible, efficient technologies to convert such intermediate streams into chemical products that are cost-competitive with petroleum equivalents. Alcohols, such as ethanol and isobutanol, are excellent molecular platforms for the sustainable production of chemical commodities and fuels. Presently, biotechnological approaches for the conversion of biomass to alcohols focus on well-established microbial fermentation processes.[1–5]

However, the conditions of fermentation processes remain restricted to the physiological limits of cellular production systems. Key barriers for the cost-effective implementation of fermentation processes include the low tolerance to temperature fluctuations, elevated temperatures in general, and diverse solvent conditions, which can result in low conversion efficiencies and yields. Additionally, the multitude of cellular metabolic pathways can often lead to the unintended use of non-productive reaction pathways. Despite advances in genetic engineering, streamlining these metabolic networks for optimal product formation at an organism level is prohibitively difficult and due to the high complexity continues to be rather unpredictable.

A prominent example is the production of isobutanol using recombinant fermentation in *Escherichia coli*. Concentrations of as low as 1–2% (v/v) isobutanol can already induce toxic effects in the microbial production host, reducing both growth rates and precursor synthesis and resulting in extremely low product yields.[1,4,5] Additionally, the cost-effective pretreatment of biomass usually produces toxic or nonfermentable components that limit microbial growth and product yields.[6] Therefore, cell-based production strategies for isobutanol and other

industrial chemicals have difficulties to compete economically with petroleum-derived equivalents.

The solution for this problem might be surprisingly simple: leave out the cells and exclusively employ purified biocatalysts. Consequently, cell-associated process barriers such as substrate or product toxicity or the undesired, substrate-induced redirection into an alternative metabolism pathway can be eliminated.[7,8] Due to their reduced molecular complexity and rapid adaptability to harsh industrial reaction conditions, designed biocatalytic processes are superior to their cellular counterparts. Indeed, the concept of cell-free synthesis was already introduced more than 100 years ago by Buchner, who accomplished ethanol production with crude yeast cell extracts.[9] Since then, enzymatic reactions have been established as valuable tools for organic synthesis, whereby most reactions comprise only one or two enzyme-catalyzed steps. Multistep reactions resembling natural pathways (>4 enzymes) are currently either being used for analytical purposes (e.g., for the identification of bottlenecks in cellular dihydroxyacetonephosphate synthesis[10,11]) or for the production of structurally complex,

[a] Dr. J.-K. Guterl, J. Carsten, F. Steffler, A. Philipp, B. Rühmann, Prof. V. Sieber
Lehrstuhl für Chemie Biogener Rohstoffe
Technische Universität München
Schulgasse 16, 94315 Straubing (Germany)
Fax: (+49) 9421187310
E-mail: sieber@tum.de

[b] Dr. D. Garbe, B. Sommer, S. Reiße, M. Haack, Prof. T. Brück
Fachgebiet Industrielle Biokatalyse
Technische Universität München
Lichtenbergstr. 4, 85748 Garching (Germany)

[c] Prof. A. Koltermann, Dr. U. Kettling
Clariant Produkte Deutschland GmbH
Staffelseestr. 6, 81477 München (Germany)

valuable compounds (such as isotope-labeled nucleotides[12, 13]), but the utilization of these processes has only recently been recognized as a promising technique for chemical synthesis of cheap and renewable base chemicals.[8]

Since many natural metabolic pathways have been shaped by evolution to regenerate cofactors such as adenosine triphosphate (ATP) and nicotinamide adenine dinucleotide phosphate (NAD(P)H), one particular issue of cell-free systems is the need for a closed cofactor balance in absence of the cell-metabolism. A particularly noteworthy example is the reconstruction of yeast Embden–Meyerhof-pathway by Scopes and coworkers which required a total of 13 enzymes and NAD(H) as well as well-defined concentrations of adenosine driphosphate (ADP) and ATP.[14] ATP, which accumulates in the absence of a viable cellular metabolism, is required for the initiation of glycolysis. To manage balanced ATP cycling, the hydrolysis of excess ATP had to be adjusted very carefully or eliminated by using highly toxic arsenate.

Consequently, to yield stable and technically feasible cell-free processes, it is essential to minimize the number of enzymes and eliminate ATP-driven reactions. This goal can be achieved by designing artificial in vitro pathways. The design of these non-natural metabolic pathways in a cell-free environment is thereby only restricted by thermodynamic limitations and enzyme performance. One recent example for a successful engineering approach to a cell-free pathway is the conversion of different sugar derivatives to molecular hydrogen by Zhang et al., who designed a novel reaction cycle based on the pentose phosphate pathway and demonstrated that their system has the necessary adaptation capability to react to changes of substrate or product requirements.[15–17]

We have now designed a completely artificial glycolytic reaction cascade for the conversion of glucose to pyruvate that is comprised of only four enzyme-catalyzed reactions, thereby also eliminating any phosphorylation requirements. The artificial pathway is completely redox balanced, and it requires only a single molecular shuttle (NAD$^+$). Pyruvate is a central intermediate from which molecules like ethanol or isobutanol can be produced with few additional enzymatic steps. The novel cell-free engineering approach allowed production of ethanol and isobutanol under reaction conditions that are prohibitive to any cell-based microbial equivalents. As our reaction cascade is designed as a general process, other products can be envisioned as future targets.

Results and Discussion

General pathway design

The production of pyruvate from glucose was achieved by a modified non-phosphorylative Entner-Doudoroff-Pathway (np-ED) derived from hyperthermophilic archaea.[18] One mole of glucose was converted into two moles pyruvate, coupled with the reduction of two NAD$^+$ equivalents (Figure 1). To eliminate phosphorylation and dephosphorylation steps of the natural np-ED pathway and thus reduce the number of required enzymes, we exploited the substrate promiscuity of an

archaeal dihydroxy acid dehydratase[19] (DHAD) which catalyzes both the transformation of glycerate to pyruvate as well as the conversion of gluconate to 2-keto-3-desoxygluconate. The molecular efficiency of DHAD (see Figure 1) allows for the consolidated conversion of glucose to pyruvate with just four enzymes: glucose dehydrogenase[20] (GDH), gluconate/glycerate/dihydroxyacid dehydratase,[19] 2-keto-3-desoxygluconate aldolase[21] (KDGA), and glyceraldehyde dehydrogenase[22, 23] (AlDH). AlDH together with DHAD redirects glyceraldehyde produced through aldol cleavage towards pyruvate formation. Enzymes of the cell-free reaction cascade were chosen based on their stability and selectivity. In general thermostable enzymes from thermophiles are preferred, as they are prone to tolerate higher process temperatures and higher solvent concentrations.[24, 25] Thus, enhanced thermostability allows for increased reaction rates, a higher rate of substrate diffusion, lower viscosities, better phase separation, and decreased bacterial contamination of the reaction medium. As demands for substrate selectivity vary at different reaction stages, enzyme fidelity has to be selected accordingly. The substrate tolerance of the *Sulfolobus solfataricus* DHAD was reported recently.[19] We found that in its recombinant form the enzyme has a specific activity of 0.66 U mg^{-1} for gluconate and 0.011 U mg^{-1} for glycerate respectively. In the conversion of glucose to the key intermediate pyruvate, DHAD allows for parallel conversion of gluconate and glycerate (Figure 1). In contrast to DHAD, an AlDH was chosen that is specific for glyceraldehyde and does not accept other aldehydes such as acetaldehyde[22] or isobutyraldehyde, which are downstream reaction intermediates. These prerequisites were met by a NADPH-dependent aldehyde dehydrogenase that was able to convert only D-glyceraldehyde to D-glycerate with excellent selectivity. In order to minimize reaction complexity, the designed pathway was further consolidated to use the coenzyme NADH as the only electron carrier. Consequently, a directed evolution approach was used to engineer an AlDH variant with a greater activity for NADH.[26] Provided that subsequent reactions maintain redox-neutrality, pyruvate can potentially be converted to an array of industrial platform chemicals without the continuous addition of any electron shuttle.

Ethanol synthesis

To demonstrate the feasibility of the cell-free synthesis toolbox, glucose was converted to pyruvate using the enzyme cascade described above. In a subsequent two-step reaction pyruvate was converted to acetaldehyde and then to ethanol by action of pyruvate decarboxylase[27] (PDC) and alcohol dehydrogenase[28, 29] (ADH). As no variants of PDC with thermophilic origin have been reported so far, the equivalent enzyme from the mesophilic bacterium *Zymomonas mobilis* was selected due to its relatively high thermal tolerance and activity. Despite its mesophilic origin, *Z. mobilis* PDC is thermostable up to 50 °C (see Table 1) which is in accord with the temperature range of more thermostable enzymes from thermophiles. Consequently, experiments were carried out at 50 °C. The six required enzymes were recombinantly expressed in *E. coli* and subjected
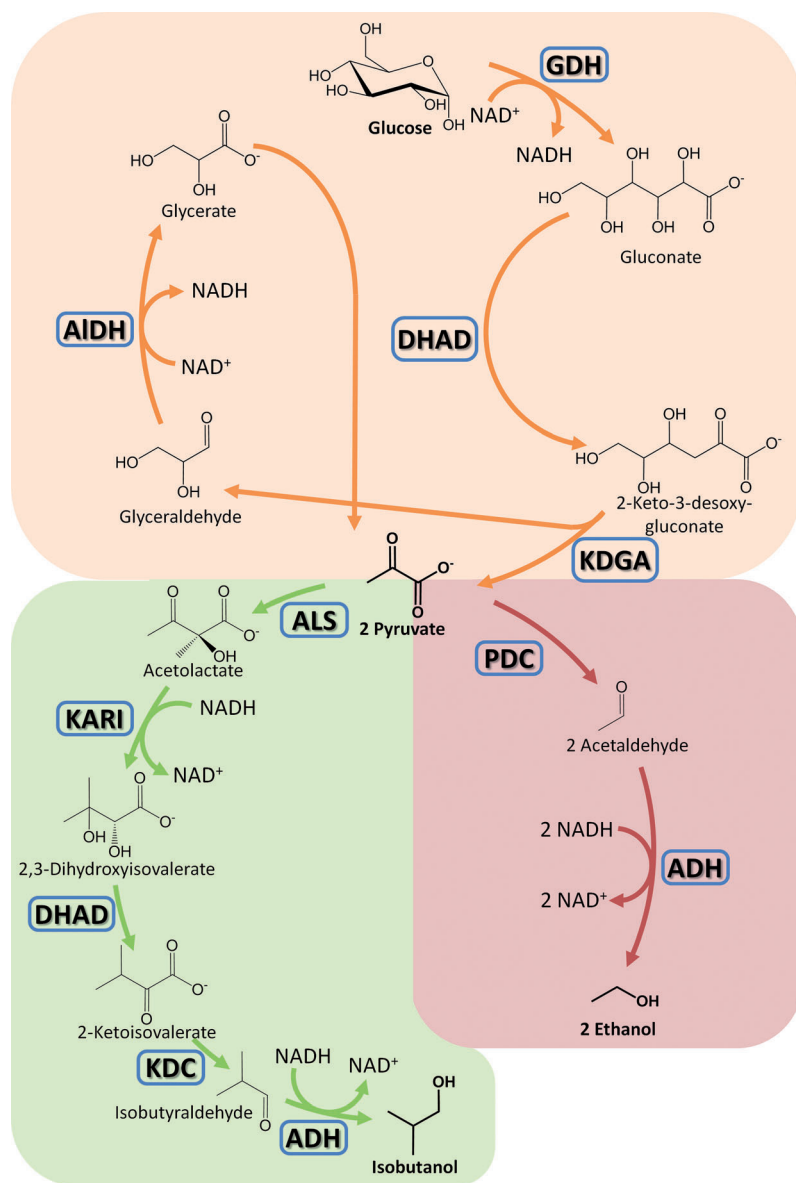
Figure 1. Schematic representation of cell-free reaction pathways to ethanol and isobutanol via minimized reaction cascades. In the first part of the reaction (top box) glucose is converted into two molecules of pyruvate. Depending on the desired final product and the enzymes applied, pyruvate can be either directed to ethanol (lower right box) or isobutanol synthesis (lower left box) in the second part of the reaction cascade. For clarity, protons and molecules of CO_2 and H_2O that are acquired or released in the reactions are not shown.

substrate of DHAD, a temporary accumulation of up to 8 mm was detected during the first 10 h of the reaction. In contrast, glycerate and acetaldehyde concentrations did not exceed 4 mm, while pyruvate was not detectable.

While residual intermediates generally accumulated at the end of the reaction cycle, the maximum gluconate concentration was measured between 8 and 10 h during the course of the reaction. Notably, undesired side-products such as lactate and acetate were not detected, indicating that the selected enzymes did provide the necessary substrate specificity. Although the enzyme-catalyzed reaction was not completed over the course of the experiment, the cumulative mass of all detectable intermediates and products gives a yield in excess of 80 %.

Isobutanol synthesis

While specialized yeasts can tolerate ethanol at higher concentrations, longer-chain alcohols ($N \geq 4$) are incompatible with microbial physiology already at low concentrations.[32] Consequently, an alcohol as large as isobutanol, despite major cell-engineering efforts, has not been synthesized using microorganisms at a concentration higher than 2–2.5 % w/v.[4]

While a non-natural isobutanol pathway has been described previously in the context of a cell-based system,[1] we have advanced the concept and converted pyruvate to isobutanol using only four additional enzymes (see Figure 1, Table 1) in a completely cell-free environment. Initially, two pyruvate molecules were joined by acetolactate synthase[30] (ALS) to yield acetolactate, which is further converted by ketolacid reductoisomerase[33] (KARI) resulting in the natural DHAD substrate dihydroxyisovalerate. DHAD then catalyzes the conversion of dihydroxyisovalerate into 2-ketoisovalerate.

The enzymes 2-ketoacid decarboxylase[27,31] (KDC) and an ADH[28,29] produced the final product, isobutanol, via isobutyraldehyde. Again the substrate tolerance of DHAD is exploited to minimize the total number of enzymes required.

to different purification regimes. Using this set of enzymes, together with 5 mm NAD^+, we were able to convert 25 mm glucose to 28.7 mm ethanol (molar yield of 57.4 %) in 19 h (Figure 2). Based on the initial substrate and coenzyme concentrations these results clearly demonstrate the successful recycling of NAD^+ and NADH. As the overall product yield exceeded 50 %, it was also shown that the glyceraldehyde resulting from 2-keto-3-desoxygluconate cleavage was successfully redirected towards pyruvate. Next to ethanol and glucose, reaction intermediates such as gluconate, 2-keto-3-desoxygluconate, pyruvate, glycerate, and acetaldehyde were monitored during the course of the reaction. Especially for gluconate, the

Table 1. Enzymes used in the cell-free synthesis of ethanol and isobutanol[a].

Enzyme	EC[b]	Source organism	Activity[c] [U mg^{-1}]	Half-life [h]	T-Optimum [°C]	E_{50}[d] [% v/v]	I_{50}[e] [% v/v]
GDH	1.1.1.47	*S. solfataricus*	15	> 24	70	30 (45 °C)	9 (45 °C)
DHAD	4.2.1.39	*S. solfataricus*	0.66 0.011 0.38	17	70	15 (50 °C)	4 (50 °C)
KDGA	4.2.1.14	*S. acidocaldarius*	4	> 24	99[21]	15 (60 °C)	> 12 (60 °C)[f]
AlDH	1.2.1.3	*Thermoplasma acidophilum*[g]	1	12	63[23]	13 (60 °C)	3 (50 °C)
PDC	4.1.1.1	*Z. mobilis*	64	22	50	20 (50 °C)	8 (45 °C)
ADH	1.1.1.1	*Geobacillus stearothermophilus*	210 83	> 24	> 60[28]	25 (50 °C)	5 (50 °C)
ALS	2.2.1.6	*Bacillus subtilis*	30	12	37[30]	n.d.	4 (50 °C)
KARI	1.1.1.86	*Meiothermus ruber*	0.7	34	55	n.d.	8 (40 °C)
KDC	4.1.1.72	*Lactococcus lactis*	150	> 24	50[31]	n.d.	4 (45 °C)

[a] For details concerning cloning and expression see methods section. Activity and half-life measurements were taken at $T = 50$ °C. [b] Enzyme classification number. [c] Activity for natural substrates, DHAD for gluconate, glycerate and dihydroxyisovalerate, ADH for acetaldehyde and isobutyraldehyde (resp.) as substrates. [d] E_{50}: Ethanol concentration which causes loss of 50% activity. n.d.: not determined. [e] I_{50}: Isobutanol concentration which causes loss of 50% activity. [f] Above solubility. [g] Enzyme was engineered.

biocatalysts with respect to thermal stability, solvent tolerance, and activity profiles (Table 1). To allow experimental comparison, the reaction conditions remained the same as described previously. Measurements indicated that 19.1 mm glucose was converted to 10.3 mm isobutanol within 23 h, which corresponds to a molar yield of 53% (Figure 3). During the first 10 h of the reaction, the product formation rate was 0.7 mm h^{-1}, which is similar to the ethanol formation rate of 2.2 mm h^{-1} (2 mol of ethanol instead of 1 mol of isobutanol is produced from 1 mol glucose). In contrast to the ethanol synthesis, only a minor accumula-

By analogy to ethanol production, the enzymes of the general pyruvate synthesis route differ from the following three tion of the DHAD substrates gluconate and glycerate was detected, resulting in a maximum concentration of 1.8 mm for
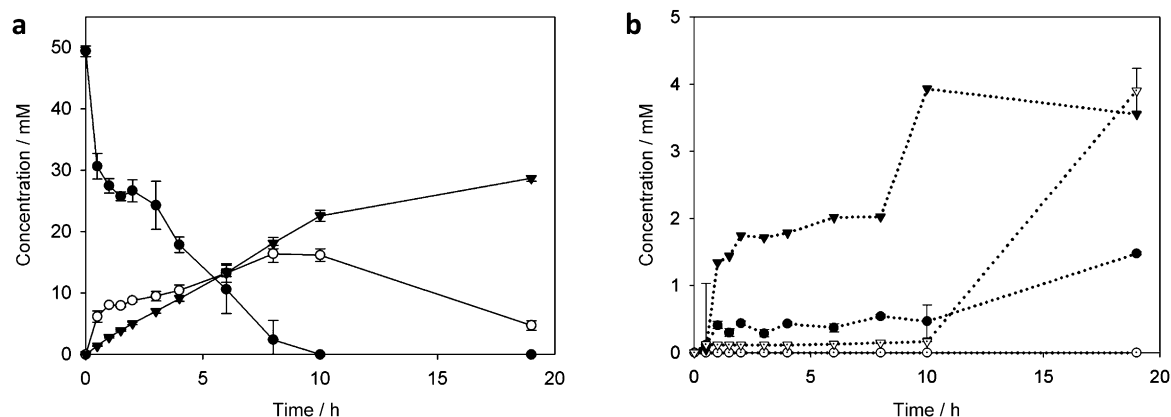

Figure 2. Cell-free synthesis of ethanol. a) Intermediates in concentrations > 5 mm; ●: glucose, ○: gluconate, ▼: ethanol. b) Intermediates in concentrations < 5 mm; ●: KDG, ○: pyruvate, ▼: glycerate, ▽: acetaldehyde. Note that the concentration of glucose, gluconate and KDG was duplicated to allow for a better comparison with the ethanol concentration (1 mol glucose is converted to 2 mol ethanol). All data points represent average values from three independent experiments.
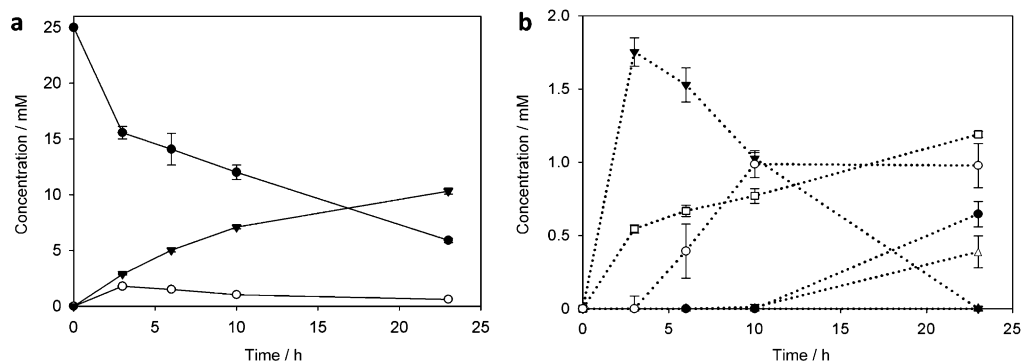

Figure 3. Cell-free synthesis of isobutanol. a) Intermediates in concentrations > 2 mm; ●: glucose, ○: gluconate, ▼: isobutanol. b) Intermediates in concentrations < 2 mm; ●: KDG, △: pyruvate, ▼: glycerate, □: isobutyraldehyde; ○: KIV. DHIV could not be detected at all. All data points represent average values from three independent experiments.

each of these intermediates. Additional reaction intermediates such as 2-keto-3-desoxygluconate, pyruvate, 2-ketoisovalerate, and isobutyraldehyde were measured at low concentrations (maximum 1.2 mM) that slowly increased towards the end of the measurement. Again substrate conversion was not completed within the monitored time. As with cell-free ethanol biosynthesis, quantification of all detectable intermediates gave a yield of 80%.

Solvent tolerance

A key characteristic of cell-free systems is their pronounced tolerance to the presence of higher alcohols. To evaluate solvent tolerance of our artificial enzyme cascade, glucose conversion to ethanol was conducted in the presence of increasing isobutanol concentrations (Figure 4). In contrast to microbial cells, where minor isobutanol concentrations (ca. 1% *v/v*) already result in a loss of productivity, presumably through the loss of membrane integrity,[5] cell-free ethanol productivity and reaction kinetics were not significantly affected by isobutanol concentrations up to 4% (*v/v*). Only in the presence of 6% (*v/v*) isobutanol, did the ethanol productivity rapidly decline (1.4 mM ethanol in 8 h). This demonstrates that cell-free processes have the potential to tolerate much higher solvent concentrations than equivalent whole-cell systems. Based on our current data AlDH has the lowest solvent tolerance, as 3% (*v/v*) isobutanol already induce adverse effects on activity. In contrast, KDGA remains completely active even in a two-phase isobutanol/water system, which forms spontaneously at product concentrations above 12% (*v/v*)[34] (see Table 1). As shown for an engineered transaminase, which remains active in a reaction medium containing 50% DMSO,[35] such shortcomings can be addressed by engineering of the respective protein. In comparison, there is neither a successful example nor a straightforward technology in place to engineer an entire cell for solvent tolerance. It is expected, that all enzymes utilized in our cell-free pathways can be engineered to be as solvent tolerant as KDGA or can be replaced by a stable naturally occurring equivalent, so that isobutanol production can be envisioned in a two-phase system. Product recovery by a simple phase separation would significantly simplify the downstream process-

ing[36] and, while conceivable with a cell-free system, it is highly unlikely to be realized by microbial fermentation.

Conclusions

The stability and minimized complexity of our cell-free system eliminate the barriers of current cell-based production, which hamper the wider industrial exploitation of bio-based platform chemicals. Pyruvate is a central intermediate, which may serve as a starting point for cell-free biosynthesis of other commodity compounds. The enzymatic approach demonstrated here has been minimized in the number of required enzymes and coenzymes and therefore it has the potential to serve as a next generation bio-production system.

Substrate and product concentrations in the herein described experiments are relatively low. For allowing easy product separation, which is a prerequisite for an economically feasible process, the product concentration should be increased above the solubility limit, which for isobutanol is 1.28 M at 20 °C (ca. 95 g L^{-1}). Although the product solubility can be reduced by increasing the process temperature and adjusting the salt concentrations, an increase of substrate concentration (and thereby product concentration) is essential. As 1 mol glucose is converted to 1 mol isobutanol in our system, substrate concentrations have to be chosen at the desired end concentration (230 g L^{-1} glucose) or higher. Furthermore, a continuously running process using a constant substrate feed (glucose syrup) and product removal (organic phase) would be advantageous, given that the enzymes and cofactors could be retained, for example, by immobilization.

Ongoing molecular optimization of individual enzymes allows for iterative improvements and extension of the presented cell-free production systems with a particular focus on activity, thermal stability and solvent tolerance. In addition, the resistance to the inhibitors that are present when hydrolyzed lignocellulosic biomass is used as feedstock can be addressed by enzyme engineering, whereas these inhibitors can be detrimental to cell-based methods.
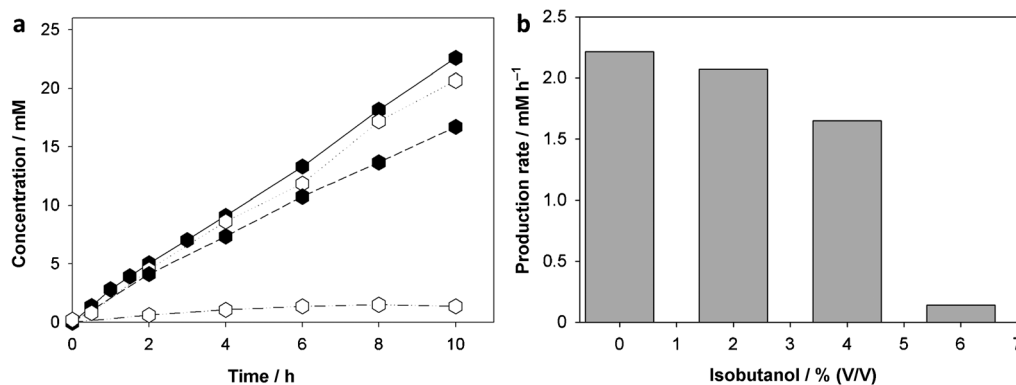

Figure 4. Ethanol production at different isobutanol concentrations. a) ● ——: 0% isobutanol; ○, ●●●●●: 2% isobutanol; ●, – – –: 4% isobutanol; ○, – – –: 6% isobutanol. b) ethanol production rate (mM h^{-1}) plotted against isobutanol concentration.

Experimental Section

Reagents

Restriction enzymes, Klenow fragment, T4 ligase and T4 kinase were purchased from New England Biolabs (Frankfurt, Germany). Phusion polymerase was from Finnzymes (Espoo, Finland), desoxy-nucleotides from Rapidozym (Berlin, Germany). All enzymes were used according to the manufacturers' recommendations, applying the provided buffer solutions. Oligonucleotides were ordered from Thermo Scientific (Ulm, Germany). Full-length genes were synthesized by Geneart (Regensburg, Germany), with optimized *E. coli* codon usage, and delivered in the company's standard plasmids. Porcine heart lactate dehydrogenase (LDH) was bought from Serva (Heidelberg, Germany), *Aspergillus niger* glucose oxidase and horseradish peroxidase from Sigma–Aldrich (Munich, Germany). All chemicals were, unless otherwise stated, purchased in analytical grade from Sigma–Aldrich, Carl Roth (Karlsruhe, Germany), Serva Electrophoresis and Merck (Darmstadt, Germany).

Strains and Plasmids

E. coli BL21(DE3) (F⁻ *ompT hsdSB* (rB⁻ mB⁻) *gal dcm* (DE3)) was purchased from Novagen (Nottingham, UK), *E. coli* XL1-Blue (*recA1 endA1 gyrA96 thi-1 hsdR17 supE44 relA1 lac* [F′ *proAB lacIqZΔM15* Tn*10* (Tetr)]) from Stratagene (Waldbronn, Germany). pET28a-DNA was provided by Novagen.

Vector construction

Plasmids pCBR, pCBRHisN and pCBRHisC were constructed on the basis of pET28a (Novagen). DNA-sequences (see Table 2) for the corresponding new multiple cloning sites were synthesized (Ge-

Table 2. Vector multiple cloning sites.

Name	DNA-Sequence (5′→3′)
pCBR	ATATATATATTCTAGAAATAATTTTGTTTAACTTTAAGAAGGAGATATACATATGATGCAGGTATATATATATTAATAGAGACCTCCTCGGATCCATATATATAT
pCBRHisN	ATATATATATCATATGATGCAGGTATATATATATTAATAGAGACCTCCTCGAATTCATATATATAT
pCBRHisC	ATATATATATTCTAGAAATAATTTTGTTTAACTTTAAGAAGGAGATATACATATGATGCAGGTATATATATATAGCGGGAGACCTGTGCTGGGCAGCAGCCACCACCACCACCACACTAATGAGATCCGGCTGCTAACAAAGCCCGAAAGGAAGCTGAGTTGGCTGCTGCCACCGCTGAGCATATATATAT

neart, Regensburg, Germany) and cloned into pET28a via *XbaI*/ *Bam*HI (pCBR), *NdeI*/*EcoRI* (pCBRHisN) or *XbaI*/*Bpu*1102I (pCBRHisC), thereby replacing the existing multiple cloning site with a new restriction site containing a *Bfu*AI- and a *Bsa*I-sequence and, in case of pCBR and pCBRHisN, a stop codon. The three new vectors allow the simultaneous cloning of any gene using the same restriction sites, enabling the user to express the respective gene without or with an N- or C-terminal His-tag, whereby a stop codon must not be attached at the 3′-end of the gene. Vector-DNA was first restricted with *Bsa*I, followed by blunt end generation with Klenow fragment. Afterwards, the linearized plasmids were digested with *Bfu*AI, generating a 5′-overhang. Genes were amplified using the Geneart vectors as templates and the corresponding oligonucleo-

tides (Table 3). After PCR, DNA fragments were digested with *Bsa*I, 3′-phosphorylated (T4 kinase) and subsequently ligated into the appropriate vectors. In some cases, phosphorylation could be replaced by digestion using *Psi*I. Plasmids were transformed into *E. coli* as described elsewhere.[37] Sequence analysis was performed by GATC Biotech (Konstanz, Germany). pET28a-HisN-LlKdcA was cloned according to Gocke et al.[31]

Table 3. Oligonucleotides.

Oligonucleotide	Gene amplified	Oligonucleotide sequence (5′→3′)
SsGDH_for	*S. solfataricus* glucose dehydrogenase	CAGCAAGGTCTCACATATGAAAGCCATTATTGTGAAACCTCCG
SsGDH_rev	*S. solfataricus* glucose dehydrogenase	TTCCCACAGAATACGAATTTTGATTTCGC
SsDHAD_for	*S. solfataricus* dihydroxyacid dehydratase	CAGCAAGGTCTCACATATGCCTGCAAAACTGAATAGCCC
SsDHAD_rev	*S. solfataricus* dihydroxyacid dehydratase	TGCCGGACGGGTAACTGC
SaKDGA_for	*S. acidocaldarius* KDG aldolase	CAGCAAGGTCTCACATATGGAAATTATTAGCCCGATTATTACCC
SaKDGA_rev	*S. acidocaldarius* KDG aldolase	ATGAACCAGTTCCTGAATTTTGCG
TaAlDH_for	*T. acidophilum* glyceraldehyde dehydrogenase	CAGCAAGGTCTCACATATGGATACCAAACTGTATATTGATGGC
TaAlDH_rev	*T. acidophilum* glyceraldehyde dehydrogenase	CTGAAACAGGTCATCACGAACG
MrKARI_for	*M. ruber* ketolacid eductoisomerase	CAGCAACGTCTCGCATATGAAGATTTACTACGACCAGGACGCAG
MrKARI_rev	*M. ruber* ketolacid reductoisomerase	GCTACCGACCTCTTCCTTCGTGAAC

Enzyme expression

Enzyme expression was performed using *E. coli* BL21(DE3) or BL21 Rosetta(DE3)-pLysS as host strains, either in shaking flask cultures or in a 10 L Biostat Cplus bioreactor (Sartorius Stedim, Göttingen, Germany). All media were supplemented with 30–50 µg mL⁻¹ kanamycin. GDH and DHAD were expressed in LB medium, acetolactate synthase in TB medium. After inoculation cells were grown at 37 °C to an optical density at 600 nm of 0.6, induced with 1 mM IPTG and the temperature lowered to 16–20 °C for 16–24 h expression. KDGA and AlDH were expressed according to the fed-batch cultivation method of Neubauer et al.[38] at 37 °C. After inoculation cells were grown for 24 h and induced with 1 mM IPTG. Enzyme expression was performed for 24 or 30 h, respectively. KDC expression was performed for 22 h at 30 °C in batch mode using Zyp-5052[39] as a medium. KARI was expressed in a batch fermentation using TB medium. Cells were grown at 37 °C to an optical density of 5.2 and induced by the addition of 0.5 mM IPTG. Afterwards, expression was performed for 24 h at 20 °C.

Enzyme purification

All protein purification steps were performed using an ÄKTA UPC-900 FPLC-system (GE Healthcare, Freiburg, Germany), equipped

with HiTrap FF-, HiPrep 26/10 Desalting- and HiTrap Q-Sepharose FF-columns (GE Healthcare). Cell lysates were prepared with a Basic-Z Cell Disruptor (Constant Systems, Northants, UK), cell debris was removed by centrifugation at 35,000×g and 4 °C for 30 min (Sorvall RC6+, SS-34 rotor, Thermo Scientific). For lyophilization an Alpha 2–4 LD Plus freeze dryer (Martin Christ GmbH, Osterode am Harz, Germany) was used. GDH and DHAD were purified by heat denaturation (30 min at 70 °C, respectively). GDH was subsequently freeze-dried (SpeedVac Plus, Thermo Scientific), DHAD concentrated using a stirred Amicon cell (Milipore, Darmstadt, Germany) and either stored at −80 °C or directly applied to experiments. KDGA, AlDH and KDC were purified as previously described[21,23,31] and stored as lyophilisates. ALS and KARI were purified via IMAC using 25 or 50 mM HEPES, pH 7. Elution was achieved with 500 mM imidazol. Enzymes were desalted and stored as a liquid stock (ALS) or lyophilisate (KARI).

Protein determination

Protein concentration was determined with the Roti-Nanoquant reagent (Carl Roth) according to the manufacturer's recommendations using bovine serum albumin as a standard.

SDS-PAGE

Protein samples were analyzed as described by Laemmli[40] using a Mini-PROTEAN system from Bio-Rad (Munich, Germany).

Enzyme assays

All photometrical enzyme assays were performed in microtiter plate format using a Thermo Scientific Multiskan or Varioskan photometer. When necessary, reaction mixtures were incubated in a waterbath (Julabo, Seelbach, Germany) for accurate temperature control. Buffers were prepared according to Stoll,[41] adjusting the pH to the corresponding temperature. Reactions using NAD$^+$ or NADH as coenzymes were followed at 340 nm (molar extinction coefficient NADH = 6.22 L mmol^{-1} cm^{-1}) and the glucose concentrations were measured at 418 nm and 480 nm as indicated.[27] One unit of enzyme activity is defined as the amount of enzyme necessary to convert 1 μmol substrate per minute. In addition to the standard reaction conditions described below, enzyme activity was tested under reaction conditions (100 mM HEPES, pH 7, 2.5 mM MgCl$_2$, 0.1 mM thiamine pyrophosphate) prior to alcohol synthesis experiments.

GDH activity: GDH activity was assayed at 50 °C by oxidizing D-glucose to gluconate, whereby the coenzyme NAD$^+$ is reduced to NADH. Assay mixture contained 50 mM HEPES (pH 7), 2 mM NAD$^+$ and 50 mM D-glucose.[20]

DHAD activity: DHAD activity was measured by an indirect assay. The assay mixture containing DHAD, 20 mM substrate and 100 mM HEPES (pH 7) was incubated at 50 °C. Afterwards the conversion of glycerate to pyruvate, gluconate to 2-keto-3-desoxygluconate or 2,3-dihydroxyisovalerate to 2-ketoisovalerate, respectively, was determined via HPLC as described below.

KDGA activity: KDGA activity was followed in cleavage direction at 50 °C. Reaction mixture contained 50 mM HEPES (pH 7), 0.1 mM thiamine pyrophosphate, 2.5 mM MgCl$_2$, 20 U PDC and 10 mM KDG. KDG cleavage was followed by HPLC as described below.

AlDH activity: AlDH activity was assayed at 50 °C by oxidizing D-glyceraldeyde to glycerate, whereby the coenzyme NAD$^+$ is re-

duced to NADH. Assay mixture contained 50 mM HEPES (pH 7), 2.5 mM MgCl$_2$, 4 mM NAD$^+$ and 5 mM D,L-glyceraldehyde.[23]

ALS activity: ALS activity was determined by following pyruvate consumption at 50 °C. Reaction mixtures contained 25 mM HEPES (pH 7), 0.1 mM thiamine pyrophosphate, 2.5 mM MgCl$_2$, 15 mM sodium pyruvate. Pyruvate concentration in the samples was determined via lactate dehydrogenase as described elsewhere.[21]

KARI activity: KARI activity was assayed by following the NADH consumption connected to the conversion of acetolactate to 2,3-dihydroxyisovalerate at 50 °C. The assay mixture contained 5 mM acetolactate, 0.3 mM NADH, 10 mM MgCl$_2$ and 50 mM HEPES, pH 7.

KDC activity: KDC activity was assayed by following the decarboxylation of 2-ketoisovalerate to isobutyraldehyde at 50 °C and 340 nm. Assay mixture contained 50 mM HEPES (pH 7), 0.1 mM thiamine pyrophosphate, 2.5 mM MgCl$_2$ and 60 mM 2-ketoisovalerate. Decarboxylation rate was calculated using the molar extinction coefficient of 2-ketoisovalerate ($\varepsilon = 0.017$ L mmol^{-1} cm^{-1}).[27]

ADH activity: ADH activity was determined by following the NADH-dependent reduction of isobutyraldehyde to isobutanol at 50 °C. Assay mixture contained 10 mM HEPES (pH 7.2), 5 mM isobutyraldehyde and 0.3 mM NADH.

Glucose analysis: Glucose oxidase was used for the quantification of glucose. Assay mixture contained 20 mM potassium phosphate (pH 6), 0.75 mM 2,2-azino-bis(3-ethylbenzthiazoline)-6-sulfonic acid (ABTS), 2 U glucose oxidase and 0.1 U peroxidase. After the addition of samples the reaction mixture was incubated for 30 min at 30 °C and the extinction at 418 and 480 nm measured. Assay calibration was performed using defined glucose standard solutions.[42]

GC–FID analysis

Isobutyraldehyde and isobutanol or acetaldehyde and ethanol were quantified by GC–FID using a Thermo Scientific Trace GC Ultra, equipped with a flame ionization detector (FID) and a Headspace Tri Plus autosampler. Alcohol and aldehyde compounds were separated by a StabilWax column (30 m, 0.25 mm internal diameter, 0.25 μm film thickness; Restek, Bellefonte, USA), whereby helium (0.8 or 1.2 mL min^{-1}) was used as the carrier gas. The oven temperature was programmed to be held at 50 °C for 2 min, raised with a gradient 10 °C min^{-1} to 150 °C and held for 1 min. Injector and detector were kept at 200 °C. Samples were incubated prior to injection at 40 °C for 15 min. Injection was done in the split mode with a flow of 10 mL min^{-1}, injecting 700 μL using headspace mode.

HPLC analysis

Gluconate, 2-keto-3-desoxygluconate, pyruvate, glycerate, 2,3-dihydroxyisovalerate and 2-ketoisovalerate were separated and quantified by HPLC, using an Ultimate-3000 HPLC system (Dionex, Idstein, Germany), equipped with autosampler and a diode-array detector. Chromatographic separation of gluconate, 2-keto-3-desoxygluconate, pyruvate and glycerate was achieved on a Metrosep A Supp10–250/40 column (250 mm, particle size 4.6 μm; Metrohm, Filderstadt, Germany) at 65 °C by isocratic elution with 12 mM ammonium bicarbonate (pH 10), followed by a washing step with 30 mM sodium carbonate (pH 10.4). Mobile phase flow was adjusted to 0.2 mL min^{-1}. 2,3-dihydroxyisovalerate and 2-ketoisovalerate were separated using a Nucleogel Sugar 810H column (300 mm, 7.8 mm internal diameter; Macherey–Nagel, Düren, Germany) at 60 °C by isocratic elution with 3 mM H$_2$SO$_4$ (pH 2.2). Mobile phase flow was adjusted to 0.6 mL min^{-1}. Sample volume was 10 μL in

each case. System calibration was performed using external standards of each of the abovementioned intermediates. Samples were prepared by filtration (10 kDa MWCO, modified PES; VWR, Darmstadt, Germany) and diluted.

Alcohol biosynthesis

All reactions were set up in 20 mL GC vials. Reaction mixtures contained 100 mm HEPES (pH 7 at 50 °C), 0.1 mm thiamine pyrophosphate, 2.5 mm $MgCl_2$, 25 mm D-glucose and 5 mm NAD^+. Enzymes were added as follows: GDH: 6 U, DHAD: 20 U for ethanol synthesis and 30 U for isobutanol synthesis, all other enzymes: 10 U. Control reactions were performed either without enzymes or without D-glucose. Reaction mixtures were placed in a water bath at 50 °C and gently stirred at 100 rpm.

[1] S. Atsumi, T. Hanai, J. C. Liao, *Nature* **2008**, *451*, 86–89.
[2] B. Blombach, B. J. Eikmanns, *Bioeng. Bugs* **2011**, *2*, 346–350.
[3] M. R. Connor, J. C. Liao, *Curr. Opin. Biotechnol.* **2009**, *20*, 307–315.
[4] S. Atsumi, T. Y. Wu, I. M. P. Machado, W. C. Huang, P. Y. Chen, M. Pellegrini, J. C. Liao, *Mol. Syst. Biol.* **2010**, *6*, 11.
[5] M. P. Brynildsen, J. C. Liao, *Mol. Syst. Biol.* **2009**, *5*, 13.
[6] N. N. Nichols, B. S. Dien, M. J. Lopez, J. Moreno, in *Biocatalysis and Biomolecular Engineering* (Eds.: C. T. Hou, J.-F. Shaw), Wiley-VCH, Weinheim **2010**, pp. 253–263.
[7] Y. H. P. Zhang, *ACS Catal.* **2011**, *1*, 998–1009.
[8] Y. H. P. Zhang, J. B. Sun, J. J. Zhong, *Curr. Opin. Biotechnol.* **2010**, *21*, 663–669.
[9] E. Buchner, R. Rapp, *Ber. Dtsch. Chem. Ges.* **1901**, *34*, 1523–1530.
[10] M. Bujara, M. Schümperli, S. Billerbeek, M. Heinemann, S. Panke, *Biotechnol. Bioeng.* **2010**, *106*, 376–389.
[11] M. Bujara, M. Schümperli, R. Pellaux, M. Heinemann, S. Panke, *Nat. Chem. Biol.* **2011**, *7*, 271–277.
[12] H. L. Schultheisz, B. R. Szymczyna, L. G. Scott, J. R. Williamson, *ACS Chem. Biol.* **2008**, *3*, 499–511.
[13] H. L. Schultheisz, B. R. Szymczyna, L. G. Scott, J. R. Williamson, *J. Am. Chem. Soc.* **2011**, *133*, 297–304.
[14] P. Welch, R. K. Scopes, *J. Biotechnol.* **1985**, *2*, 257–273.
[15] Y. H. P. Zhang, B. R. Evans, J. R. Mielenz, R. C. Hopkins, M. W. W. Adams, *PLoS One* **2007**, *2*, e456.
[16] X. H. Ye, Y. R. Wang, R. C. Hopkins, M. W. W. Adams, B. R. Evans, J. R. Mielenz, Y. H. P. Zhang, *ChemSusChem* **2009**, *2*, 149–152.
[17] Y.-R. Wang, W.-D. Huang, N. Sathitsuksanoh, Z.-G. Zhu, Y. H. P. Zhang, *Chem. Biol.* **2011**, *18*, 372–380.
[18] H. Ahmed, T. J. G. Ettema, B. Tjaden, A. C. M. Geerling, J. van der Oost, B. Siebers, *Biochem. J.* **2005**, *390*, 529–540.
[19] S. Kim, S. B. Lee, *J. Biochem.* **2006**, *139*, 591–596.
[20] C. C. Milburn, H. J. Lamble, A. Theodossis, S. D. Bull, D. W. Hough, M. J. Danson, G. L. Taylor, *J. Biol. Chem.* **2006**, *281*, 14796–14804.
[21] S. Wolterink-van Loo, A. van Eerde, M. A. J. Siemerink, J. Akerboom, B. W. Dijkstra, J. van der Oost, *Biochem. J.* **2007**, *403*, 421–430.
[22] J. H. Jung, S. B. Lee, *Biochem. J.* **2006**, *397*, 131–138.
[23] M. Reher, P. Schönheit, *FEBS Lett.* **2006**, *580*, 1198–1204.
[24] D. A. Cowan, *Comp. Biochem. Physiol. Part A* **1997**, *118*, 429–438.
[25] P. V. Iyer, L. Ananthanarayan, *Process Biochem.* **2008**, *43*, 1019–1032.
[26] F. Steffler, V. Sieber, unpublished results.
[27] D. Gocke, T. Graf, H. Brosi, I. Frindi-Wosch, L. Walter, M. Muller, M. Pohl, *J. Mol. Catal. B* **2009**, *61*, 30–35.
[28] G. Fiorentino, R. Cannio, M. Rossi, S. Bartolucci, *Protein Eng.* **1998**, *11*, 925–930.
[29] A. Guagliardi, M. Martino, I. Iaccarino, M. D. Rosa, M. Rossi, S. Bartolucci, *Int. J. Biochem. Cell Biol.* **1996**, *28*, 239–246.
[30] F. Wiegeshoff, M. A. Marahiel, *FEMS Microbiol. Lett.* **2007**, *272*, 30–34.
[31] D. Gocke, C. L. Nguyen, M. Pohl, T. Stillger, L. Walter, M. Mueller, *Adv. Synth. Catal.* **2007**, *349*, 1425–1435.
[32] K. Jia, Y. Zhang, Y. Li, *Eng. Life Sci.* **2010**, *10*, 422–429.
[33] R. Dumas, V. Biou, F. Halgand, R. Douce, R. G. Duggleby, *Acc. Chem. Res.* **2001**, *34*, 399–408.
[34] GESTIS Substance Database, **2011**.
[35] C. K. Savile, J. M. Janey, E. C. Mundorf, J. C. Moore, S. Tam, W. R. Jarvis, J. C. Colbeck, A. Krebber, F. J. Fleitz, J. Brands, P. N. Devine, G. W. Huisman, G. J. Hughes, *Science* **2010**, *329*, 305–309.
[36] A. Oudshoorn, L. A. M. van der Wielen, A. J. J. Straathof, *Ind. Eng. Chem. Res.* **2009**, *48*, 7325–7336.
[37] J. Sambrook, E. F. Fritsch, T. Maniatis, *Molecular Cloning: A Laboratory Manual*, Cold Spring Harbor Laboratory Press, Cold Spring Habor, NY, **1989**.
[38] P. Neubauer, L. Haggstrom, S. O. Enfors, *Biotechnol. Bioeng.* **1995**, *47*, 139–146.
[39] F. W. Studier, *Protein Expression Purif.* **2005**, *41*, 207–234.
[40] U. K. Laemmli, *Nature* **1970**, *227*, 680–685.
[41] V. S. Stoll, J. S. Blanchard in *Guide to Protein Purification, Vol. 466*, Elsevier Academic Press Inc, San Diego, **2009**, pp. 43–56.
[42] H. Gallati, *J. Clin. Chem. Clin. Biochem.* **1979**, *17*, 1–7.
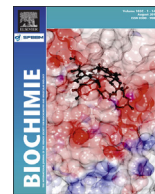
Research paper

Meiothermus ruber thiolase — A new process stable enzyme for improved butanol synthesis

CrossMark

Steven Reiße, Daniel Garbe, Thomas Brück*

Fachgebiet Industrielle Biokatalyse, Technische Universität München, Lichtenbergstr. 4, 85748 Garching, Germany

ABSTRACT

Butanol is an important renewable building block for the chemical, textile, polymer and biofuels industry due to its increased energy density. Current biotechnological butanol production is a Clostridial based anaerobic fermentation process. Thiolase (EC 2.3.1.9/EC 2.3.1.16) is a key enzyme in this biosynthetic conversion of glucose to butanol. It catalyzes the condensation of two acetyl-CoA molecules, forming acetoacetyl-CoA, which is the first committed step in butanol biosynthesis. The well characterized clostridial thiolases are neither solvent nor thermo stable, which limits butanol yields. We have isolated and characterized a new thermo- (IT_{50} 50 °C = 199 ± 0.1 h) and solvent stable (IS_{50} > 4%) thiolase derived from the thermophilic bacterium *Meiothermus ruber*. The observed catalytic constants were $K_m = 0.07 ± 0.01$ mM and $k_{cat} = 0.80 ± 0.01$ s^{-1}. In analogy to other thiolases, the enzyme was inhibited by NAD$^+$ ($K_i = 38.7 ± 5.8$ mM) and CoA ($K_i = 105.1 ± 6.6$ μM) but not NADH. The enzyme was stable under harsh process conditions ($T = 50$ °C, Butanol = 4% v/v) for prolonged time periods ($\tau = 7$ h). The new enzyme provides for targeted *in-vivo* and *in-vitro* butanol biosynthesis under industrially relevant process conditions.

© 2014 Elsevier Masson SAS. All rights reserved.

1. Introduction

Thiolases are omnipresent enzymes that can be found in prokaryotic as well as eukaryotic organisms. This enzyme family can be further subdivided into catabolic (EC 2.3.1.16) and metabolic (EC 2.3.1.9) thiolases, respectively. Both are able to catalyze a Claisen type condensation of two acetyl-CoA molecules to generate acetoacetyl-CoA. Hence, these enzymes are key in forming extended carbon skeletons from the universal metabolic precursor acetyl-CoA. Biosynthetic thiolases (EC 2.3.1.9) are utilizing only acetyl-CoA and acetoacetyl-CoA as substrates [1]. In contrast, catabolic thiolases (EC 2.3.1.16) display a varied substrate spectrum, which includes larger substrates such as 3-ketodecanoyl-CoA [2]. The catabolic enzymes are key to the β-oxidation pathway

dedicated to fatty acid degradation. Although both thiolase classes metabolize different substrates, the reaction mechanism is equivalent [1].

In this context the biochemical and biophysical features of thiolases from *Zoogloea ramigera* [1,3—8], *Thermus thermophilus* [9] and different clostridia [10—12] have been reported. Thiolases show industrial relevance throughout the acetone—butanol—ethanol fermentation process (ABE process). Therefore, multiple clostridial strains [13—16] or recombinant *Escherichia coli* [17,18] were examined in respect to good product formation rates. However, these cellular fermentation processes are limited by low tolerance to temperature, butanol concentration [19] and in case of clostridial strains, to oxygen.

A new approach to overcome these limitations could be the application of *in-vitro* enzyme cascades [20,21]. This method offers numerous benefits compared to the classical ABE fermentation. First the entire process chain and all reaction conditions, like temperature and pH-value, can be modified and controlled.

Secondly isolated enzymes originating from thermophilic organisms are prone to survive high product and organic solvent titers and further industrially relevant process parameters, like high salinity. Additionally, *in-vitro* reaction cascade do not suffer of a product drain into other non-productive metabolic pathways.

---

* Corresponding author. Tel.: +49 89 289 13253; fax: +49 89 289 13255.
E-mail addresses: steven.reisse@tum.de (S. Reiße), daniel.garbe@tum.de (D. Garbe), brueck@tum.de, thomas.brueck@gmail.com (T. Brück).

Furthermore, this approach offers the possibility to create tailor-made, artificial reaction cascades, which are not restricted to the limits of a living cell [20].

Nonetheless, cell free biosynthesis of higher alcohols is still in an early development stage. On the other hand, cell based production systems are state of the art in industrial applications [13]. Integration or exchange of more stable thiolase variants would potentially lead to better yields due to improved thermostabilities.

In our quest to isolate a robust, process relevant thiolase variant we not only concentrated on biochemical features such as kinetic performance but also focused on process stability. In this context, both solvent and thermostability were the driving forces in our screening procedures. Additionally, interactions with other co-factors and process intermediates were examined to enhance flexibility of process design.

In the present study, we report a new thiolase from *Meiothermus ruber* DSM 1279, which displayed excellent catalytic performance and enhanced thermo and solvent stability.

2. Materials and methods

2.1. Reagents and kits

Restriction enzymes, T4 DNA ligase, T4 Kinase, Shrimp alkaline phosphatase, Phusion polymerase and desoxynucleotides were purchased from Thermo Scientific (Ulm, Germany). Desoxy-ribonuclease I from bovine pancreas was from Serva (Heidelberg, Germany). All enzymes were used according to the manufacturers' recommendations, applying the provided buffer solutions. Oligo-nucleotides were ordered from Eurofins MWG Operon (Ebersberg, Germany). Porcine heart lactate dehydrogenase (LDH) was bought from Serva, bovine liver catalase from Sigma—Aldrich (München, Germany) and BSA from Roth (Karlsruhe, Germany). All chemicals were, unless otherwise stated, purchased in analytical grade from Sigma—Aldrich, Carl Roth (Karlsruhe, Germany), Serva Electro-phoresis and AppliChem (Darmstadt, Germany). Plasmids were purified by applying the GeneJET Plasmid Miniprep Kit (Thermo Scientific), PCR products and enzymatically manipulated DNA were purified via the innuPREP DOUBLEpure Kit (Analytik Jena, Germany).

2.2. Strains and media

M. ruber DSM 1279 (DSMZ, Braunschweig, Germany) was grown aerobically at 50 °C in *Thermus ruber* medium containing trypton (5 g L^{-1}), yeast extract (1 g L^{-1}) and soluble starch (1 g L^{-1}), adjusted to pH 8.

E. coli Rosetta ((F-ompT hsdSB(rB- mB-) gal dcm (DE3) pLysS-RARE (CamR)) was purchased from Merk (Darmstadt, Germany) and was grown in TB medium for protein expression. *E. coli* XL1-Blue (recA1 endA1 gyrA96 thi-1 hsdR17 supE44 relA1 lac [F′ proAB lacIqZDM15 Tn10 (Tetr)]) from Stratagene (Waldbronn, Germany) was grown in LB medium. Both media were supplemented with kanamycin (30 μg ml^{-1}), TB additionally with chloramphenicol (34 μg ml^{-1}).

2.3. Sequence alignment and structural modeling

Thiolases have been observed in several pro − and eukaryotes. A number of gene and protein sequences may be extracted from various databases. For the alignment we used only the best characterized thiolase sequences. Sources of sequence information are listed in Table 1. The HHpred server [22] and the Yasara bioinformatics suite were used to model the Mr-thiolase structure in line with manufacturers' guidelines.2.4. DNA isolation and cloning.

Table 1
Sequence sources.[a]

Strain	Gene	Protein accession number
Meiothermus ruber	Mrub_1917	YP_003507694.1
Thermus thermophilus	TTHA0559	YP_143825.1
Clostridium acetobutylicum	CA_C2873	NP_349476.1
Zoogloea ramigera	J02631.1	P07097.4

[a] www.ncbi.nlm.nih.gov.

The plasmid pET28a (Novagen) was pretreated as described by Guterl et al. [20]. The resulting vector pCBR including C-terminal His-Tag was digested with *Bve*I and *Sal*I and subsequently dephosphorylated.

Genomic DNA from *M. ruber* DSM 1279 was isolated as described by Saha [23]. The gene Mrub_1917 was amplified from genomic DNA by PCR with the phosphorylated primers listed in Table 2. Resulting PCR fragments were ligated into pCBR via *Bsm*BI and *Sal*I restriction sites. The obtained pCBR-thl-CHis plasmid was transformed in *E. coli* as described elsewhere [24]. DNA sequencing validated all cloning procedures.

2.4. Protein expression and purification

For protein expression, transformed cells were cultivated in shaking flask at 37 °C in TB medium supplemented with kanamycin (30 μg ml^{-1}) and chloramphenicol (34 μg ml^{-1}). The cells were induced with 1 mM IPTG at OD$_{600}$ 0.5−0.8 and additionally incubated at 37 °C for 4 h. Cultures were subsequently harvested and frozen at −20 °C until further use.

For cell disruption, the cell pellets were resuspended in binding buffer (50 mM HEPES pH 8, 20 mM imidazole, 10% glycerol, 0.1% tween 20), supplemented with DNAse (10 mg ml^{-1}). The cells were lysed with an Avestin EmulsiFlex-B15 homogenizer. Debris was removed by centrifugation at 20,000 × *g* and 4 °C for 30 min.

The supernatant was loaded onto Ni-NTA columns and washed with 5 column volumes of binding buffer. His-tagged Mr-thiolase was eluted in one step with two column volumes of elution buffer (50 mM HEPES pH 8, 500 mM imidazole, 10% glycerol, 0.1% tween 20). All fractions were analyzed by 12% SDS-PAGE.

Additionally a Native-PAGE was performed to study the quaternary structure of the catalytically active Mr-thiolase. Therefore, Mini-Protean TGX precast gels 4−15% (Bio-Rad, München) were used. The purified Mr-thiolase and the standard proteins BSA (67 kDa) and catalase (240 kDa, bovine liver) were diluted in Native-PAGE sample buffer according to the instruction manual (Bio-Rad). All following steps were performed in accordance with this protocol.

Protein contents were quantified photometrically by measuring the absorbance at 215 and 225 nm [25—27].

2.5. Thiolase activity assay

All assays were performed in microtiter plate format using an Enspire 2 (Perkin Elmer). The reaction was initiated by addition of 180 μl assay mixture to 20 μl enzyme solution. Assay mixtures were preincubated in a thermomixer for accurate temperature control. The pH was adjusted to the corresponding temperature. One unit of

Table 2
Oligonucleotides.

Primer	Sequence (5′−3′)
Mr_thl-fwd	CAGCAACGTCTCACATATGCGTGAGGTGTGGGTGGTTTC
Mr_thl-rev	CAGCAAGTCGACGCCCACAGCCTCCAC

enzyme activity was defined as the amount of enzyme that catalyzed the formation of 1 μmol of product per minute.

The Claisen condensation of acetyl-CoA to yield acetoacetyl-CoA performed by the purified Mr-thiolase was quantified in a coupled enzyme assay with β-Hydroxybutyryl-CoA Dehydrogenase (Hbd) by monitoring the decrease in absorbance at 340 nm due to the oxidation of NADH. The standard assay mixture contained 50 mM HEPES pH 7, 1 mM acetyl-CoA, 0.3 mM NADH and Hbd form *Clostridium acetobutylicum* [28].

Assays for pH determination were quantified via DTNB (5,5′-dithiobis-(2-nitrobenzoic acid)) according to a change in the catalyzing direction of Hbd. During this assay the thiol moiety of the released CoA molecule cleaves the disulfide bond of DTNB to form one equivalent of a yellow colored NTB^{2-} anion which can be detected at 412 nm. The standard assay mixture contained 50 mM HEPES, 0.2 mM acetyl-CoA, 0.1 mM DTNB. 5 mM DTNB stock solutions were prepared with 100 mM phosphate buffer pH 7.2. The molar extinction coefficient of 14.15 mM^{-1} cm^{-1} was used according to Riener et al. [29].

3. Results and discussion

3.1. Identification and structural comparison of Mr-thiolase

In a primary step conserved amino acid sequence stretches of characterized thiolases were aligned with a predicted *M. ruber* (Mr, YP_003507694.1) protein, which lead to identification of a putative thiolase amino acid sequence. The identified sequence showed 72% identity to *T. thermophilus* thiolase (Tth, YP_143825.1) [9]. In comparison to the sequences of *C. acetobutylicum* (Cab, NP_349476.1) and *Zoogloea ramigera* (Zr, P07097.4) thiolase, Mr-thiolase displayed much lower identities of 43% and 42% respectively (Fig. S1).

The putative Mr-thiolase sequence was used as template for a further multiple alignment and structural prediction via the HHpred server [22] to examine structural relationships more closely. The alignment and structure modeling gave e-values of $2.2 \times 10^{-66} - 3 \times 10^{-60}$, whereby the Zr-thiolase showed the highest secondary structure similarity. To create a tertiary structure alignment of these two proteins we used the MUSTANG algorithm [30] of the Yasara bioinformatics toolbox. This tertiary structure alignment between Mr- and Zr-thiolase (PDB ID: 1DM3) had an RMSD of 0.644 Å over 373 aligned residues with 42.6% primary sequence identity. We applied the substrate coordinates of Zr-thiolase to model acetyl-CoA into the active of Mr-thiolase (Fig. 1).

As the structure—function correlations have most extensively been studied in Zr-thiolase, we used this information to guide our studies on Mr-thiolase catalysis [1,4—6]. The primary step in the Zr-thiolase catalysis is the activation of the N-terminal domain Cys89 by His348. A subsequent nucleophilic attack on the substrate acetyl-CoA forms a covalent acyl-enzyme intermediate [1,8]. An additional acetyl-CoA is then added to the initial enzyme—substrate complex. Subsequently, the second, C-terminal located Cys378 deprotonates the enzyme substrate complex intermediate by a second nucleophilic attack to yield acetoacetyl-CoA, which is ultimately released from the active site [4,6]. In our Mr-thiolase model the catalytically relevant amino acids Cys88, Cys382 and His352 are corresponding to Cys89, Cys378 and His348 of Zr-thiolase. The presence of equivalent catalytic residues implied a similar catalytic mechanism for these two enzymes. To validate the bioinformatics data set, we carried out a detail experimental characterization of the putative Mr-thiolase activity.

3.2. Cloning, heterologous expression and purification

The gene of Mr-thiolase was fused to a C-terminal His-tag and transformed into *E. coli* Rosetta (DE3) cells to overexpress the recombinant enzyme, which was subsequently purified and examined by SDS-PAGE (Fig. 2a). More than 50% of the recombinant enzymes were present in the soluble cell fraction. This was the highest yield of soluble, active enzyme of any tested thiolase in our screening panel. The purified enzyme was stable in HEPES buffer at 4 °C for several weeks. On denaturing SDS-PAGE the recombinant Mr-thiolase monomer subunit displayed a molecular weight of 44 kDa. Analysis of Mr-thiolase on Native-PAGE (Fig. 2b) indicated a molecular weight of almost 240 kDa, which is consistent with calculated molecular weight of 176 kDa, suggesting that the native enzyme has a tetrameric architecture. This data is also consistent with previous reports on thiolase structure [7,10,31].

3.3. Evaluation of optimal reaction conditions

To determine the optimal reaction conditions the experiments were performed at various temperatures and pH values.

3.3.1. pH optimum

As our thiolase activity measurements were coupled to the reactivity and pH dependence of Hbd, the data sets beyond pH 8 were of limited information, since Hbd preferentially switches towards ß-hydroxybutyryl-CoA hydrolysis at pH higher than 8 [28,32]. Consequently, at pH values beyond 8 the activity of Mr-thiolase could not be measured, but reliably using a coupled assay with Hbd. To circumvent this limitation we have developed a new DTNB dependent assay (Fig. 3).
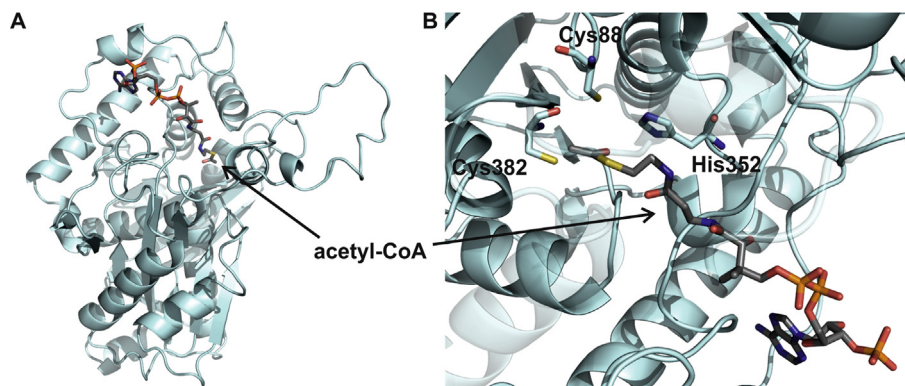

Fig. 1. Modeled Mr-thiolase structure. (A) Structural overview with the substrate acetyl-CoA. (B) A detailed view of the active site including the catalytic relevant residues Cys88, Cys382 and His352.
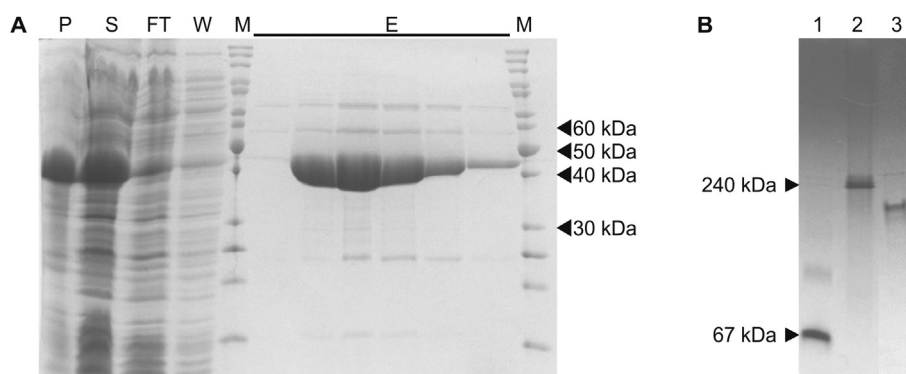
Fig. 2. Purification of C-terminal His-tagged thiolase from Meiothermus ruber after expression in *E. coli* Rosetta (DE3) cells. (A) SDS-PAGE: showing protein fractions from pellet (P), supernatant (S), flow through (FT), washing step (W), eluted enzyme (E) and marker (M, PageRuler Unstained Protein Ladder, Thermo Fisher Scientific). (B) Native-PAGE: showing the native Mr-thiolase in reference to commercial enzymes: 1 BSA (67 kDa); 2 catalase (240 kDa, bovine liver); 3 Mr-thiolase.

As depicted in Fig. 3 the DTNB based assay relies on the reaction of the thiolate anion moiety from the released CoA-molecule with Ellman's reagent, which subsequently leads to the formation of a mixed disulfide and one equivalent of yellow colored NTB^{2-} [29]. This spectrophotometric measurement of NTB^{2-} allows a direct observation of thiolase activity over an extended pH range (pH 6–11, Fig. 4a) leading to the detection of Mr-thiolase's pH optimum at pH 10.

3.3.2. Temperature optimum

The Mr-thiolase temperature stability was measured by incubating the enzyme at 40–60 °C (Fig. 4b), followed by determination of the residual activity at 50 °C, which also marked the temperature optimum. Hence, the observed temperature optimum of Mr-thiolase is 15 °C less than for the thiolase of the hyperthermophilic organism *T. thermophilus* [9]. Nevertheless, Mr-thiolase showed an extended time-dependent stability at temperatures higher than 50 °C (Table 3). The notable Mr-thiolase half-life at 60 °C was 6 days, indicating a significant resistance to elevated reaction temperatures.

3.4. Kinetic properties

Kinetic characterization of Mr-thiolase was carried out with a coupled assay using acetyl-CoA as a primary substrate for the condensation reaction. All investigations were performed under aerobic conditions.

Table 4 demonstrates Mr-thiolase reaction rates for acetyl-CoA condensation to be considerably smaller compared to thiolase enzymes from several other organisms [12,31,33,34]. Comparison of the Mr kinetic data with literature reports reveals significant differences in the kinetic performance between catabolic and biosynthetic thiolases. Interestingly, catabolic thiolases are characterized by relative low K_m and k_{cat} values and subsequently lower catalytic efficiencies compared to the biosynthetic ones. With respect to the kinetic properties, biosynthetic thiolases were found in *Z. ramigera* ($K_m = 1.2$ mM; $k_{cat} = 71$ s^{-1}) [6] and *Rhizobium* sp. ($K_m = 1.1$ mM; $k_{cat} = 26$ s^{-1}) [31]. However, kinetic parameters of Mr-thiolase are in line with the best performing catabolic thiolase from pig heart ($K_m = 0.3$ mM; $k_{cat} = 0.8$ s^{-1}) [6,35]. For this reason, it can be deduced Mr-thiolase belongs to the family of catabolic thiolases (EC 2.3.1.16).

State of the art biological butanol production is based on microbial systems using *C. acetobutylicum* as host [13] or its butanol pathway enzymes [17,36], including thiolase. The thiolases of *C. acetobutylicum* and *Clostridium butyricum* are partially characterized with a reported K_m of 0.27 mM [12] and 0.67 mM [10], respectively. Interestingly, the C. *pasteurianum* thiolase, which only operates under strictly anaerobic conditions, showed a K_m of 0.06 mM [11] similar to the value determined in this study for Mr-thiolase. The pronounced activity of Mr-thiolase under aerobic conditions makes this enzyme particularly suitable for *in-vitro* butanol production systems.

3.4.1. Enzyme inhibition

In line with previous literature reports we could confirm inhibitory effects of NAD^+ for Mr-thiolase. By contrast, the previously reported thiolase inhibition by NADH [31] could not be observed for Mr-thiolase. With respect to the NAD^+ inhibition, the double reciprocal plots of activity versus acetyl-CoA concentration in presence of different concentrations of NAD^+ were linear and intersected on the ordinate (Fig. 5a). This is consistent with a competitive inhibition effect. Based on this data set an inhibition constant (K_i) for NAD^+ of 38.7 ± 5.8 mM was determined (Table 1).

In the context of CoA dependent butanol formation, we have examined the CoA inhibitory effect on Mr-thiolase. Kinetic data revealed free CoA to be a more potent inhibitor than NAD^+. In the presence of 1 mM acetyl-CoA as substrate the IC_{50} (CoA) was 200 μM. Subsequent collection of kinetic data (Fig. 5b) implicated CoA to act also as a competitive inhibitor. This data set is consistent with previous reports on CoA [10,12,31,34]. The determined K_i value for CoA of 105.1 ± 6.6 μM indicates Mr-thiolase to be 5–10 times less sensitive to CoA inhibition than previously described thiolases e.g. from *Rhizobium* sp. or *Alcanigenes latus* with detected K_i values of 11 μM [31] and 20 μM [34], respectively. This feature is particularly advantageous to achieve a high titer in butanol production.
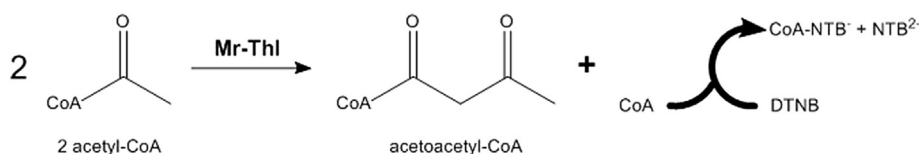

Fig. 3. Reaction of Mr-thiolase in the presence of Ellman's reagent (DTNB). The assay contained 50 mM HEPES, 0.2 mM acetyl-CoA, 0.1 mM DTNB. The formation of the yellow colored NTB2- anion could be followed at 412 nm.
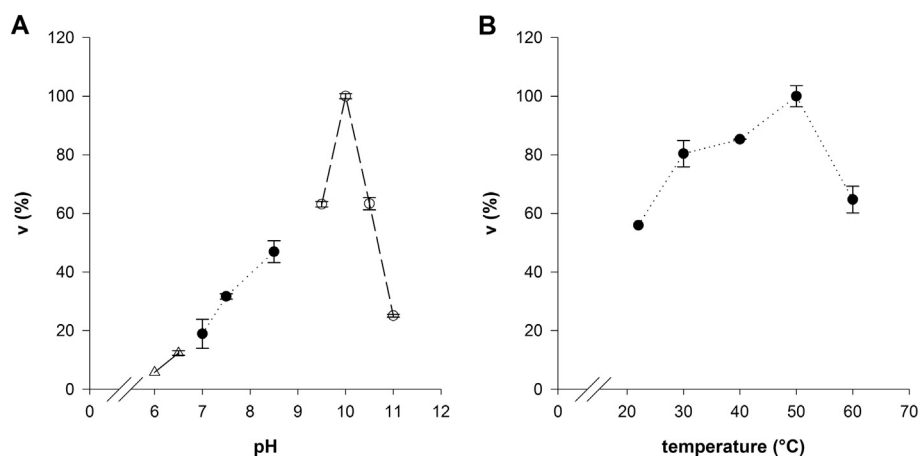
Fig. 4. Effects of different conditions on the condensation reaction of Mr-thiolase. The obtained activity is depicted in relative values. (A) pH profile: The reactions were carried out with the following buffers: △ −−−−: 50 mM Phosphate buffer, pH 6—6.5; ● •••••: 50 mM HEPES, pH 7—8.5; □ − − − 50 mM CAPS pH 9.5—11. (B) Temperature profile: The reactions were carried out in a range from 22 to 60 °C in 50 mM HEPES pH 7.

Table 3
Thermal stability of Mr-thiolase.[a]

Temperature (°C)	Half-life (h)
40	436 ± 0.1
50	199 ± 0.1
60	136 ± 0.1

[a] Enzyme solutions were incubated at various temperatures and measured regularly according to our predefined assay conditions.

3.5. Solvent tolerance

An additionally important aspect for the use of isolated thiolases in butanol biosynthesis pathways is the tolerance against high titers of the end product. Hence, Mr-thiolase was evaluated in the presence of different butanol concentrations (Fig. 6). Our data set depicts that 90% of the Mr-thiolase activity remains up to the presence of 4% (v/v) butanol in the reaction medium.

Additionally, we conducted in-vitro stability experiments under process relevant conditions, i.e. elevated temperatures and solvent concentration. The resulting data demonstrated a thiolase half-life of approximately 7 h at 50 °C and 4% (v/v) butanol. To our knowledge this is the first report that demonstrates that thiolase remains active for an extended time period under such harsh reaction conditions.

Table 4
Kinetic constants of Mr-thiolase in direction of the condensation reaction.[a]

Reaction parameter	Value
K_m (mM)[b]	0.07 ± 0.01
k_{cat} (s^{-1})	0.80 ± 0.01
k_{cat}/K_m (M^{-1} s^{-1})	11,400 ± 1000
$K_{i\ CoA}$ (μM)[c]	105.1 ± 6.6
$K_{i^+ NAD}$ (mM)[d]	38.7 ± 5.8

[a] All assays applied purified recombinant enzyme. Each value represents the average of three separate measurements.
[b] The Michaelis−Menten constant for acetyl-CoA was measured with varying concentrations of acetyl-CoA (0.1−6 mM) in 50 mM HEPES pH 7 at 50 °C.
[c] The inhibition constant for CoA was determined with varying concentrations of CoA (50−200 μM) and acetyl-CoA.
[d] The inhibition constant for NAD$^+$ was determined with varying concentrations of NAD$^+$ (1−20 mM) and acetyl-CoA.

In cell based butanol production systems, end product toxicity at solvent concentrations above 2% (v/v) remains a major challenge, limiting both product titers and process viability [36—38]. Hydrophobic alcohols, such as butanol, exert their toxic effects on cellular production systems predominantly by damaging cell wall components [16]. Therefore, metabolic integration of solvent tolerant enzyme components would not significantly enhance solvent resistant of the cell or improve butanol product titers.

By contrast, we recently reported on a cell-free system for production of ethanol, whose reaction kinetics and product yields were not affected even in the presence of 4% (v/v) isobutanol [20]. The data indicated that in cell-free systems the upper limit of process productivity is governed by solvent resistance of individual enzyme components that constitute the reaction cascade. The pronounced solvent tolerance observed for Mr-thiolase reported in this study suggest, that this enzyme is a suitable component for the construction of a cell-free butanol production cascade. In this context, we recently reported on a consolidated cell-free reaction cascade converting crotyl alcohol to butanol [39]. Further, we have recently identified an oxygen tolerant crotonase activity, whose identification and characterization will be reported elsewhere. The identification of Mr-thiolase and crotonase activities together with our previous results on the cell-free conversion of glucose to pyruvate and crotyl alcohol to butanol provide a platform for a consolidated cell-free reaction cascade that allows direct, aerobic conversion of glucose to butanol with potential product yields exceeding 4% (v/w).

4. Conclusion

The traditional biobutanol production is based on an anaerobic fermentation process applying different Clostridia species. By-products such as butyrate, acetone and ethanol accompanied with low tolerance to temperature and butanol concentration lead to a low product yield and impede industrial process realization. Alternatively, a completely cell-free approach using in-vitro enzyme cascades has the potential to simplify product separation and may also provide higher total yields of biobutanol [20,21,39]. In this regard, identification of process relevant enzymes with enhanced solvent and temperature tolerance as well as good catalytic features is essential.

Here we report a new thiolase derived from M. ruber DSM 1279, which catalyzes the first committed step in the butanol biosynthesis cascade. The new Mr-thiolase was cloned, heterologously
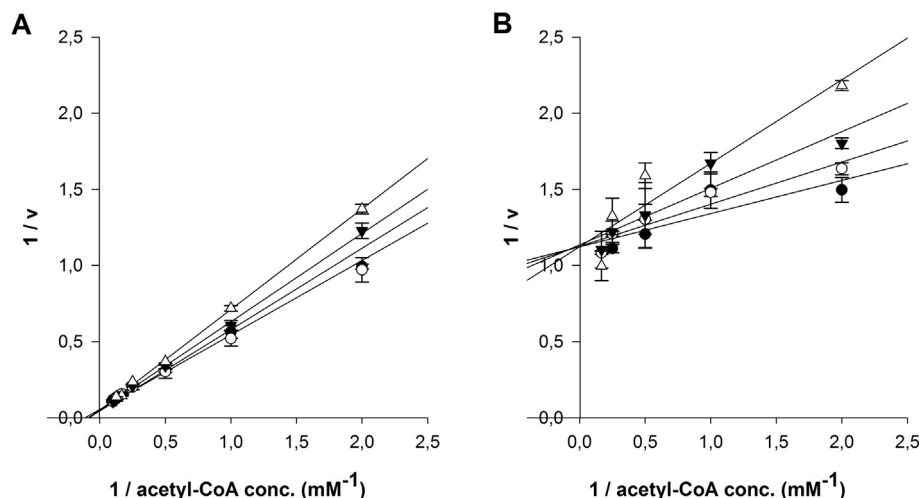
Fig. 5. Kinetics of Mr-thiolase in direction of the condensation reaction. (A) Inhibition of the thiolase by NAD^+. Double reciprocal plot of velocity versus acetyl-CoA concentration. Reactions were assayed according to the described conditions in the presence of varying NAD^+ concentrations: ● 0 mM NAD^+; ○ 1 mM NAD^+; ▼ 10 mM NAD^+; △ 20 mM NAD^+. (B) Inhibition of the thiolase by CoA. Double reciprocal plot of velocity versus acetyl-CoA concentration. Reactions were conducted as mentioned above in the presence of varying CoA concentrations: ● 0 μM CoA; ○ 50 μM CoA; ▼ 100 μM CoA; △ 200 μM CoA.

expressed in *E. coli* and finally characterized with respect to in-dustrial applications, such as butanol synthesis.

The structural and kinetic properties of the enzyme indicate that it belongs to the family catabolic thiolases. In contrast to previous reports we examined the interaction of Mr-thiolase with alterna-tive cofactors and process intermediates. We could demonstrate that NAD^+ and CoA are both competitive inhibitors, of while CoA seems to be most inhibitory. Particularly noteworthy in this context is the lower sensitivity of Mr-thiolase towards CoA compared to other reported thiolases. This particular feature could be used to improve metabolic flux in order to achieve higher butanol titer in cell-free as well as cell based approaches.
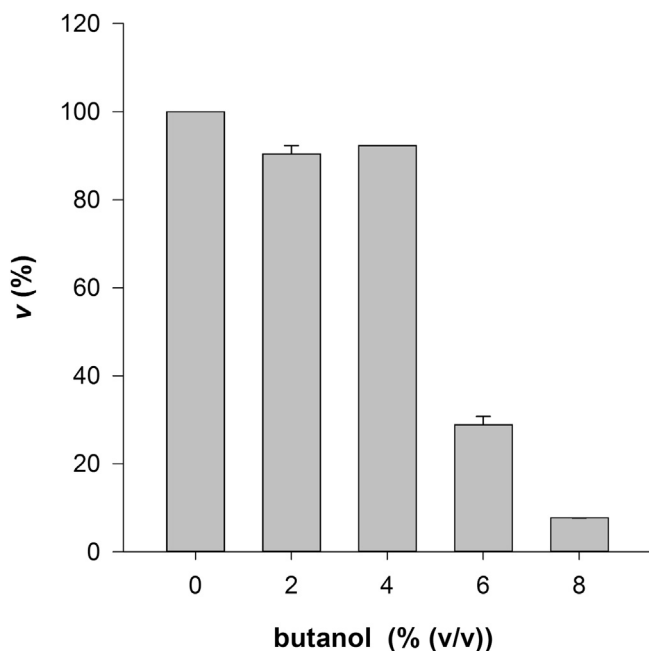

Fig. 6. Butanol tolerance of Mr-thiolase. The assays were carried out in the presence of various butanol concentrations. Each measurement was performed after incubation at 50 °C for 30 min.

In this study we have developed a new DTNB based assay, which, for the first time, allowed to overcome limitations of the coupled assay with Hbd. The new DTNB assay allowed the deter-mination of the Mr-thiolase pH optimum at 10. The half-life at the dedicated process temperature of 50 °C was 199 h, which corre-spondence to a dwell time in the process over one week. Further, the dwell time was of particular importance with respect to determining the enzymes solvent tolerance. Interestingly, the Mr-thiolase activity remained stable over extended time periods even under extreme temperatures and high solvent (T = 50 °C, Butanol = 4% v/v) concentrations. Therefore, Mr-thiolase opens new avenues to improve both cell and cell-free processes for in-dustrial production of biobutanol.

However, further studies towards CoA sensitivity and improved catalytic characteristics are required. Although the Mr-thiolase operates at neutral pH conditions, the shift of the pH optimum in direction of a more neutral pH with a focus on the catalytic pa-rameters is desirable to enhance the cooperation with the other enzymes in the butanol pathway.

Nevertheless, for demonstration purposes the functional incor-poration of Mr-thiolase into a cell-free butanol production system is feasible as the enzyme is still operational at neutral pH. In this study we have demonstrated the functional cooperation of Mr-thiolase with Hbd resulting in the efficient conversion of acetyl-CoA to β-hydroxybutyryl CoA. Further, we have shown that the downstream cascade converting crotyl alcohol to butanol is oper-ational at neutral pH [39]. In our previous cell-free cascade for production of isobutanol we have demonstrated the conversion of glucose to pyruvate at neutral pH [20]. The implementation of a consolidated cell-free reaction cascade enabling direct conversion of glucose to butanol and operating at neutral pH is therefore within reach. Currently, implementation of an enzyme reaction cascade at neutral pH represents a feasible compromise that maintains activity of all required enzyme components albeit not at their pH optimum [40]. Moreover, we have recently, isolated an oxygen resistant crotonase enzyme that operates also at neutral pH. The description of this enzyme will be published elsewhere. The newly isolated crotonase activity will complete our cell-free system for the conversion of glucose to butanol under aerobic condition.

However, for a process relevant cell-free butanol production system, the Mr-thiolase inhibition by CoA is still a limiting step,

which impedes the metabolic flux in cell free biobutanol production systems. The molecular optimization towards a less sensitive and more active thiolase at neutral pH conditions can be addressed by e.g. rational or random enzyme engineering methods.

Conflict of interest

Acknowledgments

Appendix A. Supplementary data

Supplementary data related to this article can be found at http://dx.doi.org/10.1016/j.biochi.2014.03.013.

References

[1] P. Kursula, J. Ojala, A.M. Lambeir, R.K. Wierenga, The catalytic cycle of biosynthetic thiolase: a conformational journey of an acetyl group through four binding modes and two oxyanion holes, Biochemistry 41 (2002) 15543—15556.

[2] H. Staack, J.F. Binstock, H. Schulz, Purification and properties of a pig heart thiolase with broad chain length specificity and comparison of thiolases from pig heart and Escherichia coli, J. Biol. Chem. 253 (1978) 1827—1831.

[3] J.T. Davis, R.N. Moore, B. Imperiali, A.J. Pratt, K. Kobayashi, S. Masamune, A.J. Sinskey, C.T. Walsh, T. Fukui, K. Tomita, Biosynthetic thiolase from Zoogloea ramigera. I. Preliminary characterization and analysis of proton transfer reaction, J. Biol. Chem. 262 (1987) 82—89.

[4] G. Merilainen, V. Poikela, P. Kursula, R.K. Wierenga, The thiolase reaction mechanism: the importance of Asn316 and His348 for stabilizing the enolate intermediate of the Claisen condensation, Biochemistry 48 (2009) 11011—11025.

[5] G. Merilainen, W. Schmitz, R.K. Wierenga, P. Kursula, The sulfur atoms of the substrate CoA and the catalytic cysteine are required for a productive mode of substrate binding in bacterial biosynthetic thiolase, a thioester-dependent enzyme, FEBS J. 275 (2008) 6136—6148.

[6] Y. Modis, R.K. Wierenga, Crystallographic analysis of the reaction pathway of Zoogloea ramigera biosynthetic thiolase, J. Mol. Biol. 297 (2000) 1171—1182.

[7] T. Nishimura, T. Saito, K. Tomita, Purification and properties of beta-ketothiolase from Zoogloea ramigera, Arch. Microbiol. 116 (1978) 21—27.

[8] M.A. Palmer, E. Differding, R. Gamboni, S.F. Williams, O.P. Peoples, C.T. Walsh, A.J. Sinskey, S. Masamune, Biosynthetic thiolase from Zoogloea ramigera. Evidence for a mechanism involving Cys-378 as the active site base, J. Biol. Chem. 266 (1991) 8369—8375.

[9] A.A. Pantazaki, A.K. Ioannou, D.A. Kyriakidis, A thermostable beta-ketothiolase of polyhydroxyalkanoates (PHAs) in Thermus thermophilus: purification and biochemical properties, Mol. Cell. Biochem. 269 (2005) 27—36.

[10] M. Klein, P. Wenk, M.B. Ansorge-Schumacher, M. Fritsch, W. Hartmeier, Heterologous expression and characterisation of a biosynthetic thiolase from Clostridium butyricum DSM 10702, Enzym. Microbiol. Technol. 45 (2009) 361—366.

[11] Y. Meng, J. Li, Cloning, expression and characterization of a thiolase gene from Clostridium pasteurianum, Biotechnol. Lett. 28 (2006) 1227—1232.

[12] D.P. Wiesenborn, F.B. Rudolph, E.T. Papoutsakis, Thiolase from Clostridium acetobutylicum ATCC 824 and its role in the synthesis of acids and solvents, Appl. Environ. Microbiol. 54 (1988) 2717—2722.

[13] P. Durre, Fermentative butanol production: bulk chemical and biofuel, Ann. N.Y. Acad. Sci. 1125 (2008) 353—362.

[14] S. Dusseaux, C. Croux, P. Soucaille, I. Meynial-Salles, Metabolic engineering of Clostridium acetobutylicum ATCC 824 for the high-yield production of a biofuel composed of an isopropanol/butanol/ethanol mixture, Metab. Eng. 18 (2013) 1—8.

[15] Y.L. Lin, H.P. Blaschek, Butanol production by a butanol-tolerant strain of Clostridium acetobutylicum in Extruded Corn Broth, Appl. Environ. Microbiol. 45 (1983) 966—973.

[16] K. Vollherbst-Schneck, J.A. Sands, B.S. Montenecourt, Effect of butanol on lipid composition and fluidity of Clostridium acetobutylicum ATCC 824, Appl. Environ. Microbiol. 47 (1984) 193—194.

[17] S. Atsumi, A.F. Cann, M.R. Connor, C.R. Shen, K.M. Smith, M.P. Brynildsen, K.J. Chou, T. Hanai, J.C. Liao, Metabolic engineering of Escherichia coli for 1-butanol production, Metab. Eng. 10 (2008) 305—311.

[18] M. Inui, M. Suda, S. Kimura, K. Yasuda, H. Suzuki, H. Toda, S. Yamamoto, S. Okino, N. Suzuki, H. Yukawa, Expression of Clostridium acetobutylicum butanol synthetic genes in Escherichia coli, Appl. Microbiol. Biotechnol. 77 (2008) 1305—1316.

[19] S.H. Baer, H.P. Blaschek, T.L. Smith, Effect of butanol challenge and temperature on lipid composition and membrane fluidity of butanol-tolerant Clostridium acetobutylicum, Appl. Environ. Microbiol. 53 (1987) 2854—2861.

[20] J.K. Guterl, D. Garbe, J. Carsten, F. Steffler, B. Sommer, S. Reisse, A. Philipp, M. Haack, B. Ruhmann, A. Koltermann, U. Kettling, T. Bruck, V. Sieber, Cell-free metabolic engineering: production of chemicals by minimized reaction cascades, ChemSusChem 5 (2012) 2165—2172.

[21] Y.H.P. Zhang, Simpler is better: high-yield and potential low-cost biofuels production through cell-free synthetic pathway biotransformation (SyPaB), ACS Catal. 1 (2011) 998—1009.

[22] J. Soding, A. Biegert, A.N. Lupas, The HHpred interactive server for protein homology detection and structure prediction, Nucleic Acids Res. 33 (2005) W244—W248.

[23] S.K. Saha, L. Uma, G. Subramanian, An improved method for marine cyanobacterial DNA isolation, World J. Microbiol. Biotechnol. 21 (2005) 877—881.

[24] J. Sambrook, D.W. Russell, Molecular Cloning: a Laboratory Manual, Cold Spring Harbor Laboratory, 2001.

[25] A. Aitken, M. Learmonth, Protein determination by UV absorption, in: J. Walker (Ed.), The Protein Protocols Handbook, Humana Press, 2002, pp. 3—6.

[26] W.J. Waddell, A simple ultraviolet spectrophotometric method for the determination of protein, J. Lab. Clin. Med. 48 (1956) 311—314.

[27] P. Wolf, A critical reappraisal of Waddell's technique for ultraviolet spectrophotometric protein estimation, Anal. Biochem. 129 (1983) 145—155.

[28] B. Sommer, D. Garbe, P. Schrepfer, T. Brück, Characterization of a highly thermostable ß-hydroxybutyryl CoA dehydrogenase from Clostridium acetobutylicum ATCC 824, J. Mol. Catal. B Enzym 98 (2013) 138—144.

[29] C.K. Riener, G. Kada, H.J. Gruber, Quick measurement of protein sulfhydryls with Ellman's reagent and with 4,4'-dithiodipyridine, Anal. Bioanal. Chem. 373 (2002) 266—276.

[30] A.S. Konagurthu, J.C. Whisstock, P.J. Stuckey, A.M. Lesk, MUSTANG: a multiple structural alignment algorithm, Proteins 64 (2006) 559—574.

[31] S.A. Kim, L. Copeland, Acetyl coenzyme a acetyltransferase of Rhizobium sp. (Cicer) strain CC 1192, Appl. Environ. Microbiol. 63 (1997) 3432—3437.

[32] R.C. Taylor, A.K. Brown, A. Singh, A. Bhatt, G.S. Besra, Characterization of a beta-hydroxybutyryl-CoA dehydrogenase from Mycobacterium tuberculosis, Microbiology 156 (2010) 1975—1982.

[33] M. Hedl, A. Sutherlin, E.I. Wilding, M. Mazzulla, D. McDevitt, P. Lane, J.W. Burgner 2nd, K.R. Lehnbeuter, C.V. Stauffacher, M.N. Gwynn, V.W. Rodwell, Enterococcus faecalis acetoacetyl-coenzyme A thiolase/3-hydroxy-3-methylglutaryl-coenzyme A reductase, a dual-function protein of isopentenyl diphosphate biosynthesis, J. Bacteriol. 184 (2002) 2116—2122.

[34] B. Maekawa, N. Koyama, Y. Doi, Purification and properties of 3-ketothiolase from Alcaligenes latus, Biotechnol. Lett. 15 (1993) 691—696.

[35] H.F. Gilbert, B.J. Lennox, C.D. Mossman, W.C. Carle, The relation of acyl transfer to the overall reaction of thiolase I from porcine heart, J. Biol. Chem. 256 (1981) 7371—7377.

[36] E.J. Steen, R. Chan, N. Prasad, S. Myers, C.J. Petzold, A. Redding, M. Ouellet, J.D. Keasling, Metabolic engineering of Saccharomyces cerevisiae for the production of n-butanol, Microb. Cell Fact. 7 (2008) 36.

[37] S. Atsumi, T. Hanai, J.C. Liao, Non-fermentative pathways for synthesis of branched-chain higher alcohols as biofuels, Nature 451 (2008) 86—89.

[38] D.R. Nielsen, E. Leonard, S.H. Yoon, H.C. Tseng, C. Yuan, K.L. Prather, Engineering alternative butanol production platforms in heterologous bacteria, Metab. Eng. 11 (2009) 262—273.

[39] B. Sommer, M. Haack, D. Garbe, T. Brück, Catalytic modules in non-natural butanol biosynthesis: conversion of the key intermediate crotylalcohol to N-butanol via a designed enzyme cascade, JSM Biotechnol. Bioeng. 1 (2013).

[40] A.D. Neale, R.K. Scopes, R.E. Wettenhall, N.J. Hoogenraad, Pyruvate decarboxylase of Zymomonas mobilis: isolation, properties, and genetic expression in Escherichia coli, J. Bacteriol. 169 (1987) 1024—1028.
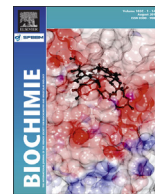
Research paper

Identification and optimization of a novel thermo- and solvent stable ketol-acid reductoisomerase for cell free isobutanol biosynthesis

Steven Reiße, Daniel Garbe, Thomas Brück*

Fachgebiet Industrielle Biokatalyse, Technische Universität München, Lichtenbergstr. 4, 85748 Garching, Germany

ABSTRACT

Due to its enhanced energy content and hydrophobicity, isobutanol is flagged as a next generation biofuel and chemical building block. For cellular and cell-free isobutanol production, NADH dependent (over NADPH dependent) enzyme systems are desired. To improve cell-free isobutanol processes, we characterized and catalytically optimized a NADH dependent, thermo- and solvent stable ketol-acid reductoisomerase (KARI) derived from the bacterium *Meiothermus ruber* (Mr). The wild type Mr-KARI has the most temperature tolerant KARI specific activity reported to date. The KARI screening procedure developed in this study allows accelerated molecular optimization. Thus, a KARI variant with a 350% improved activity and enhanced NADH cofactor specificity was identified. Other KARI variants gave insights into Mr-KARI structure–function relationships.

© 2014 Elsevier B.V. and Société française de biochimie et biologie Moléculaire (SFBBM). All rights reserved.

1. Introduction

Ketol-acid reductoisomerase (KARI, EC 1.1.1.86) catalyzes the unusual two-step conversion of 2-acetolactate into 2,3-dihydroxyisovalerate via an initiating alkyl migration and a following NAD(P)H dependent reduction [1]. The Mg^{2+} dependent KARI activity is present in plants, fungi and microorganisms [1]. Recently, the KARI dependent part of branched-chain amino acid biosynthesis has attracted great interest in both sustainable agrochemical- and biofuel research. Especially isobutanol is flagged as a next generation biofuel and sustainable chemical building block due to its enhanced energy content and hydrophobicity compared to ethanol. The metabolic conversion of the 2-keto acid to the target alcohols involves the host specific oxidoreductase activities of KARI and an alcohol dehydrogenase (ADH).

Recently, *E. coli* specific KARI has been successfully engineered to accept NADH to significantly improve isobutanol yields [2]. A generally applicable method for modification of the KARI superfamily has been reported by Brinkmann-Chen et al. [3]. Although,

significant improvements in isobutanol biosynthesis have been implemented at a molecular level, current fermentative processes have a product ceiling of 2% (v/v) due to toxicity effects and non-productive metabolic side reactions [4].

More recently, a cell-free isobutanol production system based on a designed enzyme cascade has been reported [5], which holds the promise of higher isobutanol titers and simplified product recovery. This redox–neutral reaction cascades utilizes NAD^+ as the universal cofactor and operates at elevated temperatures (i.e. 50 °C) and solvent concentrations. These process parameters enable isobutanol titers in excess of those obtainable with cellular systems. Further, since process conditions and substrate/intermediate specificities are strictly controlled, unproductive side reactions are eliminated, which allows a targeted conversion of sugars into isobutanol. The final process configuration of the cell-free isobutanol production system is only limited by the operational parameters of the individual enzyme components [5]. Key to implementation of this cell-free reaction cascade was the exchange of NADPH dependent oxidoreductase activities with equivalents accepting NADH as the cofactor. While aldehyde and alcohol dehydrogenases could be substituted by reported NADH dependent alternatives [6,7], the search for a NADH dependent KARI activity remained challenging, especially as process stability at high temperature and high solvent concentrations were additional enzyme selection criteria. None of the reported KARI enzyme activities met the desired process parameters with respect to temperature tolerance, while no data was available for solvent tolerance.

Abbreviations: KARI, ketol-acid reductoisomerase; Mr, *Meiothermus ruber*; Cg, *Corynebacterium glutamicum*; Ss, *Sulfolobus solfataricus*; Se, *Slackia exigua*; Ec, *Escherichia coli*; τ, half-life; ADH, alcohol dehydrogenase; WT, wild-type; CV, coefficient of variance; Z′, dimensionless parameter for the quality of an assay itself; Z, dimensionless parameter for the quality of an array of tested variants.

* Corresponding author.

E-mail addresses: steven.reisse@tum.de (S. Reiße), daniel.garbe@tum.de (D. Garbe), brueck@tum.de (T. Brück).

In this study, we present a new NADH dependent KARI activity isolated from the bacterium *Meiothermus ruber* DSM 1279 (Mr-KARI). This enzyme features an excellent catalytic performance together with pronounced thermal- and solvent stabilities. The ideal combination of these process relevant parameters, allowed successful incorporation of the wild type Mr-KARI activity in our designed cell-free isobutanol production system [5].

Since the catalytic performance of the wild type KARI was a limiting factor in achieving even higher isobutanol yields, we addressed this issue by combining directed evolution with targeted genetic engineering strategies. Here we report on the detailed characterization of wild type KARI and present a new KARI directed *in-vivo* screening methodology. Application of this new methodology allowed identification of various KARI variants with enhanced catalytic efficiency. The variant T84S could be purified to homogeneity and was thoroughly characterized.

2. Materials and methods

2.1. Reagents and kits

Restriction enzymes, T4 DNA ligase, T4 Kinase, Shrimp alkaline phosphatase, Phusion polymerase and desoxynucleotides were purchased from Thermo Scientific (Ulm, Germany). Desoxyribonuclease I from bovine pancreas was from Serva Electrophoresis (Heidelberg, Germany). All enzymes were used according to the manufacturers' recommendations, applying the provided buffer solutions. Oligonucleotides were ordered from Eurofins MWG Operon (Ebersberg, Germany). All chemicals were, unless otherwise stated, purchased in analytical grade from Sigma-Aldrich (München, Germany), Carl Roth (Karlsruhe, Germany), Serva Electrophoresis and AppliChem (Darmstadt, Germany). Plasmids were purified applying the GeneJET Plasmid Miniprep Kit (Thermo Scientific), PCR products and enzymatically manipulated DNA were purified via the innuPREP DOUBLEpure Kit (Analytik Jena, Germany).

2.2. Strains and media

Meiothermus ruber DSM 1279 (DSMZ, Braunschweig, Germany) was grown aerobically at 50 °C in *Thermus ruber* medium containing trypton (5 g L^{-1}), yeast extract (1 g L^{-1}) and soluble starch (1 g L^{-1}), adjusted to pH 8. *E. coli* Rosetta cells (F- ompT hsdSB(rB-mB-) gal dcm (DE3) pLysSRARE (CamR)) were purchased from Merck (Darmstadt, Germany) and were grown in TB medium for protein expression. The KARI knockout strain *E. coli* JW3747 (F-, Δ(araD-araB)567, ΔlacZ4787(::rrnB-3), λ-, rph-1, ΔilvC725:kan, Δ(rhaD-rhaB)568, hsdR514) was obtained from the Keio collection [8]. This strain was grown in M9 minimal medium. *E. coli* XL1-Blue cells (recA1 endA1 gyrA96 thi-1 hsdR17 supE44 relA1 lac [F' proAB lacIqZDM15 Tn10 (Tetr)]) from Stratagene (Waldbronn, Germany) were grown in LB medium. All media were supplemented with kanamycin (30 μg ml^{-1}), TB additionally with chloramphenicol (34 μg ml^{-1}).

2.3. Sequence alignment and structural modeling

KARIs have been observed in several pro– and eukaryotes. A number of gene and protein sequences may be found in various databases, although not all are characterized. For the amino acid alignment we chose only bacterial sequences retrieved from the UniProt database [9]. Clustal Omega [10–12] was used to conduct the sequence alignment and ESPript [13] for further editing. Examination of structure–function relationships based on a modeled Mr-KARI structure conducted by the Phyre^2 server [14]. After

primary sequence alignment the published crystal structure of *Pseudomonas aeruginosa* (PDB 1NP3) KARI was used as a template to compute the Mr-KARI structural features. Subsequently, respective KARI ligands Mg^{2+}, 2,3-dihydroxy-3-methylvalerate and NADP$^+$ were adopted from the spinach scaffold (PDB 1YVE and 1QMG).

2.4. DNA isolation and cloning

The plasmid pET28a (Merck) was pretreated as described by Guterl et al. [5]. Genomic DNA from *Meiothermus ruber* DSM 1279 was isolated as described by Saha [15]. The gene *mrub_1907* was amplified from genomic DNA by PCR with the phosphorylated primers listed in Table 1. PCR fragments were ligated into pCBR via the BsmBI restriction site. The obtained pCBR-Mr-KARI-CHis plasmid was transformed in *E. coli* as described elsewhere [16]. DNA sequencing validated all cloning procedures.

2.5. Protein expression and purification

For protein expression, transformed cells were cultivated in a shaking flask at 37 °C in TB medium supplemented with kanamycin (30 μg ml^{-1}) and chloramphenicol (34 μg ml^{-1}). The cells were induced with 1 mM IPTG at OD$_{600}$ 0.5–0.8 and afterwards incubated at 20 °C for 20 h.

The basal expression of Mr-KARI in the knockout strain JW3747 was conducted in M9 minimal medium supplemented with 0.4% (w/v) glucose and kanamycin (30 μg ml^{-1}) as indicated [16]. The culture was inoculated with transformed cells and cultivated at 37 °C overnight. Cultures were subsequently harvested and frozen at −20 °C until further use.

For cell disruption the cell pellets were resuspended in binding buffer (50 mM HEPES pH 8, 20 mM imidazole, 10% (v/v) glycerol, 0.1% (v/v) Tween 20), supplemented with DNAse (10 mg ml^{-1}). The cells were lysed with an Avestin EmulsiFlex-B15 homogenizer. Debris was removed by centrifugation at 20,000 × g and 4 °C for 30 min. The supernatant was loaded onto Ni-NTA columns and washed with 5 column volumes of binding buffer. His-tagged Mr-KARI was eluted in one step with two column volumes of elution buffer (50 mM HEPES pH 8, 500 mM imidazole, 10% glycerol, 0.1% Tween 20). All fractions were analyzed by 12% SDS-PAGE.

The purified enzyme was subsequently desalted via HiPrep 26/10 Desalting-column (GE Healthcare Europe; Freiburg, Germany) in either 20 mM ammonium carbonate for lyophilization or in 50 mM HEPES pH 7.5 plus 10% glycerol for storing at −80 °C.

Protein contents were quantified spectrophotometrically by measuring the absorbance at 215 and 225 nm as indicated [17–19].

2.6. Enzyme characterization

All assays were performed in microtiter plate format using an Enspire 2 (Perkin Elmer; Rodgau, Germany). The reaction was initiated by addition of 180 μl assay mixture to 20 μl enzyme solution. Assay mixtures were preincubated in a thermomixer for accurate temperature control. The pH was adjusted to the corresponding temperature. One unit of enzyme activity was defined as the amount of enzyme that catalyzed the formation of 1 μmol of product per minute.

Table 1
Oligonucleotides.

Primer	Sequence (5′ – 3′)
Mr-KARI fwd	CAGCAACGTCTCGCATATGAAGATTTACTACGACCAGGACGCAG
Mr-KARI rev	GCTACCGACCTCTTCCTTCGTGAAC

The KARI activity was quantified spectrophotometrically by the NADH consumption connected to the conversion of 2-acetolactate to 2,3-dihydroxyisovalerate at 50 °C. The assay mixture contained 5 mM acetolactate, 0.3 mM NADH, 10 mM MgCl$_2$ and 50 mM HEPES pH 7 (50 °C). Before every experiment, 2-acetolactate was freshly synthesized with a purified acetolactate synthase (ALS) from *Bacillus subtillis*, existing in our lab. The reaction mixture contained 50 mM HEPES pH 7, 0.1 mM thiamine pyrophosphate, 2.5 μM FAD, 50 mM sodium pyruvate. After addition of ALS the reaction was incubated at 40 °C for 40 min. The 2-acetolactate concentration was determined via NMR: 500 MHz, D$_2$O, δ = 1.46 (s, 3H, COHC*H*3); δ = 2.26 (s, 3H, COC*H*3). Sodium 3-(trimethylsilyl)propanoate (TSP) was used as internal standard: δ = 0.00 (s, 9H).

2.7. Library construction and screening procedure

The primary library was constructed via error prone PCR in accordance to Jaeger et al. [20] and subsequently cloned in the pCBR vector using *Nde*I and *Sal*I restriction sites. The plasmids were transformed into the KARI knockout strain JW3747 via electroporation. As control we used the pET28a vector without insert. The library was plated on M9 minimal medium agar plates supplemented with 30 μg ml^{-1} kanamycin (M9 + kana). Grown colonies were transferred into 96-well microtiter plates containing 200 μl M9 + kana and incubated at 37 °C for 24 h. Afterwards, deep-well plates containing 1.5 ml M9 + kana were inoculated with this sub culture and grown at 37 °C for 48 h. The cells were harvested and resuspended in 100 μl of 50 mM HEPES pH 7 (50 °C), 0.5 mg ml^{-1} lysozyme and 10 mg ml^{-1} DNAse to prepare the crude cell extracts. The crude extracts were incubated for 60 min and subsequently centrifuged. All activity measurements were performed in 96-well microtiter plates at 50 °C with 20 μl of the supernatant according to the protocol described above.

The whole screening procedure was validated according to the methods of Zhang et al. [21]. Potential hits were verified by rescreening. Plasmids of improved variants were subsequently isolated and sequenced. Individual amino acid exchanges, received by the error prone PCR, were segregated via quick change mutagenesis protocol according to Papworth et al. [22] Applied oligonucleotides can be found in Table S2.

Site saturation mutagenesis was carried out with primers (Table S3) degenerated at specific target sites according to the same protocol. Caster 2.0 [23,24] was used to calculate the individual library sizes and the number of variants to be screened.

3. Results and discussion

3.1. Mr-KARI identification and sequence analysis

Amino acid sequences of representative prokaryotic KARI enzymes were aligned and searched against the reported *Meiothermus ruber* genome. Sequence alignment resulted in identification of a predicted *Meiothermus ruber* (Mr, UniProt: D3PT81) protein, representing a putative KARI activity. The putative protein shared 53% and 50% sequence identity with the KARI activities of *Corynebacterium glutamicum* (Cg, UniProt: Q57179) and *Sulfolobus solfataricus* (Ss, UniProt: Q9UWX9), respectively. In contrast, the Mr-KARI protein only shared 34% identity with the reported *E. coli* KARI sequence (Ec, UniProt: P05793) (Fig. S1).

Interestingly, the *E. coli* KARI features ~150 additional residues, which are absent in the former. These additional residues are an evolutionary evolved duplication of the C-terminal α-helical domain of the *E. coli* polypeptide. The origin of the *E. coli* KARI is therefore comparable to the plant KARI enzymes, which are typified as class II KARI. In contrast to the former short, class I, KARI

enzymes, the *E. coli* KARI is consequently classified as a bacterial class II [25]. Nevertheless, despite this observation all of the evaluated KARI sequences harbor conserved regions that define the KARI enzyme family [1]. The predicted secondary structure of Mr-KARI encompasses the signature 182-residue N-terminal domain and a 157-residue C-terminal domain. While the N-terminal domain (residues 1–182) features a mixed α/β structure, which includes the canonical dinucleotide (cofactor) binding fold (Rossmann-fold), the C-terminal domain (residues 183–339) is predominately composed of α-helical motifs. The Rossmann-fold was identified by the highly conserved GxGxxG motif (Fig. 1A), which is characteristic for NAD(P)$^+$ depending oxidoreductases [26].

The binding site for the 2′-phosphate moiety of NAD(P)H was identified in a loop region 18 amino acids downstream of the GxGxxG motif.

The NAD(P)H binding site of all KARI sequences analyzed in this study contain 7 amino acid residues, with the exception of the *E. coli* motif which features 12 residues [2,3]. The differences in the NAD(P)H binding site segregates the *E. coli* KARI from other KARI enzymes examined in this study.

To examine structure–function relationships of the class I Mr-KARI in more detail, the putative sequence was submitted to the Phyre^2 bioinformatics tools [14]. The resulting structural model had a confidence interval of 98% over 332 residues with more than 90% accuracy to the best fitting scaffold of *P. aeruginosa* (PDB 1NP3). In the resulting Mr-KARI model (Fig. 1B) we adopted all ligands from the structural data of the spinach KARI (PDB 1YVE and 1QMG).

Examination of the resulting Mr-KARI model indicated that the NADPH binding site adopts the characteristic βαβαβ motif (Fig. 1C) [27]. As additionally depicted in Fig. 1C, the green loop representing the putative NADPH binding site, is only six residues (Leu46 - Arg51) in length. This modeling data contrasts the sequence alignment analysis, which indicated a seven amino acid co-factor binding motif. The model shows that Asn52 is not part of the loop of the putative NADPH binding site but is rather a part of the adjacent α-Helix domain. Further NADPH binding motif analyses revealed that the six-residue loops are characterized by conserved Lys/Arg and Ser residues at the C-terminus. By contrast, seven-residue loops end with a conserved SxS amino acid arrangement [3]. Consequently, these structural features of our Mr-KARI model imply a six-residue loop encompassing the positively charged Arg47 and Arg51 residues at either end, which are probably responsible for binding of the NADPH [27]. However, compared to other KARI family members featuring a six-residue loop NADPH binding motif, the positions of the small polar residue Ser50 and Arg51 are reversed in Mr-KARI [3]. This unusual feature of the NADPH binding loop in Mr-KARI warranted further experimental investigation to define the cofactor preference of the enzyme.

3.2. Cloning, heterologous expression and purification

The gene of Mr-KARI was fused to a C-terminal His-tag and transformed into *E. coli Rosetta* (DE3) cells. The heterologous enzyme was purified to homogeneity and examined by SDS-PAGE (Fig. S2). More than 90% of the recombinant enzymes were present in the soluble cell fraction. The Mr-KARI monomer exhibited a single band at approximately 40 kDa, which is consistent with a calculated molecular weight of 39 kDa. The purified enzyme could be stored either as lyophilisate or as frozen stock at −80 °C. The lyophilisate was stable for several months, but accompanied with a reduced thermal stability compared to the liquid stock. The latter can be stored over one year without any changes in the biochemical characteristics.
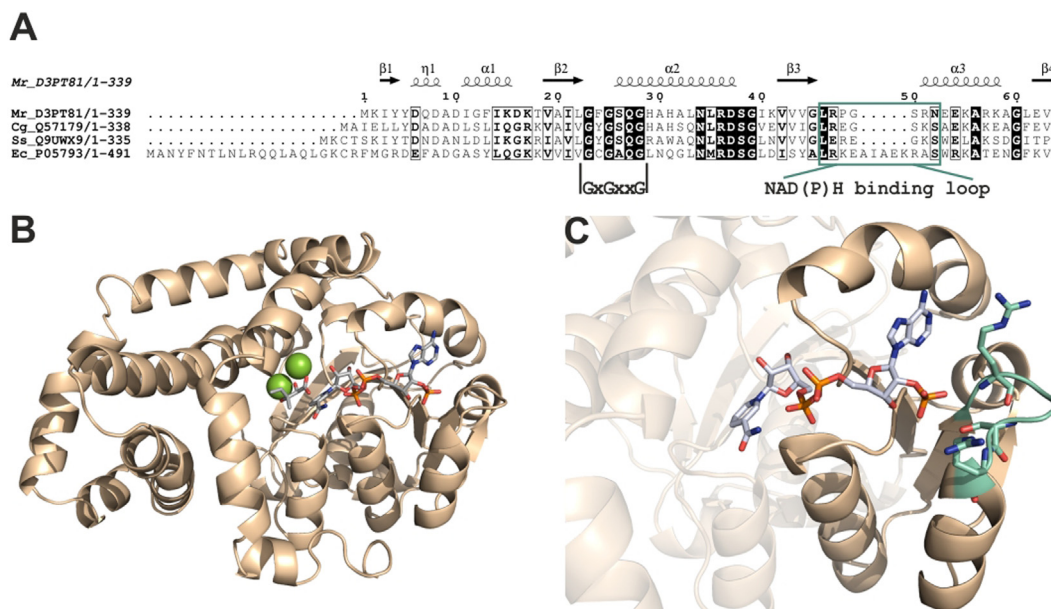
Fig. 1. Mr-KARI identification and sequence. (A) Amino acid sequence alignment of the Rossmann fold between *Meiothermus ruber* (Mr, UniProt: D3PT81), *Corynebacterium glutamicum* (Cg, UniProt: Q57179), *Sulfolobus solfataricus* (Ss, UniProt: Q9UWX9) and *Escherichia coli* (Ec, UniProt: P05793). The GxGxxG motif and the positively charged loop for NAD(P)H binding are labeled and boxed. (B) Modeled Mr-KARI structure. The ligands were adopted from spinach KARI (PDB 1YVE: Mg^{2+}, green spheres; $NADP^+$, gray stick structure; PDB 1QMG: 2,3-dihydroxy-3-methylvalerate, gray stick structure). (C) Cofactor binding site. The positively charged loop, which interacts with the 2′-phosphate of the $NADP^+$, is highlighted in green.

3.3. Biochemical characterization of wild type Mr-KARI

To examine if Mr-KARI was a suitable building block for designed cellular or cell-free isobutanol production, its kinetic and biochemical characteristics were determined. In addition to the Mr-KARI NADPH/NADH cofactor preference, its operational pH and temperature profiles, we also evaluated its solvent stability. This is the first time that solvent stability for any member of the KARI family is reported. In this context, we consider solvent stability as a crucial process parameter for the suitability of Mr-KARI in the cell-free isobutanol biosynthesis processes.

Since the desired operating temperature of our cell-free isobutanol process was 50 °C [5], all biochemical features of Mr-KARI were measured at this temperature, with exception of the temperature optimum.

The obtained pH optimum for Mr-KARI was 7.0 (Fig. 2A). This is consistent with previous values described for KARI enzymes. For comparison, the KARI enzymes of *C. glutamicum* [28], *Hordeum vulgare* [29], *Neurospora crassa* [30] and *Spinacea oleracea* [31] all display a pH optimum at 7.5. In line with our data observed for Mr-KARI, all other reported enzyme activities exhibited a significant activity decrease below pH 7.

The temperature profile of Mr-KARI was measured by incubating the enzyme at 30–65 °C for 10 min (Fig. 2B), followed by determination of the residual activity at the corresponding temperatures. Fig. 2B shows that the temperature optimum of Mr-KARI is beyond 65 °C, which also marks the instrumental limit of our assay procedure. This is the highest operational temperature ever measured for any KARI enzyme.

At the desired process temperature of 50 °C, Mr-KARI showed an extended time-dependent stability (half-life (IT_{50}) = 71 ± 0.2 h; Fig. 2C). The previously stated lower value of 34 h [5] published by us, was due to the application of lyophilized enzyme preparation applied in the reported experimental procedures. Clearly, the freshly prepared or frozen stock used in this study showed enhanced viability.

In the context of cell-free isobutanol production, the solvent stability of Mr-KARI was of utmost importance. Therefore, we evaluated the Mr-KARI activity in presence of various isobutanol concentrations. As depicted in Fig. 2D 60% of the Mr-KARI remains active even in the presence of 6% (v/v) isobutanol. In comparison, a two-phase isobutanol/water system is formed at product concentrations above 12% (v/v) [32]. This data is consistent with solvent stabilities observed for other enzyme systems derived from *Meiothermus ruber* [33].

3.4. Kinetic properties

To evaluate the catalytic performance of the Mr-KARI assay we initially validated reported assay conditions using *E. coli* KARI [2]. We could reproduce the kinetics of *E. coli* KARI. Interestingly, the NADH dependent K_m value (0.24 ± 0.02 mM) determined by us was in line with data reported by Rane and Calvo [34].

In contrast to *E. coli* KARI, the Mr equivalent featured a 10 times higher specific activity combined with a 15 times higher catalytic efficiency with respect to NADH as a cofactor (Table 2).

Detailed examination of the cofactor specificity of Mr-KARI showed that NADPH dependent K_m and k_{cat} values were 0.02 ± 0.00 mM and 0.98 ± 0.01 s^{-1}, respectively. Therefore, the NADPH dependent catalytic efficiency of Mr-KARI was calculated as 54.5 ± 11.1 mM^{-1} s^{-1}. This k_{cat}/K_m value is lower than the values reported for *E. coli* (88 ± 11 mM^{-1} s^{-1}), *Shewanella* sp. (4500 ± 450 mM^{-1} s^{-1}) and *Slackia exigua* (Se, 800 ± 100 mM^{-1} s^{-1}) KARI [3].

Subsequently, we examined the 2-acetolactate (native substrate) dependent catalytic performance in the presence of either NADH or NADPH. In the presence of NADPH as a cofactor Mr-KARI showed a considerably reduced catalytic efficiency (k_{cat}/K_m = 10.2 ± 1.8 mM^{-1} s^{-1}) compared to *E. coli* KARI [35], which was caused by a relatively high K_m (2-acetolactate) of 0.08 ± 0.01 mM and low k_{cat} (2-acetolactate) of 0.77 ± 0.01 s^{-1}. A detailed overview of kinetic parameters is provided in Table S1.
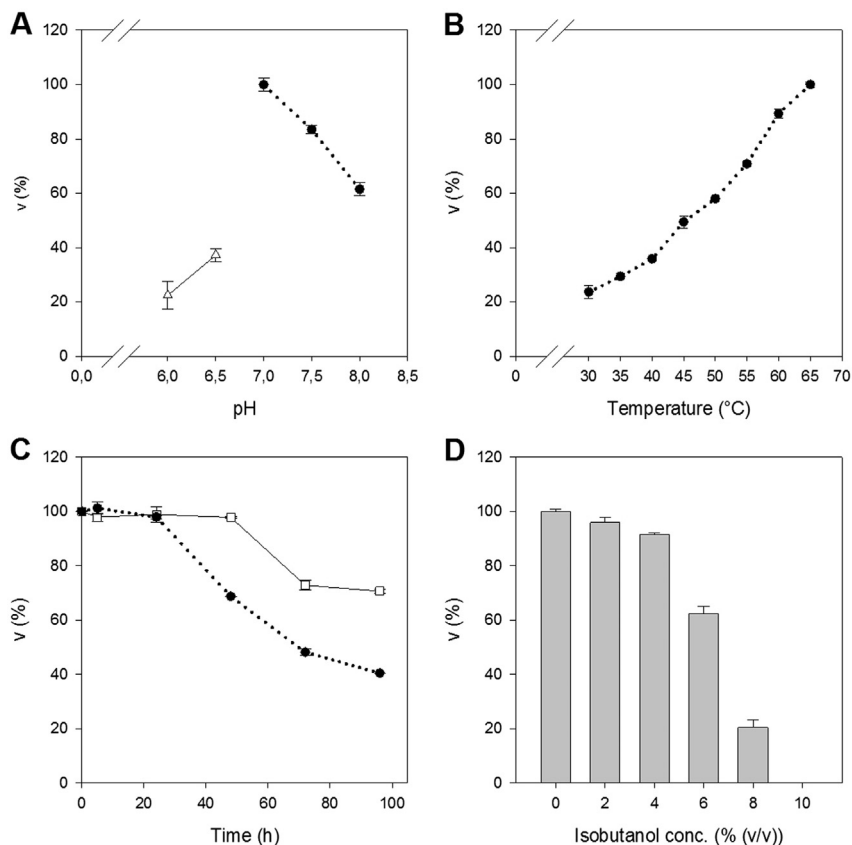
Fig. 2. Effects of different conditions on the activity of purified Mr-KARI. The highest obtained activity was defined as 100%. (A) pH profile: The reactions were carried out at described conditions with following buffers: —Δ— 50 mM Phosphate buffer, pH 6–6.5; ⋯●⋯ 50 mM HEPES, pH 7–8; (B) Temperature profile: The reactions were carried out at described conditions in a range from 30 to 65 °C. (C) Thermal stability of Mr-KARI. Enzyme solutions were incubated at various temperatures and measured regularly under our predefined assay conditions: —□—40 °C; ⋯●⋯ 50 °C. (D) Isobutanol tolerance: The assays were carried out under described conditions in the presence of various isobutanol concentrations.

The kinetic data clearly indicate that Mr-KARI can utilize NADH more efficiently than any other reported KARI activity. This feature is particularly important for improving both cellular and cell-free isobutanol production systems. To optimize the physical characteristics of Mr-KARI we set out to generate consolidated mutant libraries. This however required the design of a high-throughput screening platform for KARI specific activity.

3.5. Development of KARI specific high-throughput screening platform

Since the catalytic efficiency of the wild type (WT) Mr-KARI activity was limiting in our cell-free isobutanol production

Table 2
Characteristics of Mr-KARI measured for the cofactor NADH.

Property	Value
Specific enzyme activity (50 °C)	0.7 U mg^{-1}
Optimum temperature	>65 °C
Thermal stability (50 °C)	τ = 71 h
Solvent tolerance (isobutanol)	≥6% (v/v)
Optimum pH	7
Molecular weight	39 kDa
K_m[a]	0.24 mM
k_{cat}	1.09 s^{-1}
k_{cat}/K_m	4.6 mM^{-1} s^{-1}

[a] The kinetic constants were measured with varying concentrations of NADH (0.1–0.5 mM) and saturating concentrations of 2-acetolactate in 50 mM HEPES pH 7 at 50 °C.

approach, we have developed a new KARI specific screening platform, which enables rapid selection of catalytically improved variants. The underlying mechanism of the screening platform was the application of an *E. coli* KARI knockout strain as *in-vivo* selection tool. This strain allowed us to establish a simple and rapid analysis of large KARI variant libraries by selecting viable phenotypes. In the absence of the amino acids valine, leucine and isoleucine the knockout strain was not able to grow on minimal medium, unless a functional KARI activity was introduced into the cell.

For cellular supplementation of functional KARI activities we utilized the basal expression provided by the pET vector system. Fig. 3A shows that Mr-KARI was successfully expressed in the knockout strain. On SDS-PAGE the protein at 40 kDa correlates well with previous expression experiments carried out in corresponding *E. coli* hosts. However, the basal expression level in our cellular screening system is low, which leads to relative faint activity signals in a 96-well screen.

For qualification of the new screening approach, we primarily simulated the procedure using the Mr-KARI WT enzyme in order to determine the dynamic range of the assay. To quantify the sensitivity of the applied screening procedure the coefficient of variance (CV) and the Z′-factor was determined [21]. The Z′-factor is a dimensionless parameter that provides a qualitative sensitivity measure of the applied assay. Whereas negative Z′ or zero values indicate poor assay quality, values close to one, mark ideal assay conditions [21].

Data in Fig. 3B indicate that the separation between the WT KARI and the control (no KARI supplementation) is relative small.
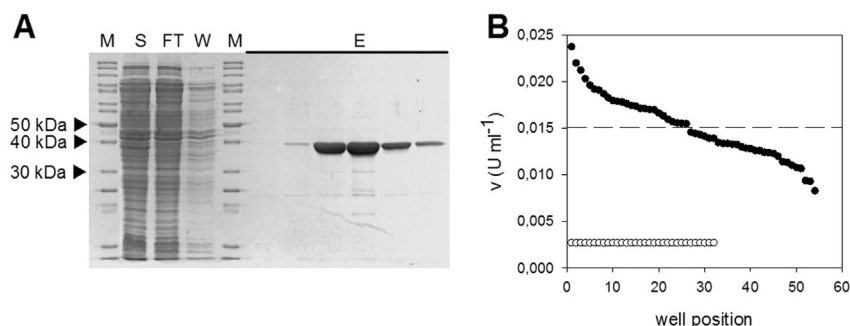
Fig. 3. Assay development for Mr-KARI screening. (A) SDS-PAGE of heterologously expressed Mr-KARI in *E. coli* JW3747. Showing protein fractions from supernatant (S), flow through (FT), washing step (W), eluted enzyme (E) and marker (M, PageRuler Unstained Protein Ladder, Thermo Scientific). (B) Scatter plot of Mr-KARI WT activities versus the well position of the clones. Crude extracts were tested in a 96-well microtiter plate with 50 mM HEPES pH 7, 5 mM acetolactate, 0.3 mM NADH and 10 mM MgCl$_2$. The distribution is shown in ordered sequence (Mr-KARI WT: ●; control: ○). The dash line indicates the mean of all measured WT reactions.

This is in agreement with the calculated Z′-factor of 0.2. The calculated CV of 22% indicates that in our screening system we can only segregate variants with significantly improved activities. Even though this is in line with our experimental goals, the design of a more sensitive assay procedure would require a lower CV.

The application of the knockout strain has the advantage of almost no background signal, because control clones with just the pET vector inside cannot grow in minimal medium. Hence, the measured background signal correlates with the buffer blank control. Importantly, the small dynamic range of the assay avoids false positive signals due to native KARI activities derived from the expression host.

In essence the present methodology selects only KARI variants with significantly improved activity, which provides for consolidated (smart) mutant libraries. These consolidated libraries carrying active KARI variants can be rapidly screened by hand and do not require expensive robotic procedures.

3.6. Screening for optimized Mr-KARI derivatives

Our reported cell-free isobutanol synthesis is based on a synchronized reaction cascade to achieve high glucose to isobutanol conversion rates [5]. In this process NADH was used as exclusive electron carrier to minimize the reaction complexity. In the reported experimental set-up the relatively low catalytic activity of

Mr-KARI (0.7 U mg^{-1}) was a significant bottleneck in achieving high product titers. Hence, large amounts of enzyme had to be supplied to the reaction to compensate the low catalytic performance. Therefore, we set-out to generate Mr-KARI variants with improved catalytic efficiency and NADH selectivity.

Initially, we applied a directed evolution based KARI optimization using an error prone PCR strategy. The substitution frequency could be controlled by buffer composition and was adjusted at around 5 − 7 base pair substitutions per kilobase of DNA.

The resulting library was cloned into the pCBR vector [5] with a C-terminal His-tag and transferred into the *E. coli* knockout strain. In the primary screening procedure improved KARI variants were selected from a library of 432 clones. As illustrated in Fig. 4A, KARI mutants displayed a wide range of both increased and reduced activity values compared to the WT Mr-KARI control. Comparable to the WT, the negative control was likewise close to zero and did not affect the screening procedure. The calculated Z-factor for the initial library screen was 0.3 and therefore in line with the expected quality values for the procedure. Our analysis indicated that 11 clones showed an enhanced activity of 150−200 % compared to the Mr-KARI WT. Two clones were identified with a significantly increased activity of more than 200% with respect to the WT (Fig. 4A and B).

Genotypic characterization of the Mr-KARI mutants revealed the molecular changes and allowed a refinement of the primary screen
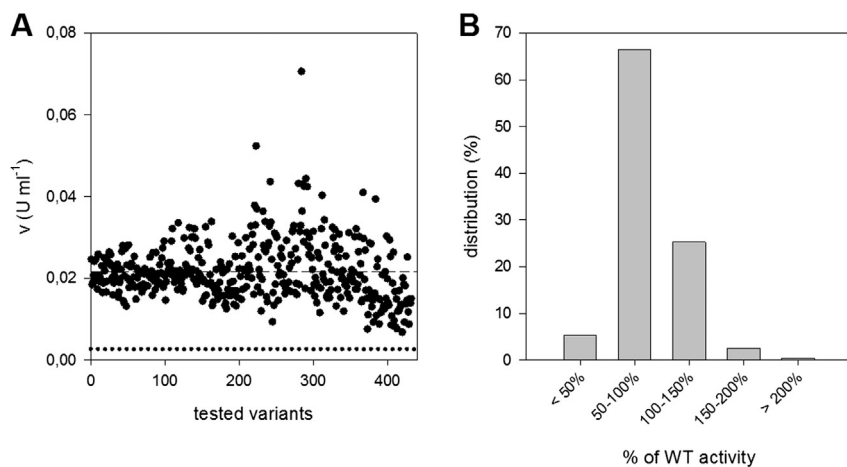

Fig. 4. High-throughput-screening Mr-KARI derivatives. (A) Scatter plot of the first screening round. The activity of the Mr-KARI derivatives was measured in crude extract and 50 mM HEPES pH 7, 5 mM acetolactate, 0.3 mM NADH and 10 mM MgCl$_2$. The dash line indicates the mean value of tested variants. The dotted line indicates the mean value of the control. (B) Relative distribution as percent of wild-type Mr-KARI activity.

Table 3
Kinetic parameters of Mr-KARI WT compared to the T84S Mutant for the substrate with saturating concentrations of NADH[a].

	U mg^{-1}	K_m [mM]	k_{cat} [s^{-1}]	k_{cat}/K_m [mM^{-1} s^{-1}]
WT$_{NADH}$	0.74 ± 0.02	0.55 ± 0.06	0.50 ± 0.01	0.9 ± 0.2
WT$_{NADPH}$	1.11 ± 0.03	0.08 ± 0.01	0.77 ± 0.01	10.2 ± 1.8
T84S$_{NADH}$	2.66 ± 0.27	0.04 ± 0.01	1.30 ± 0.06	34.1 ± 6.0
T84S$_{NADPH}$	1.5 ± 0.02	0.15 ± 0.03	3.81 ± 0.12	25.9 ± 4.7

[a] The Michaelis—Menten constants for the substrate were determined with varying concentrations of 2-acetolactate (0—10 mM) and saturating concentrations of NADH/NADPH in 50 mM HEPES pH 7 at 50 °C.

via site directed segregation of the most promising amino acid sites. The greatest impact could be attributed to a substitution of threonine at position 84 by serine.

The resulting T84S mutant exhibited a specific activity of 2.66 U mg^{-1}, which was an enhancement of ≥350% compared to the WT (0.74 U mg^{-1}). This data set represents a top-level activity for a KARI enzyme operating with NADH as a cofactor (Table 3).

The T84S K_m value (0.04 mM) for 2-acetolactate in the presence of NADH was half of the corresponding NADPH dependent value ($K_m = 0.08$ mM) of the WT Mr-KARI (Table 3). Therefore, the catalytic efficiency of T84S for 2-acetolacte in the presence of NADH is 132% of the NADPH dependent activity measured for the WT enzyme. In comparison, the catalytic efficiency of the WT enzyme with NADH was considerably lower, with only 9% of the NADPH dependent WT efficiency.

The catalytic efficiency of the WT towards NADH as a cofactor was 8% with respect to NADPH and subsequently 60% for T84S (Table S1). Therefore, the T84S modification altered the binding characteristics of both the cofactor and the substrate. However, this mutation is accompanied by a reduced structural and thermal stability, which affected the activity measurements at higher temperatures. In consequence, there was a decrease of the k_{cat} mean values over the time and hence a drop between these values and the specific activity (Table S1).

In analogy to our data, mutagenesis studies with *E. coli* and *Slackia exigua* (Se-KARI) KARI identified amino acid positions equivalent to T84 as optimization hot spots. Particularly, the position Q110 of the *E. coli* KARI is equivalent to I95 of Se-KARI and T84 of Mr-KARI positioned at the start of the α5-helix crossing the Rossmann-fold. Additionally, Q110 and I95 were selected for their potential to affect the cofactor orientation through interaction with the adenine moiety [2,3].

Consequently, we aligned our Mr-KARI model with the crystal structure of Se-KARI. As illustrated in Fig. 5, the position of both substitutions in Mr-KARI (T84) and Se-KARI (I95) are comparable. In both instances we can refer to conservative missense mutations. In case of Se-KARI (I95) the nonpolar residue isoleucine was replaced by a similar one, valine [3]. In Mr-KARI the polar threonine was substituted by serine. The difference consists only in the hydrophobicity of the residues.

In contrast, for *E. coli* KARI a different approach was chosen. Here the polar glutamine was substituted by the nonpolar amino acids valine as well as alanine [2]. Positive effects on the catalytic activity could be detected for all mutations at this position. However, we could detect an additional positive effect on the cofactor preference in Mr-KARI. This can be attributed to an increased influence of the mutation on the whole active side, because of an altered fold located within the cofactor binding motif of Mr-KARI.

3.7. Site saturation mutagenesis of Mr-KARI

Using a rational approach we identified several amino acid residues as further targets for molecular engineering of Mr-KARI in
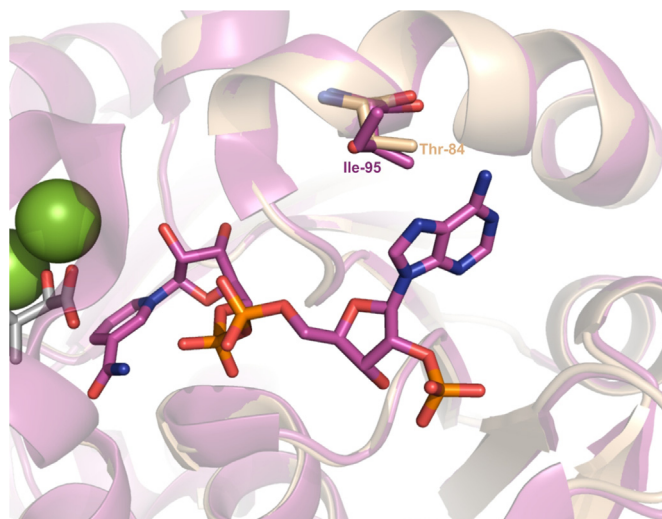

Fig. 5. Structural alignment of modeled Mr-KARI and native Se-KARI. The modeled Mr-KARI structure is colored in gold. The crystal structure of the native Se-KARI (PDB 4KQW) is colored in magenta. Here the NADP$^+$ was adopted from Se-KARI and is also colored in magenta. The other ligands were adopted from spinach KARI as mentioned before. Specific positions for substitutions are labeled.

accordance with structural and kinetic analysis of the *E. coli* KARI [2,3]. Based on these references, we selected the residues Arg47, Arg51 and Ser50 because of their position within the NAD(P)H binding loop and their supposed interaction with the phosphate group of NADPH [2,3,27]. Residues Gln85 and Val88 located within the α5-helix across the Rossmann-fold were selected for site saturation based optimization due to their presumed effect in analogy to T84S. As depicted in Fig. 6, the best improvements with respect to the relative activity were achieved at the positions Ser50 within in the loop region and Val88, which is part of the α5-helix. Surprisingly, the libraries at positions Arg47 and Arg51 resulted in variants with only low enhanced activities or, in case of Arg51, no improvements (data not shown). This data contrast previous reports on *E. coli* KARI optimization, where amino acid exchanges of the basic arginine to the acidic aspartate resulted in increased catalytic properties towards NADH [2,3,34].
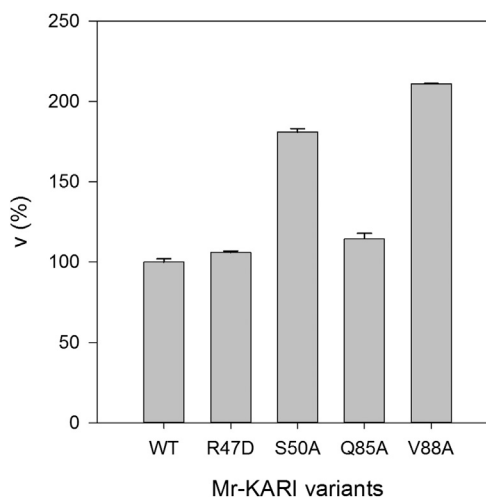

Fig. 6. Comparison of relative activities of different Mr-KARI variants. Relative activity of Mr-KARI WT compared to the variants (R47D, S50A, Q85A, V88A) resulting from the site saturation mutagenesis.

The different enzyme behavior may be due to a difference between the loop regions of the Mr-KARI and other analyzed KARI sequences, where the positions of Ser50 and Arg51 at the end of the loop are reversed. Fig. 1C illustrates that only Ser50 is positioned to build a hydrogen bond to an oxygen atom of the phosphate group. By contrast, the arginine residues are not able to build salt bridges as they are too far removed from the phosphate moiety. The low catalytic effects induced by the mutation of the arginine residues confirmed this hypothesis.

In contrast to previous reported KARI enzymes, our data indicates that the enhanced NADH acceptance of WT Mr-KARI can be attributed to minor interactions between the residues of the binding loop and the cofactor.

The substitution of valine by alanine at position 88 is, like T84S, a conservative missense mutation. The enhanced catalytic activity can therefore be attributed to the same effects.

However, the new Mr-KARI variants obtained by site-saturation could not be purified in the active form and were thus deemed not to be process relevant. Nevertheless, the obtained results gave us new insights into the structure–function relationships and catalytic interactions of Mr-KARI.

4. Conclusion

Here we report a new KARI activity derived from *Meiothermus ruber* DSM 1279, which catalyzes the reductive isomerization of 2-acetolactate to 2,3-dihydroxyisovalerate. The reaction requires both Mg^{2+} and NAD(P)H as cofactors.

Mr-KARI could be expressed in *E. coli* with a very high expression level of over 90% soluble protein in the supernatant cell fraction. The purified enzyme displayed distinct biochemical properties from other members of the KARI family. Most notably Mr-KARI was active over a broad temperature range (30–65 °C) and demonstrated an extremely high stability under process condition ($\tau = 71$ h). Therefore, Mr-KARI represents the most temperature tolerant KARI activity reported to date.

Further, the neutral pH optimum and the high tolerance towards isobutanol ($IS_{50} \geq 6\% (v/v)$) did also meet our process specifications. Moreover, kinetic examinations demonstrated that Mr-KARI accepts NADH as cofactor with a 10 times higher specific activity and even a 15 times higher catalytic efficiency compared to *E. coli* KARI. The overall features of Mr-KARI make this enzyme an ideal candidate for *in-vitro* isobutanol synthesis, but also suitable for *in-vivo* production systems. Hence, this enzyme could be successfully applied in our previously reported cell-free isobutanol production system [5].

Nevertheless, compared to other enzymes in our process the specific activity of Mr-KARI was relative low (0.7 U mg^{-1}). To provide an efficient metabolic flux and minimize enzyme quantities in the reaction cascade, it was necessary to enhance the catalytic activity of the enzyme. Therefore, we developed a new screening method, which was based on an *E. coli* knockout strain as *in-vivo* selection tool. This simple procedure allowed selection of significantly improved KARI variants by simple phenotype selection. The obtained Mr-KARI mutant T84S exhibited an increased preference for NADH as a co-factor and demonstrated a specific activity of 2.7 U mg^{-1}, which is a 350% improvement over the WT. We refined the molecular optimization via site-saturation mutagenesis, generating an array of catalytically improved variants. These variants gave significant insights into the structure–function relationships of Mr-KARI. We could demonstrate that the arginines of the NADPH binding loop of Mr-KARI have a minor influence on the cofactor septicity, which contrasts data for other KARI enzymes [2,34,36,37] and NADPH depending oxidoreductases [27]. Nevertheless, this data was in line with our sequence and structural analysis and could explain the relative high affinity towards NADH of the WT enzyme.

Conflict of interest

The authors declare that they have no competing interests.

Acknowledgment

Appendix A. Supplementary data

Supplementary data related to this article can be found at http://dx.doi.org/10.1016/j.biochi.2014.10.024.

References

[1] R. Dumas, V. Biou, F. Halgand, R. Douce, R.G. Duggleby, Enzymology, structure, and dynamics of acetohydroxy acid isomeroreductase, Acc. Chem. Res. 34 (2001) 399–408.

[2] S. Bastian, X. Liu, J.T. Meyerowitz, C.D. Snow, M.M. Chen, F.H. Arnold, Engineered ketol-acid reductoisomerase and alcohol dehydrogenase enable anaerobic 2-methylpropan-1-ol production at theoretical yield in Escherichia coli, Metab. Eng. 13 (2011) 345–352.

[3] S. Brinkmann-Chen, T. Flock, J.K.B. Cahn, C.D. Snow, E.M. Brustad, J.A. McIntosh, P. Meinhold, L. Zhang, F.H. Arnold, General approach to reversing ketol-acid reductoisomerase cofactor dependence from NADPH to NADH, Proc. Natl. Acad. Sci. U. S. A. 110 (2013) 10946–10951.

[4] S. Atsumi, T. Hanai, J.C. Liao, Non-fermentative pathways for synthesis of branched-chain higher alcohols as biofuels, Nature 451 (2008) 86–89.

[5] J.K. Guterl, D. Garbe, J. Carsten, F. Steffler, B. Sommer, S. Reisse, A. Philipp, M. Haack, B. Ruhmann, A. Koltermann, U. Kettling, T. Bruck, V. Sieber, Cell-free metabolic engineering: production of chemicals by minimized reaction cascades, ChemSusChem 5 (2012) 2165–2172.

[6] M. Reher, P. Schonheit, Glyceraldehyde dehydrogenases from the thermoacidophilic euryarchaeota Picrophilus torridus and Thermoplasma acidophilum, key enzymes of the non-phosphorylative Entner–Doudoroff pathway, constitute a novel enzyme family within the aldehyde dehydrogenase superfamily, FEBS Lett. 580 (2006) 1198–1204.

[7] G. Fiorentino, R. Cannio, M. Rossi, S. Bartolucci, Decreasing the stability and changing the substrate specificity of the Bacillus stearothermophilus alcohol dehydrogenase by single amino acid replacements, Protein Eng. 11 (1998) 925–930.

[8] T. Baba, T. Ara, M. Hasegawa, Y. Takai, Y. Okumura, M. Baba, K.A. Datsenko, M. Tomita, B.L. Wanner, H. Mori, Construction of Escherichia coli K-12 in-frame, single-gene knockout mutants: the Keio collection, Mol. Syst. Biol. 2 (2006) 2006, 0008.

[9] C. UniProt, Update on activities at the Universal Protein Resource (UniProt) in 2013, Nucleic acids Res. 41 (2013) D43–D47.

[10] M. Goujon, H. McWilliam, W. Li, F. Valentin, S. Squizzato, J. Paern, R. Lopez, A new bioinformatics analysis tools framework at EMBL-EBI, Nucleic acids Res. 38 (2010) W695–W699.

[11] H. McWilliam, W. Li, M. Uludag, S. Squizzato, Y.M. Park, N. Buso, A.P. Cowley, R. Lopez, Analysis tool web services from the EMBL-EBI, Nucleic acids Res. 41 (2013) W597–W600.

[12] F. Sievers, A. Wilm, D. Dineen, T.J. Gibson, K. Karplus, W. Li, R. Lopez, H. McWilliam, M. Remmert, J. Soding, J.D. Thompson, D.G. Higgins, Fast, scalable generation of high-quality protein multiple sequence alignments using Clustal Omega, Mol. Syst. Biol. 7 (2011) 539.

[13] P. Gouet, X. Robert, E. Courcelle, ESPript/ENDscript: extracting and rendering sequence and 3D information from atomic structures of proteins, Nucleic acids Res. 31 (2003) 3320–3323.

[14] L.A. Kelley, M.J. Sternberg, Protein structure prediction on the Web: a case study using the Phyre server, Nat. Protoc. 4 (2009) 363–371.

[15] S.K. Saha, L. Uma, G. Subramanian, An improved method for marine cyanobacterial DNA isolation, World J. Microb. Biot. 21 (2005) 877–881.

[16] J. Sambrook, D.W. Russell, Molecular Cloning: a Laboratory Manual, Cold Spring Harbor Laboratory, 2001.

[17] A. Aitken, M. Learmonth, Protein determination by UV Absorption, in: J. Walker (Ed.), The Protein Protocols Handbook, Humana Press, 2002, pp. 3—6.

[18] W.J. Waddell, A simple ultraviolet spectrophotometric method for the determination of protein, J. Lab. Clin. Med. 48 (1956) 311—314.

[19] P. Wolf, A critical reappraisal of Waddell's technique for ultraviolet spectro-photometric protein estimation, Anal. Biochem. 129 (1983) 145—155.

[20] K.E. Jaeger, T. Eggert, A. Eipper, M.T. Reetz, Directed evolution and the creation of enantioselective biocatalysts, Appl. Microbiol. Biotechnol. 55 (2001) 519—530.

[21] J.H. Zhang, T.D. Chung, K.R. Oldenburg, A simple statistical parameter for use in evaluation and validation of high throughput screening assays, J. Biomol. Screen. 4 (1999) 67—73.

[22] C. Papworth, J.C. Bauer, J. Braman, D.A. Wright, QuikChange site-directed mutagenesis, Strategies 9 (1996) 3—4.

[23] M.T. Reetz, Caster 2.0, http://www.kofo.mpg.de/de/forschung/organische-synthese.

[24] M.T. Reetz, J.D. Carballeira, Iterative saturation mutagenesis (ISM) for rapid directed evolution of functional enzymes, Nat. Protoc. 2 (2007) 891—903.

[25] R. Tyagi, S. Duquerroy, J. Navaza, L.W. Guddat, R.G. Duggleby, The crystal structure of a bacterial class II ketol-acid reductoisomerase: domain con-servation and evolution, Protein Sci. : a Publ. Protein Soc. 14 (2005) 3089—3100.

[26] A.M. Lesk, NAD-binding domains of dehydrogenases, Curr. Opin. Struct. Biol. 5 (1995) 775—783.

[27] N.S. Scrutton, A. Berry, R.N. Perham, Redesign of the coenzyme specificity of a dehydrogenase by protein engineering, Nature 343 (1990) 38—43.

[28] D. Leyval, D. Uy, S. Delaunay, J.L. Goergen, J.M. Engasser, Characterisation of the enzyme activities involved in the valine biosynthetic pathway in a valine-producing strain of *Corynebacterium glutamicum*, J. Biotechnol. 104 (2003) 241—252.

[29] J. Durner, O.C. Knorzer, P. Boger, Ketol-acid reductoisomerase from Barley (*Hordeum vulgare*) (purification, properties, and specific inhibition), Plant physiol. 103 (1993) 903—910.

[30] K. Kiritani, S. Narise, R.P. Wagner, The dihydroxy acid dehydratase of *Neurospora crassa*, J. biol. Chem. 241 (1966) 2042—2046.

[31] R. Dumas, J. Joyard, R. Douce, Purification and characterization of acetohy-droxyacid reductoisomerase from spinach chloroplasts, Biochem. J. 262 (1989) 971—976.

[32] GESTIS Substance Database.

[33] S. Reisse, D. Garbe, T. Bruck, Meiothermus ruber thiolase — a new process stable enzyme for improved butanol synthesis, Biochimie 104 (2014) 16—22.

[34] M.J. Rane, K.C. Calvo, Reversal of the nucleotide specificity of ketol acid reductoisomerase by site-directed mutagenesis identifies the NADPH binding site, Arch. Biochem. Biophys. 338 (1997) 83—89.

[35] A. Aulabaugh, J.V. Schloss, Oxalyl hydroxamates as reaction-intermediate ana-logues for ketol-acid reductoisomerase, Biochemistry 29 (1990) 2824—2830.

[36] E.W. Leung, L.W. Guddat, Conformational changes in a plant ketol-acid reductoisomerase upon Mg(2+) and NADPH binding as revealed by two crystal structures, J. Mol. Biol. 389 (2009) 167—182.

[37] K. Thomazeau, R. Dumas, F. Halgand, E. Forest, R. Douce, V. Biou, Structure of spinach acetohydroxyacid isomeroreductase complexed with its reaction product dihydroxymethylvalerate, manganese and (phospho)-ADP-ribose, Acta crystallogr. D Biol. Crystallogr. 56 (2000) 389—397.

Identification and characterization of a highly thermostable crotonase from *Meiothermus ruber*

Steven Reiße, Daniel Garbe, Thomas Brück*

Division of Industrial Biocatalysis, Technische Universität München, Lichtenbergstr. 4, 85748 Garching, Germany

ABSTRACT

Butanol is deemed a second generation biofuel due to its enhanced energy content and improved hydrophobicity compared to ethanol. The state of the art production is the *Clostridia* based anaerobic acetone, butanol and ethanol (ABE) fermentation process. However, the classical ABE fermentation is capped at 2% (v/v) butanol yield, due to end-product toxicity effects. By contrast, cell-free bio-butanol production systems based on designed enzyme cascades hold the promise of higher butanol yields and simplified end-product recovery. Crotonases catalyze the reversible hydration of crotonyl-CoA and are key enzymes in butanol biosynthesis. In this study, we present the isolation, heterologous expression and characterization of a new highly thermostable crotonase (Crt) derived from the bacterium *Meiothermus ruber* (Mr). Mr-Crt displays a broad activity range of 50–70 °C, with optimal reactivity at pH 7.0 and 55 °C. Moreover, Mr-Crt displays an extended half-life of over 1 month (IT$_{50}$ (50 °C) = 743 ± 0.7 h) at elevated temperatures. Robust enzyme activities, such as Mr-Crt, with high temperature and solvent tolerance will ultimately contribute to an improved cell-free butanol process.

© 2014 Elsevier B.V. All rights reserved.

1. Introduction

Enoyl-CoA-hydratase (EC 4.2.1.17) catalyzes the reversible addition of water to α,β-unsaturated enoyl-CoA thioesters. The enzyme is commonly referred as crotonase because of its most active substrate, crotonyl-CoA. Crotonase is part of the physiological important fatty acid β-oxidation pathway and is an essential enzyme component of the related CoA-dependent butanol biosynthesis in microbial cells. At present only a few crotonase type enzyme activities have been reported from pro- and eukaryotic organisms [1–6]. Moreover, only the crystal structure and catalytic mechanism of the crotonase from *Rattus norvegicus* was examined in detail [7–9].

Crotonase activities have attracted significant research attention due to their essential role in biological production of butanol, which is flagged as a second generation biofuel due to its enhanced energy content and improved hydrophobicity compared to first generation fuel options, such as ethanol. Conventionally, bio-butanol production is based on the anaerobic acetone, butanol and ethanol (ABE) fermentation process using clostridial [10–13] or recombinant *Escherichia coli* [14,15] strains. At present, low temperature and solvent (butanol) tolerance [16] and, in case of clostridial strains, oxygen sensitivity hamper industrial process application. To circumvent the limitations of living cell targeted butanol production can be achieved via cell-free bio-butanol production systems utilizing tailor made enzyme cascades [17,18]. These cell-free systems allow the selective production of butanol and hold the promise of higher butanol yields, which provides for simplified end-product recovery. This approach has the potential to control, modify or individually adapt the process conditions [19]. To improve either fermentative or cell-free butanol production requires the identification of process relevant biosynthetic enzyme systems, which display advanced catalytic properties like significant temperature and solvent tolerance.

In this study, we describe a new crotonase activity derived from the mesophilic bacterium *Meiothermus ruber* DSM 1279 (Mr-Crt), which demonstrated excellent thermal stability. The enzyme may assist in improving cell-free butanol production processes.

2. Materials and methods

2.1. Reagents and kits

Restriction enzymes, T4 DNA ligase, T4 Kinase, Shrimp alkaline phosphatase, Phusion polymerase and desoxynucleotides were

---

* Corresponding author.
E-mail addresses: steven.reisse@tum.de (S. Reiße), daniel.garbe@tum.de (D. Garbe), brueck@tum.de (T. Brück).

purchased from Thermo Scientific (Ulm, Germany). Desoxyribonuclease I from bovine pancreas was from Serva Electrophoresis (Heidelberg, Germany). All enzymes were used according to the manufacturers' recommendations, applying the provided buffer solutions. Oligonucleotides were ordered from Eurofins MWG Operon (Ebersberg, Germany). All chemicals were, unless otherwise stated, purchased in analytical grade from Sigma–Aldrich (Munich, Germany), Carl Roth (Karlsruhe, Germany), Serva Electrophoresis and AppliChem (Darmstadt, Germany). Plasmids were purified by GeneJET Plasmid Miniprep Kit (Thermo Scientific), while the innuPREP DOUBLEpure Kit (Analytik Jena; Jena, Germany) was used for purification of PCR products and enzymatically manipulated DNA.

2.2. Strains and media

M. ruber DSM 1279 (DMSZ, Braunschweig, Germany) was grown aerobically at 50 °C in *Thermus ruber* medium containing trypton ($5 \, g \, L^{-1}$), yeast extract ($1 \, g \, L^{-1}$) and soluble starch ($1 \, g \, L^{-1}$), adjusted to pH 8.

E. coli Rosetta ((F-ompT hsdSB(rB-mB-) gal dcm (DE3) pLysSRARE (CamR)) was purchased from Merck (Darmstadt, Germany) and was grown in Terrific Broth (TB) medium for protein expression. *E. coli* XL1-Blue (recA1 endA1 gyrA96 thi-1 hsdR17 supE44 relA1 lac [F′ proAB lacIqZDM15 Tn10 (Tetr)]) from Stratagene (Waldbronn, Germany) was grown in Luria-Bertani (LB) medium. Both media were supplemented with kanamycin ($30 \, \mu g \, ml^{-1}$), TB additionally with chloramphenicol ($34 \, \mu g \, ml^{-1}$).

2.3. Sequence analysis

The predicted amino acid sequence of Mr-Crt was obtained from the UniProt database [20] and aligned to other published sequences by using Clustal W [21]. ESPript [22] was used for further editing. The structural alignment with *R. norvegicus* (PDB: 1DUB) based on a modeled Mr-Crt structure was performed by the Phyre^2 server [23].

2.4. DNA isolation and cloning

The plasmid pET28a (Merck) was pretreated as described by Guterl et al. [19]. The resulting vector pCBR including C-terminal His-Tag was digested with BveI and SalI and subsequently dephosphorylated.

Genomic DNA from *M. ruber* DSM 1279 was isolated as described by Saha [24]. The gene Mrub_2284 was amplified from genomic DNA by PCR with the phosphorylated primers Mr-Crt fwd (5′-CAGCAAGGTCTCGCATATGGCACAGACCTTTGAACTC-3′) and Mr-Crt rev (5′-CAGCAAGTCGACCTCCCCTTTAAACTGCGCC-3′). Resulting PCR fragments were ligated into pCBR via BsaI and SalI restriction sites. The obtained pCBR-Crt-CHis plasmid was transformed in *E. coli* as described elsewhere [25].

2.5. Protein expression and purification

For protein expression, transformed cells were cultivated in shaking flask at 37 °C in TB medium supplemented with kanamycin ($30 \, \mu g \, ml^{-1}$) and chloramphenicol ($34 \, \mu g \, ml^{-1}$). The cells were induced with 1 mM IPTG at OD_{600} 0.5–0.8 and additionally incubated at 37 °C for 4 h. Cultures were subsequently harvested and frozen at −20 °C until further use.

For cell disruption, the cell pellets were resuspended in binding buffer (50 mM HEPES pH 7.5, 20 mM imidazole), supplemented with DNAse ($10 \, mg \, ml^{-1}$). The cells were lysed with an Avestin EmulsiFlex-B15 homogenizer (Mannheim, Germany). Debris was removed by centrifugation at $20,000 \times g$ and 4 °C for 30 min.

The supernatant was loaded onto Ni-NTA columns and washed with 5 column volumes of binding buffer. His-tagged Mr-Crt was eluted in one step with two column volumes of elution buffer (50 mM HEPES pH 7.5, 500 mM imidazole). All fractions were analyzed by 12% SDS-PAGE.

The purified enzyme was subsequently desalted via HiPrep 26/10 Desalting-column (GE Healthcare Europe; Freiburg Germany) in 50 mM HEPES pH 7.5 plus 10% (v/v) glycerol for storing at −80 °C as liquid stock.

Protein contents were quantified spectrophotometrically by measuring the absorbance at 215 and 225 nm as indicated [26–28].

2.6. Analytical methods

3-Hydroxybutyryl-CoA and crotonyl-CoA were analyzed via high performance liquid chromatography (HPLC; Agilent 1100 Series; Agilent, Santa Clara, USA). The system was equipped with an autosampler, a thermostatic column compartment and a diode-array detector. Separation of the CoA-esters was achieved on a Luna 3 μm C18(2) 100 Å column (Phenomenex; Aschaffenburg, Germany) at 25 °C. The two step elution started with a mixture of buffer A (10 mM potassium-phosphate buffer, pH 6.5) and 30% buffer B (10 mM potassium-phosphate buffer, pH 6.5 and methanol, ratio 60/40), followed by a gradient up to 80% buffer B within 10 min. The level of 80% buffer B was finally kept for 5 min, whereby the overall mobile phase flow was adjusted to $0.4 \, ml \, min^{-1}$. System calibration was performed using external standards of each CoA-ester. All samples were pretreated by filtration (10 kDa MWCO; modified PES; VWR, Darmstadt, Germany) before injection. The injection volume was 10 μl in each case.

2.7. Enzymatic characterization

Enzyme activities of Mr-Crt were determined by HPLC analysis, monitoring the formation of 3-hydroxybutyryl-CoA at 50 °C. The assay mixture contained 50 mM HEPES (pH 7) and 50 μM crotonyl-CoA and was preincubated in a thermomixer for accurate temperature control. The pH was adjusted to the corresponding temperature. Reactions were performed in 1.5 ml safe-lock tubes and initiated by addition of 180 μl assay mixture to 20 μl enzyme solution and finally stopped on ice. One unit of enzyme activity was defined as the amount of enzyme that catalyzed the formation of 1 μmol of product per minute.

3. Results and discussion

3.1. Identification and sequence analysis

The alignment of different amino acid sequences of characterized crotonases with a predicted protein from *M. ruber* allowed putative identification of a new crotonase activity (Fig. S1). Although this amino acid based homology study was carried out with different phylogenetic groups, the putative crotonase from *M. ruber* showed sequence homology to the crotonases of *Clostridium acetobutylicum* (Ca, 48%) and *R. norvegicus* (Rn, 39%) [29].

Supplementary material related to this article can be found in the online version, at http://dx.doi.org/10.1016/j.molcatb.2014.11.011.

The putative Mr-thiolase sequence was used as template for a further structural prediction via the Phyre^2 server [23] to examine structural relationships of aforementioned crotonases more closely. The resulting structural model had a confidence interval of 97% over 258 residues with more than 90% accuracy (Fig. 1a).

The alignment data clearly indicated conserved, signature regions between Mr, Ca and Rn crotonase variants, encompassing the amino acid residues, which constitute the crotonase specific
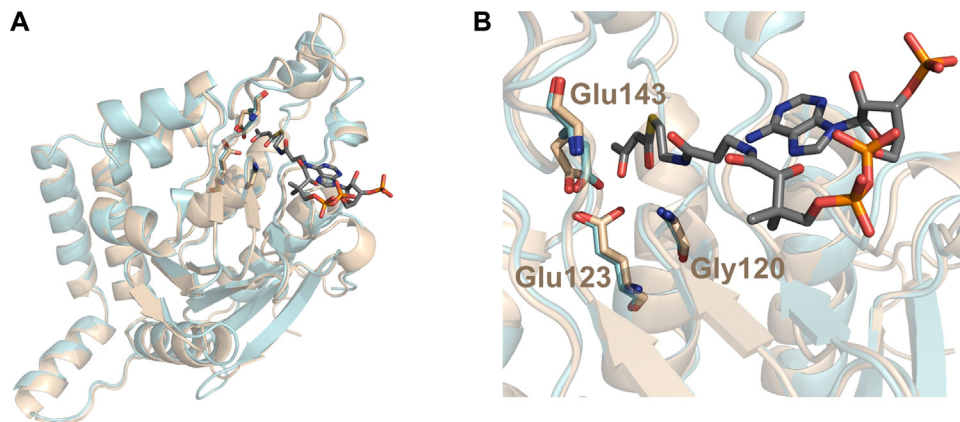
Fig. 1. Structural alignment of modeled Mr-Crt and Rn-Crt. (A) Structural overview. The modeled Mr-Crt structure is colored in gold. The crystal structure of the native Rn-Crt (PDB 1DUB) is colored in blue. The carbon backbone of the CoA-ester is colored in gray. (B) Active site of the aligned crotonases. The amino acids of the catalytic triad of Mr-Crt are labeled. (For interpretation of the references to colour in this figure legend, the reader is referred to the web version of this article.)

catalytic triad [7,9,30]. The Mr-Crt catalytic triad was identified as Gly120, Glu123 and Glu143, which is homologous to Rn crotonase, implicating a similar catalytic mechanism (Fig. 1b).

Consequently, the Mr-Crt catalytic mechanism constitutes a concerted attack by the two glutamate residues. While Glu143 of Mr-Crt protonates the substrate, Glu123 abstracts a proton from a bound water molecule. The Gly120 activates the substrate by a hydrogen bond to the oxygen of the enoyl moiety of the CoA ester [7,30]. The binding pocket for the CoA moiety is formed by characteristic hydrophobic amino acids and lysine residues [7] as shown in Fig. S1. Based on these *in-silico* results, we expected the putative Mr-Crt enzyme could possess crotonase activity.

3.2. Cloning, heterologous expression and purification

The Mr-Crt gene was isolated, cloned and subsequently expressed in *E. coli Rosetta* (DE3) fused to a C-terminal His-Tag. Above 90% of the recombinant Mr-Crt could be recovered from the soluble cell fraction.

The heterologous enzyme was purified to homogeneity and examined by SDS-PAGE. The purified enzyme could be stored as liquid stock at −80 °C over one year without any changes in the biochemical characteristics. In accordance with the theoretical (+ His-tag) molecular weight of the Mr-Crt monomer a single band at approximately 30 kDa was detected on SDS-PAGE (Fig. 2a). Hence, the observed Mr-Crt molecular weight is in line with other crotonases derived from *C. acetobutylicum* (29 kDa) [1], *Bacillus subtilis* (28 kDa) [4] and the eukaryotic crotonase from *R. norvegicus* (28 kDa) [7].

Analysis of Mr-Crt on Native-PAGE (Fig. 2b) indicated a molecular weight of almost 140 kDa, which is consistent with a calculated molecular weight of 120 kDa, suggesting that the native enzyme has a tetrameric architecture. This data is also consistent with previous reports for the prokaryotic crotonase from *C. acetobutylicum* [6].

3.3. Reaction conditions

To reduce microbial contamination in the reaction vessel and enhance space–time yields butanol production is preferably carried out at elevated temperatures. Therefore, in this study measurements for Mr-Crt were carried out at 50 °C or above.

Initial pH effects on Mr-Crt reactivity were studied at 50 °C (Fig. 3a). Mr-Crt was operational in a rather narrow, neutral pH region with an optimal activity at pH 7.0. Notably, a 40% activity reduction was already observed at pH 6.5 and 7.5.

The operational temperature range was determined by incubating Mr-Crt between 30 and 75 °C for 5 min. The reaction was stopped on ice. The formation of 3-hydroxybutyryl-CoA was subsequently monitored via HPLC (Fig. 3b). The enzyme retained 80% activity over a temperature range of 50–70 °C with an optimal activity at 55 °C, indicating that Mr-Crt is highly thermostable.

Enzyme thermo-tolerance is a key process parameter to establish improved butanol production. Therefore, we initially tested the residence time of Mr-Crt by incubating the purified enzyme at 50 °C, followed by determination of the residual activity.

Former conclusion on Mr-Crt temperature optimum could be confirmed by the current assay configuration. The data indicated
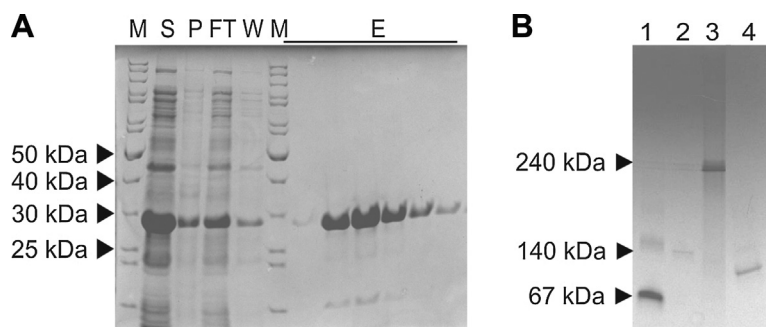

Fig. 2. Purification of C-terminal His-Tagged Mr-Crt. (A) SDS-PAGE analysis after expression in *E. coli* Rosetta (DE3) cells: showing protein fractions from supernatant (S), pellet (P), flow through (FT), washing step (W), eluted enzyme (E) and marker (M, PageRuler Unstained Protein Ladder, Thermo Scientific). (B) Native-PAGE: showing the native Mr-Crt in reference to commercial enzymes: 1 BSA (67 kDa); 2 lactate dehydrogenase (140 kDa); 3 catalase (240 kDa, bovine liver); 4 Mr-Crt.
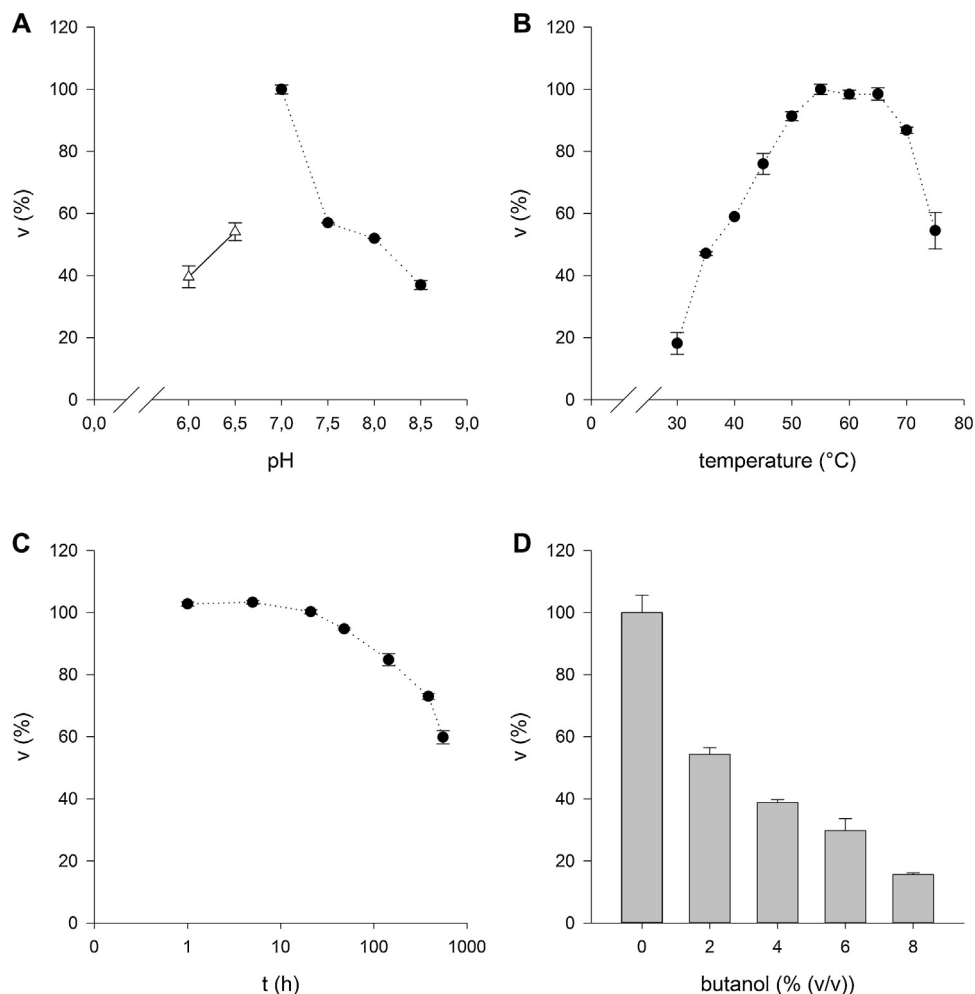
Fig. 3. Effects of different conditions on the activity of purified Mr-Crt. The obtained activity maximum was defined as 100%. (A) pH profile: the reactions were carried out at described conditions with following buffers: −−△−− 50 mM phosphate buffer, pH 6–6.5; ···•··· 50 mM HEPES, pH 7–8,5; (B) Temperature profile: the reactions were carried out at described conditions in a range from 30 to 75 °C for 5 min. (C) Temperature dependant stability at 50 °C, in logarithmic scale. (D) Butanol tolerance. The assays were carried out under described conditions in the presence of various butanol concentrations.

that Mr-Crt has an extraordinary time-dependent stability (IT_{50}) of 743 h ± 0.7 h at 50 °C (Fig. 3c).

As solvent tolerance is a crucial parameter to enhance butanol productivity in biotechnological production processes we have determined the Mr-Crt activity in the presence of increasing butanol concentrations.

Notably, this is the first time that butanol stability is reported for any member of the crotonase family (Fig. 3d). Interestingly, Mr-Crt retained 60% of its activity in the presence of 2% (v/v) butanol. The calculated $IS_{50} > 2$% is lower compared to other thermostable enzyme systems derived from *M. ruber*. Specifically, Mr-thiolase remained 90% of the initial activity up to the presence of 4% (v/v) butanol in the reaction medium [31].

3.4. Catalytic performance

Kinetic experiments were carried out under aerobic conditions. The specific activity of Mr-Crt determined by the increase of 3-hydroxybutyryl-CoA was 20.9 ± 0.3 U mg^{-1}, which is comparable to the specific activity of *C. acetobutylicum* crotonase (19.0 U mg^{-1}) [15].

Kinetic constants were measured with varying concentrations of crotonyl-CoA (0–0.2 mM) in 50 mM HEPES (pH 7 at 50 °C). Observed data of several experiments were fitted to the Michaelis–Menten

equation. The experimentally obtained kinetic constants are stated in Table 1 together with other characteristic values of Mr-Crt.

The measured substrate specificity of 0.03 mM was in line with the previously reported wild type crotonases of *B. subtilis* (0.05 mM) [4], *C. acetobutylicum* (0.03 mM) [6] and *R. norvegicus* (0.015 mM) [8]. However, in contrast to the model enzyme from *R. norvegicus* ($k_{cat}/K_m = 1.2 \times 10^8$ M^{-1} s^{-1} [8]) the catalytic efficiency of Mr-Crt was 1000 fold lower. Nevertheless, the pronounced activity of Mr-Crt under aerobic conditions combined with its excellent therma

Table 1
Physical characteristics of Mr-Crt.

Property	Value
Specific enzyme activity (50 °C)	20.9 ± 0.3 U mg^{-1}
Optimum temperature	55 °C
Thermal stability (50 °C)	$\tau = 743 \pm 0.7$ h
Solvent tolerance (butanol)	<4% (v/v)
Optimum pH	7
Molecular weight (monomeric unit)	30 kDa
K_m[a]	0.03 ± 0.01 mM
k_{cat}	14.9 ± 0.9 s^{-1}
k_{cat}/K_m	$(5.0 \pm 0.9) \times 10^5$ M^{-1} s^{-1}

[a] The kinetic constants were measured with varying concentrations of crotonyl-CoA (0–0.2 mM) in 50 mM HEPES pH 7 at 50 °C.

stability makes this enzyme suitable for *in vitro* butanol production systems.

4. Conclusion

Climate change and rising energy costs drive development of sustainable, bio-based processes for platform chemicals and bio-fuels. Butanol has attracted significant attention as a potential next generation biofuel due to its enhanced energy content and hydrophobicity compared to ethanol.

The classical butanol biosynthesis via anaerobic clostridial fermentation is limited by end product toxicity, low temperature and oxygen tolerance. By contrast, cell-free approaches using *in vitro* enzyme cascades hold the promise of potentially higher product titers and simplified product recovery [17,19,32]. In this context, identification of robust enzyme systems with enhanced temperature and/or solvent tolerance is essential.

Here we present a new crotonase activity derived from *M. ruber* DSM 1279, which catalyzes the reversible hydration of crotonyl-CoA. The new Mr-Crt was cloned, heterologously expressed in *E. coli* and its physical parameters were characterized.

Our experimental data demonstrated that the new enzyme had crotonase activity, in line with our bioinformatic predictions. Optimal Mr-Crt activities were determined at pH 7.0 and 55 °C. Interestingly, the enzyme was active over a very broad temperature range of 50–70 °C where it retained 80% of its initial activity. Moreover, Mr-Crt displayed an extended half-life of over 1 month (IT_{50} (50 °C) = 743 ± 0.7 h) at elevated temperatures, which has not been reported for any other member of the crotonase enzyme family.

A further aspect concerns butanol toxicity. Cell based butanol production systems are limited in both product titers and process viability at 2% (v/v) butanol [33–35] due to toxic effects on cell wall components [13]. A metabolic integration of Mr-Crt would therefore not lead to any improvement. However, the pronounced butanol stability beyond 2% (v/v) suggests, that this enzyme is a suitable component for the construction of a cell-free butanol production cascade.

In light of process-engineering perspectives the excellent thermostability of Mr-Crt at neutral pH conditions provide extended operation capacity and reduced enzyme costs for cell-free butanol production approaches [18].

In this context, we have recently identified a thiolase activity, whose biochemical properties also promise *in vitro* butanol biosynthesis under industrially relevant process conditions [31]. In this regard, the identification of the new Mr-Crt and thiolase enzyme together with our previous results on the cell-free conversion of glucose to pyruvate provide a platform for a consolidated cell-free reaction cascade that allows direct, aerobic conversion of glucose to butanol.

Conflict of interest

The authors declare that they have no competing interests.

References

[1] Z.L. Boynton, G.N. Bennet, F.B. Rudolph, J. Bacteriol. 178 (1996) 3015–3024.
[2] A. Dhar, K. Dhar, J.P. Rosazza, J. Ind. Microbiol. Biotechnol. 28 (2002) 81–87.
[3] M. Dieuaide-Noubhani, D. Novikov, J. Vandekerckhove, P.P. Veldhoven, G.P. Mannaerts, Biochem. J. 321 (Pt 1) (1997) 253–259.
[4] A. Frandi, P. Zucca, M. Marvasi, G. Mastromei, E. Sanjust, B. Perito, Ann. Microbiol. 61 (2011) 371–374.
[5] S.J. Park, S.Y. Lee, J. Bacteriol. 185 (2003) 5391–5397.
[6] R.M. Waterson, R.L. Hill, G.M. Hass, F. Castelli, J. Biol. Chem. 247 (1972) 5266–5271.
[7] C.K. Engel, M. Mathieu, J.P. Zeelen, J.K. Hiltunen, R.K. Wierenga, EMBO J. 15 (1996) 5135–5145.
[8] Y. Feng, H.A. Hofstein, J. Zwahlen, P.J. Tonge, Biochemistry 41 (2002) 12883–12890.
[9] H.A. Hofstein, Y. Feng, V.E. Anderson, P.J. Tonge, Biochemistry 38 (1999) 9508–9516.
[10] P. Durre, Ann. N.Y. Acad. Sci. 1125 (2008) 353–362.
[11] S. Dusseaux, C. Croux, P. Soucaille, I. Meynial-Salles, Metab. Eng. 18 (2013) 1–8.
[12] Y.L. Lin, H.P. Blaschek, Appl. Environ. Microbiol. 45 (1983) 966–973.
[13] K. Vollherbst-Schneck, J.A. Sands, B.S. Montenecourt, Appl. Environ. Microbiol. 47 (1984) 193–194.
[14] S. Atsumi, A.F. Cann, M.R. Connor, C.R. Shen, K.M. Smith, M.P. Brynildsen, K.J. Chou, T. Hanai, J.C. Liao, Metab. Eng. 10 (2008) 305–311.
[15] M. Inui, M. Suda, S. Kimura, K. Yasuda, H. Suzuki, H. Toda, S. Yamamoto, S. Okino, N. Suzuki, H. Yukawa, Appl. Microbiol. Biotechnol. 77 (2008) 1305–1316.
[16] S.H. Baer, H.P. Blaschek, T.L. Smith, Appl. Environ. Microbiol. 53 (1987) 2854–2861.
[17] B. Krutsakorn, K. Honda, X. Ye, T. Imagawa, X. Bei, K. Okano, H. Ohtake, Metab. Eng. 20 (2013) 84–91.
[18] B. Sommer, M. Haack, D. Garbe, T. Brück, JSM Biotechnol. Bioeng. 1 (2013).
[19] J.K. Guterl, D. Garbe, J. Carsten, F. Steffler, B. Sommer, S. Reisse, A. Philipp, M. Haack, B. Ruhmann, A. Koltermann, U. Kettling, T. Bruck, V. Sieber, ChemSusChem 5 (2012) 2165–2172.
[20] C. UniProt, Nucleic Acids Res. 41 (2013) D43–D47.
[21] M.A. Larkin, G. Blackshields, N.P. Brown, R. Chenna, P.A. McGettigan, H. McWilliam, F. Valentin, I.M. Wallace, A. Wilm, R. Lopez, J.D. Thompson, T.J. Gibson, D.G. Higgins, Bioinformatics 23 (2007) 2947–2948.
[22] P. Gouet, X. Robert, E. Courcelle, Nucleic Acids Res. 31 (2003) 3320–3323.
[23] L.A. Kelley, M.J. Sternberg, Nat. Protoc. 4 (2009) 363–371.
[24] S.K. Saha, L. Uma, G. Subramanian, World J. Microbiol. Biotechnol. 21 (2005) 877–881.
[25] J. Sambrook, D.W. Russell, Molecular Cloning: A Laboratory Manual, Cold Spring Harbor Laboratory, 2001.
[26] A. Aitken, M. Learmonth, Protein determination by UV absorption, in: J. Walker (Ed.), The Protein Protocols Handbook, Humana Press, Totowa, New Jersey, 2002, pp. 3–6.
[27] W.J. Waddell, J. Lab. Clin. Med. 48 (1956) 311–314.
[28] P. Wolf, Anal. Biochem. 129 (1983) 145–155.
[29] G. Agnihotri, H.W. Liu, Bioorg. Med. Chem. 11 (2003) 9–20.
[30] C.K. Engel, T.R. Kiema, J.K. Hiltunen, R.K. Wierenga, J. Mol. Biol. 275 (1998) 847–859.
[31] S. Reisse, D. Garbe, T. Bruck, Biochimie 103 (2014) 16–22.
[32] Y.H.P. Zhang, ACS Catal. 1 (2011) 998–1009.
[33] S. Atsumi, T. Hanai, J.C. Liao, Nature 451 (2008) 86–89.
[34] D.R. Nielsen, E. Leonard, S.H. Yoon, H.C. Tseng, C. Yuan, K.L. Prather, Metab. Eng. 11 (2009) 262–273.
[35] E.J. Steen, R. Chan, N. Prasad, S. Myers, C.J. Petzold, A. Redding, M. Ouellet, J.D. Keasling, Microb. Cell Factories 7 (2008) 36.